

Alma Mater Studiorum – Università di Bologna

DOTTORATO DI RICERCA IN

Scienze ambientali: tutela e gestione delle risorse naturali

Ciclo XXVII

Settore Concorsuale di afferenza: 04/A1

Settore Scientifico disciplinare: GEO/08

TITOLO TESI

**HYDROGEOCHEMICAL MONITORING AND MODELLING OF
SALTWATER INTRUSION IN LOWLANDS (FERRARA, IT)**

Presentata da: Nicolò Colombani

Coordinatore Dottorato

Prof. Enrico Dinelli

Relatori

**Prof. Enrico Dinelli
Prof.ssa Maria Dolores Fidelibus**

Esame finale anno 2014

Acknowledgments

Prof. Ramon Aravena, Prof. Enrico Dinelli and Prof. Maria Dolores Fidelibus are gratefully acknowledged for their precious comments and suggestions.

Many thanks are also due to Dr. Dario Di Giuseppe, Dr. Renzo Tassinari and Dr. Umberto Tessari for laboratory assistance and to Dr. Mariachiara Caschetto, Dr. Massimo Marchesi, Dr. Enzo Salemi and Dr. Fabio Vincenzi for field assistance.

Beatrice Maria Sole Giambastiani and Micòl Mastrocicco are acknowledge for all the rest!

THESIS CONTENTS

List of figures	iii
List of tables	viii
RIASSUNTO	ix
Contesto e motivazione	ix
Significato del sito di test selezionato	xii
Obiettivi della tesi	xiii
Implicazioni e prospettive	xvi
1. INTRODUCTION	1
1.1 Background and motivation	1
1.2 Significance of the selected test site	5
1.3 Objectives of the thesis	6
2. SITE DESCRIPTION	9
2.1 Study area	9
2.2 Morphological evolution during the last glacial period	10
2.3 Recent anthropogenic activity	12
2.4 Hydrogeological setting	13
3. MATERIALS AND METHODS	16
3.1 Field activities	16
3.1.1 Monitoring wells installation	16
3.1.2 Continuous monitoring of piezometric heads and surface waters levels	17
3.1.3 Depth profiles acquisition	17
3.1.4 Constant rate pumping tests	19
3.2 Analytical methods	21
3.2.1 Sedimentological characterization	21
3.2.2 Chemical analysis of water samples	22
3.2.3 Geochemical analysis of soil samples	22
3.3 Numerical modelling activities	24
3.3.1 Site wide steady-state simulation	24
3.3.2 Two dimensional transient simulation	28
3.3.3 Scenario modelling	32

CONTENTS

4. RESULTS AND DISCUSSION	34
4.1 Characterization of the lowland coastal aquifer of Ferrara: hydrology, hydrochemistry and evolution of the system	34
4.1.1 Hydrostratigraphic characterization	34
4.1.2 Hydrochemical characterization	39
4.1.3 The origin of the salinization processes	43
4.2 The importance of data acquisition techniques in saltwater intrusion monitoring	47
4.2.1 Open-Borehole Logging and Multi-Level Sampling	48
4.2.2 Integrated-Depth Sampling and Multi-Level Sampling	53
4.2.3 Discrepancy between an integral-depth and a depth-dependent monitoring	55
4.3 Numerical modelling to predict salinization trends in a lowland coastal aquifer	58
4.3.1 Three-dimensional model calibration and sensitivity analysis	59
4.3.2 Three-dimensional model results	62
4.3.3 Tidal forcing effects on groundwater fluctuation	63
4.3.4 Two-dimensional model calibration and validation	65
4.3.5 Future scenarios	68
4.4 Ammonium occurrence in a salinized lowland coastal aquifer	71
4.4.1 Water table elevation and ammonium mapping	72
4.4.2 Core samples depth profiles	73
4.4.3 Groundwater quality depth profiles	75
4.4.4 Groundwater mineralization processes	77
4.5 Trace elements mobility in a saline coastal aquifer of the Po river lowland	78
4.5.1 Sediment composition	78
4.5.2 Hydrochemical conditions of the shallow aquifer	81
4.5.3 Trace elements distribution in the shallow aquifer	81
4.5.4 Trace elements profiles in sediments and groundwater	83
4.5.5 Trace elements partitioning between groundwater and sediments	85
5. SUMMARY AND CONCLUSIONS	87
5.1 Synthesis	87
5.2 Conclusions	87
5.3 Recommendations	90
5.3.1 Practical implications	90
5.3.2 Remaining challenges	91
5.4 Related publications	92
6. REFERENCES	95

LIST OF FIGURES

Figure 1.1 – Wheat fields in the Ferrara lowland (www.estense.com).

Figure 2.1 - Ferrara Province topography map and location of the coastal lowland study area (dashed rectangle).

Figure 2.2 – Upper panel: Location of the 13 monitoring wells, the sandy paleochannel belts, the dunes and paleodunes in the study area. Lower panel: sketch of the study area showing the location of the two boreholes P33, P34 and of the courses of the main rivers. Below is shown the hydro-stratigraphic reconstruction along the transect AA', with geological logs and piezocone resistance profiles.

Figure 2.3 – Waterworks in the Ferrara Province at the beginning of the XX century (www.bonificaferrara.it).

Figure 2.4 – “Valle Lepri” dewatering station in the Ferrara Province lowland (www.bonificaferrara.it).

Figure 2.5 - Excerpt of the coastal territory of the Duchy of Ferrara in 1648 (ilmuseodimirabello.com).

Figure 3.1 - Multilevel Sampler set up and installation.

Figure 3.2 - Grid discretization and boundary conditions applied to the model domain: no flow cells (grey), constant heads cells (blue) drain cells (yellow) and river cells (cyan).

Figure 3.3 - Hydraulic conductivity (m/s) discretization of the model domain based on surface geology and the decreasing hydraulic conductivity pattern found during the multi-level pumping tests.

Figure 3.4 - Variogram fitted with a power law function (left plot), and distribution of Specified Concentration in layer 10 derived from the interpolated measured TDS and pilot points (right plot).

Figure 3.5 - Numerical grid, with the optimized k_h discretization, in yellow the Drain cell and in light blue the Time-Variant Specified-Head cells pertaining to the canal and to the pro-delta silty clays connected with the Adriatic sea.

Figure 3.6 - In the upper left hand side plot, the actual cumulative transpiration (blue line) and evaporation rates (black line) computed by Hydrus-1D are shown. In the upper right hand

LIST OF FIGURES

side plot, the recharge rate computed by Hydrus-1D (blue line) and its discretization as input in SEAWAT (red bars) are shown. In the lower left hand side plot, the modelled (blue line) and observed (black line) canal water levels are shown. In the lower right hand side plot, the modelled (blue line) and observed (black open circles) canal TDS values are shown.

Figure 4.1 - (a) Profiles of hydraulic conductivity measured by constant rate pumping tests in the four monitoring wells and (b) Scatterplot of K values calculated by pedotransfer formula (Kped) and K values resulting from permeability tests in P33 and P34.

Figure 4.2 - Transect AA' across the coastal aquifer (trace in Figure 2.2) showing freshwater head (h_f in green color) and seepage (q_z in red color). Note: positive value means flow from the bottom toward the surface, while negative values indicate downward flow (recharge).

Figure 4.3 - Salinity (TDS in g/l) and concentration of the anions of major salts. The purple line indicates the TDS concentration of the current Adriatic Sea water.

Figure 4.4 - Saturation index for gypsum, calcite and dolomite along the aquifer depth calculated with PHREEQC.

Figure 4.5 - Plots of the concentration of Br^- , Na^+ , SO_4^{2-} , and Mg^{2+} with respect to Cl^- . The purple lines indicate the non-reactive mixing line between freshwater and modern seawater; the star symbol indicates the concentration of the modern Adriatic Sea water.

Figure 4.6 - Variation of sample concentration of Na^+ , K^+ , Mg^{2+} , and Ca^{2+} with respect to the theoretical composition expected for a non-reactive mixing of Adriatic Sea water and freshwater. Note: positive values indicate enrichment, while negative values indicate depletion.

Figure 4.7 - TDS versus Depth, blue circles indicate the MLS samples and red crosses indicate the IDS samples. Water quality classes are drawn according to Davis and De Wiest (1996).

Figure 4.8 - TDS distribution along the coastal aquifer. Dashed lines indicate TDS values of monitoring campaign in November 2011.

Figure 4.9 - Plot of Cl^-/Br^- molar ratio versus Cl^- (meq/l) for the groundwater samples (left panel). Plot of Cl^- versus Br^- (meq/l) for the groundwater samples (right panel). Black lines indicate the ideal mixing line between actual freshwater and seawater, while the grey shaded areas represent the mixing area.

Figure 4.10 - Gibbs diagrams for cations (left panel) and anions (right panel).

LIST OF FIGURES

Figure 4.11 - Plots of salinity with MLS versus OBL data for each monitoring well along transect AA'; stratigraphy (core logs data) from figure 2.2 is displayed on each plot to assist the interpretation.

Figure 4.12 - Plots of pH with MLS versus OBL data for each monitoring well along the transect AA'; stratigraphy (core logs data) from figure 2.2 is displayed on each plot to assist the interpretation.

Figure 4.13 - Plots of Eh with MLS versus OBL data for each monitoring well along the transect AA'; stratigraphy (core logs data) from figure 2.2 is displayed on each plot to assist the interpretation.

Figure 4.14 - Plots of O₂ with MLS versus OBL data, for each monitoring well along the transect AA'; stratigraphy (core logs data) from figure 2.2 is displayed on each plot to assist the interpretation.

Figure 4.15 - TDS versus Depth, blue circles indicate the MLS samples and red crosses indicate the IDS samples. Water quality classes are drawn according to Davis and De Wiest (1996).

Figure 4.16 - Eh versus depth for selected monitoring wells. Blue circles indicate the MLS values and red lines indicate the IDS values.

Figure 4.17 - Eh versus pH plot. Grey shaded areas identify the main TEAP environments.

Figure 4.18 - Cl⁻ distribution maps, according to Stuyfzand classification (1989), derived using IDS data (left panel) and MLS data from the upper aquifer portion (mid panel) and from the lower aquifer portion (right panel).

Figure 4.19 - Subdivision of the model in drainage basins.

Figure 4.20 - Scatter diagrams of calculated and measured hydraulic head (left plot) and of salt concentrations (right plot).

Figure 4.21 - Piezometric map of the calculated heads (m a.s.l.).

Figure 4.22 - Three-dimensional isoconcentration map of the calculated salt concentrations, along the transect AA'.

Figure 4.23 - Plots of continuous piezometric head monitoring of monitoring well P8 (black line) and sea level (red line). The left plot shows the entire monitoring period, while the right plot shows a zoomed timeframe of one week when the tidal oscillation is more evident. Note that the y scales have different ranges.

LIST OF FIGURES

Figure 4.24 - Location of the study area and conceptual model of the transect across monitoring well P8 and Canale della Gronda, selected for the two-dimensional numerical model.

Figure 4.25 - In the left hand side plots: comparison of modelled hydraulic heads (blue lines) versus observed hydraulic heads (grey lines) and their running average with daily period (black lines), In the right hand side plots: comparison of modelled TDS (blue lines) versus observed TDS (grey lines) and their running average with daily period (black lines). The observed water levels and TDS in the drain ditch are plotted with black open circles.

Figure 4.26 - In the upper panels the simulated TDS contours for 12/12/2012 (left panel) and for 26/02/2013 (right panel) are shown with the location of P8. Profiles in P8 of modelled (black lines) versus observed (black open circles) TDS used to validate the numerical model are shown in the lower plots.

Figure 4.27 - In the upper panels the actual average TDS contours for the end of the summer (left panel) and for the end of the winter (right panel) are plotted, while the future scenarios are all plotted for the end of the summer conditions. The projected LSLR are shown in the left panels and HSLR are shown in the right panels. The black line represents the 2.5 g/L TDS isoline.

Figure 4.28 - Location of the study area with the piezometric contour map (black lines); circles represent the groundwater NH_4^+ concentration at 1 m below the water table in the 59 piezometer investigated; in black colour the four selected piezometers along a flow line (dashed line corresponding to transect AA' in Fig. 2.2).

Figure 4.29 - Distribution of NO_3^- and NH_4^+ concentrations for the 59 monitoring wells with respect to redox values (Eh).

Figure 4.30 - Depth profiles of sediment TOC, TLN and NH_4^+ ; stratigraphy (core logs data) is plotted on each graph to facilitate the interpretation.

Figure 4.31 - Transect along the selected flow line (refer to figure 4.28 for the location) with concentration profiles of NH_4^+ , NO_3^- and NO_2^- ; unconfined aquifer thickness (shaded grey area), water table (blue line) and core logs stratigraphy are also shown. Note that curves are plotted at different horizontal scale to facilitate the graph interpretation.

Figure 4.32 - Transect along the selected flow line (refer to figure 4.28 for the location) with concentrations profiles of NH_4^+ and TDS; unconfined aquifer thickness (shaded grey area), water table (blue line) and core logs data are also shown. Note that curves are plotted at different horizontal scale to facilitate the graph interpretation.

LIST OF FIGURES

Figure 4.33 - Salinity versus Sr^{2+} concentration in deep (from -25 to -9 m a.s.l.), medium (from -9 to -7 m a.s.l.), and shallow (from -7 to +1 m a.s.l.) samples (left graph); grey bars represent salinity and Sr^{2+} concentration of the Adriatic seawater. NH_4^+ versus Sr^{2+} concentration in deep (from -25 to -9 m a.s.l.), medium (from -9 to -7 m a.s.l.), and shallow (from -7 to +1 m a.s.l.) samples (right graph); grey bars represent NH_4^+ and Sr^{2+} concentration of the Adriatic seawater.

Figure 4.34 - Scatter plots of selected TE in sediments versus clay content and their relative regression coefficients (R^2) for linear fitting.

Figure 4.35 - Depth profiles of TDS, Eh and selected redox species in groundwater and sediments; stratigraphy (core logs data) is reported on each plot to facilitate the interpretation.

Figure 4.36 - Depth profiles of TE in groundwater and sediments; stratigraphy (core logs data) is reported on each plot to facilitate the interpretation.

LIST OF TABLES

Table 3.1 - Flow and transport parameters used for the simulations.

Table 4.1 - Core sample analyses of monitoring wells P33 and P34.

Table 4.2 - Values of measured total porosity (n), calculated total porosity by Vukovic and Soro (1992) (n_v), respective effective porosity (n_e , n_{ev}) and pore-water velocity (v and v_v), and measured hydraulic conductivity (k) in monitoring wells P33 and P34.

Table 4.3 - Discrepancy between MLS and IDS values concerning the major ions, the symbol – is used when concentrations are below detection limit.

Table 4.4 - Discrepancy between MLS and IDS values concerning the physical-chemical parameters.

Table 4.5 - Comparison between the observed and calculated volume of water (m^3/s) discharged to the sea by the 5 main dewatering stations.

Table 4.6 - Hydraulic heads composite scale sensitivity values calculated by PEST.

Table 4.7 - Absolute mean error between observed and calculated values of the calibrated and validated models.

Table 4.8 - Scenario modelling of the predicted variations of freshwater maximum thickness respect to the actual situation, with sub-scenarios of projected low sea level rise (LSLR) and high sea level rise (HSLR). Positive values indicate thinning of freshwater lens, while negative values indicate thickening.

Table 4.9 - Chemical composition of samples from P33 and P34. Depth are expressed as relative to mean sea level.

Table 4.10 – Derived parameter values in the sediment samples collected from P33 and P34 (in italics). SOM and clay content reported from Mastrocicco et al. (2012). Depth are expressed as relative to mean sea level.

Table 4.11 - TE concentrations in groundwater samples from P33 and P34. Depth are expressed as relative to mean sea level.

RIASSUNTO

Contesto e motivazione

Le risorse idriche sotterranee delle aree costiere sono sottoposte ad una crescente attenzione come fonte di approvvigionamento idrica grazie alla loro minor vulnerabilità all'inquinamento rispetto alle acque superficiali ed alla elevata capacità di stoccaggio degli acquiferi (Dillon, 2005). Tuttavia, in assenza di sistemi di gestione sostenibile delle risorse idriche, un incontrollato uso del suolo ed il sovrasfruttamento delle falde, possono portare ad un deterioramento significativo e di lunga durata delle risorse idriche e degli ecosistemi da esse dipendenti (Candela et al., 2009; Grassi et al., 2007; Park et al., 2005).

Per queste ragioni, negli ultimi decenni la ricerca sugli acquiferi costiere si è intensificata soprattutto per quanto riguarda i processi di salinizzazione (Barlow e Reichard, 2010; Custodio, 2010; Post e Abarca, 2010; Werner et al., 2013). Tuttavia, l'individuazione delle sorgenti di salinizzazione delle falde costiere non è semplice in quanto essa può derivare sia da fonti naturali che antropiche e, in molti casi, più sorgenti possono agire contemporaneamente in uno stesso acquifero (Cartwright et al., 2004; Fakir et al., 2002; Lenahan e Bristow, 2010; Sanchez Martos et al., 2002). In alcune zone costiere, la questione della salinizzazione delle acque sotterranee vede il coinvolgimento non solo di acqua marina attuale ma anche di acque di mare relitte e acque ipersaline (Fass et al., 2007; Ridd e Stieglitz, 2002; Wood et al., 2003). In questi casi, la distinzione tra intrusione attuale e relitta è fondamentale per costruire un modello concettuale robusto con il quale definire un programma di gestione sostenibile (Werner e Gallagher, 2006). Qualunque sia la sorgente salina, la sua identificazione è spesso complicata dalle interazioni suolo-acqua, per altro amplificate dall'aumento della forza ionica dell'acqua (de Montety et al., 2008), e dai processi di miscelazione spesso accelerati dalle attività antropiche come l'eccessivo pompaggio o l'escavazione di canali artificiali (Barlow e Reichard, 2010; Custodio, 2010; Kass et al., 2005; Yamanaka e Kumagai, 2006).

Un tema chiave per comprendere i processi di salinizzazione è quello della corretta caratterizzazione verticale delle proprietà fisico-chimiche degli acquiferi (de Louw et al., 2010; 2011; Netzer et al., 2011). La variabilità nella composizione chimica verticale delle acque sotterranee è stata descritta sia tra diverse unità idrogeologiche della medesima falda (Nativ e Weisbrod, 1994) che su piccole sezioni di una data unità idrologica (Dhar et al., 2008). Gli acquiferi costieri sono spesso costituiti da sequenze di strati con differenti proprietà idrauliche (Bear et al., 1999), che possono complicare l'andamento dell'interfaccia acqua dolce/acqua salata (Kim et al., 2008) e quindi i pozzi di monitoraggio delle zone costiere possono agire come cortocircuiti verticali fra strati (Werner et al., 2013) inducendo un flusso verticale locale (Elci et al., 2003) che può causare il trasporto dei soluti (Konikow e Hornberger, 2006) compromettendo le misure concernenti la distribuzione della salinità (Shalev et al., 2009).

Le diagrafie (OBL) sono spesso impiegate per individuare l'interfaccia acqua dolce/acqua salata negli acquiferi costieri e per caratterizzarne le zone redox (Jorstad et al., 2004; Kim et al., 2008). Tuttavia, anche se questo metodo di monitoraggio è semplice, economico e veloce, la tecnica OBL ha alcune limitazioni, in particolare nelle zone costiere dove i valori misurati (di salinità o di qualsiasi altra proprietà dell'acqua) potrebbero essere rappresentativi della colonna d'acqua stratificatasi all'interno del pozzo, ma non necessariamente del mezzo poroso circostante (Balugani e Antonellini, 2010; Kurtzman et al., 2011; Shalev et al., 2009).

Allo stesso modo, il campionamento integrato (IDS) fornisce campioni d'acqua che rappresentano un'integrazione indefinita della qualità delle acque sotterranee per l'intera lunghezza del pozzo (Robbins e Hayden-Martin, 1991) ed è quindi in gran parte carente ai fini dello studio dei processi di salinizzazione, dal momento che in un acquifero costiero la stratificazione delle acque in funzione della loro densità è la regola piuttosto che l'eccezione.

Al contrario, il campionamento multilivello (MLS) della falda acquifera è in grado di fornire una distribuzione tridimensionale della qualità delle acque sotterranee all'interno di un sistema acquifero costiero (Mastrocicco et al., 2012c). La tecnica MLS è abitualmente applicata in siti contaminati per mappare la diffusione dei contaminanti e quantificare i percorsi di reazione biogeochimici (Colombani et al., 2009; Henderson et al., 2009; Mastrocicco et al., 2012b; Prommer et al., 2006), ma è meno frequentemente utilizzata nel monitoraggio della salinizzazione nelle zone costiere a causa dei costi elevati e dei tempi lunghi (Einarson e Cherry, 2002). La spesa, tuttavia, non cancella la necessità di una caratterizzazione in funzione della profondità per stimare correttamente la composizione chimica delle acque sotterranee e migliorare quindi la comprensione dei processi che agiscono nelle zone costiere.

La discretizzazione verticale negli acquiferi è fondamentale non solo per comprendere i processi di salinizzazione ma anche nello studio della distribuzione e la speciazione di alcuni composti maggiori ed in tracce che, in seguito all'aumentata della forza ionica delle acque sotterranee, potrebbero essere rimobilizzati. Dalla diffusione di contaminanti geogenici o di origine antropica disciolti nelle acque sotterranee, derivano potenziali rischi non solo per le acque superficiali (Li et al., 2014) ma anche per le colture (Li et al., 2010). Ad esempio, un aumento delle concentrazioni di azoto reattivo (N) può essere responsabile di pericoli per la salute (Gelberg et al., 1999; Guliš et al., 2002), dell'eutrofizzazione delle acque superficiali (Jayasingha et al., 2011) e della crescita di alghe nelle acque marino costiere con conseguenti danni non solo ambientali ma anche alle attività turistiche (Linderfelt e Turner, 2001). L'aumento del contenuto di N nelle acque superficiali e sotterranee è stato comunemente attribuito a fonti antropiche, quali la presenza di scarichi civili o di attività agricole e/o industriali (Rodvang e Simpkins, 2001). Minore attenzione è stata data alle sorgenti naturali di N nelle acque sotterranee, quali ad esempio un arricchimento dovuto al contributo di processi di interazione acqua/sedimento, la mineralizzazione della sostanza organica, (Lorite-Herrera et al., 2009) e il rilascio di NH_4^+ per scambio cationico in condizioni anossiche (Appelo e Postma, 2005; Lewandowski e Nützmann, 2010; Seitzinger et al., 1991).

Un altro argomento in cui la discretizzazione verticale è inevitabile è lo studio della distribuzione degli elementi in traccia (TE) nelle acque sotterranee con salinità variabile e nei sedimenti associati. I TE possono derivare da fonti antropiche quali attività agricole, industriali e

minerarie (Buggy e Tobin, 2008; Du Laing et al., 2009), ma possono anche essere legati alla naturale composizione delle formazioni da cui derivano i sedimenti erosi o alle reazioni di scambio promosse dall'intrusione di acque saline (Teuchies et al., 2013). La contaminazione da metalli geogenici è infatti possibile soprattutto nelle zone costiere dove la forza ionica delle acque sotterranee può essere molto elevata, favorendo così la consistente mobilitazione di TE (Acosta et al., 2011; Wang et al., 2012; Cidu et al., 2013; Delaune et al., 2008. Dévai et al., 2005; Du Laing et al., 2008).

Un caso particolare è rappresentato dalle zone costiere che si trovano sotto il livello del mare, che in futuro, con l'aumento del livello del mare previsto dai cambiamenti climatici (Werner et al., 2013), potrebbero sperimentare un aumento della risalita delle acque saline presenti alle base degli acquiferi, grazie ai flussi verticali indotti dalle attività di bonifica indispensabili per mantenere asciutti i terreni delle pianure alluvionali utilizzati per l'agricoltura (Louw et al., 2013; Giambastiani et al., 2013; Mollema et al., 2013; Hinsby et al., 2008; Vandecasteele et al., 2006).

Con il recente perfezionamento delle proiezioni dei cambiamenti climatici, è aumentato il numero degli studi che valutano gli effetti delle crescenti pressioni sugli acquiferi costiere (Ranjan et al., 2006; Werner et al., 2013). Diversi studi hanno cercato di quantificare l'effetto dell'innalzamento del livello marino (SLR) sull'intrusione di acque marine in acquiferi costieri. Considerando l'Europa, la vulnerabilità delle aree costiere al SLR è stata indagata da Lebbe et al. (2008) e da Vandenbohede et al. (2008) per la pianura costiera del Belgio, da Oude Essink (2010) per i Paesi Bassi, da Feseker (2007) per il Nord-ovest della Germania, da Fujinawa et al. (2009) per la regione orientale della Turchia, da Giambastiani et al. (2007) e da Colombani et al. (2015a) per le falde acquifere costiere di Ravenna e Ferrara. La maggior parte di questi studi sottolineano la salinizzazione dell'acquifero costiero spesso mette a rischio anche le risorse idriche superficiali. Recenti studi hanno esaminato le interazioni quantitative a grande scala tra acque superficiali e sotterranee in prossimità della costa (Oude Essink et al., 2010; Vandenbohede et al., 2008) ma meno è stato fatto per chiarire le interazioni a piccola scala tra acque sotterranee e canali di irrigazione e drenaggio. Solo di recente sono stati pubblicati alcuni studi dettagliati in cui i processi di flusso e trasporto del sale in pianure agricole bonificate sono stati quantificati e modellati (de Louw et al., 2010; 2011; 2013).

Una volta che un modello concettuale affidabile è stato costruito, l'implementazione di modelli numerici di flusso e trasporto densità-dipendenti, come SEAWAT (Guo e Langevin, 2002; Langevin et al., 2007) e MODFLOW (Harbaugh et al., 2005; McDonald e Harbaugh, 1988), costituisce un valido approccio per capire: (i) i meccanismi di salinizzazione (da intrusione di acqua di mare attuale e per risalita di acque saline relitte), (ii) il loro effetto sulla mobilitazione di contaminanti geogenici e (iii) gli impatti che i diversi scenari di cambiamenti climatici avranno su questi fenomeni. L'utilizzo di tali strumenti, vincolati ai rilievi di campo, consentirà migliorare la gestione dell'interazione tra acque superficiali e sotterranee e di individuare eventuali misure di mitigazione degli impatti per evitare il deterioramento delle risorse idriche.

Significatività dell'area di studio prescelta

Le aree soggette a deterioramento delle acque sotterranee sono prevalentemente pianure costiere densamente popolate, che più di altre sono esposte alle perturbazioni antropiche e alle conseguenze dei cambiamenti climatici. Tra i problemi che queste aree devono affrontare, la salinizzazione delle risorse sia di superficie che sotterranee sembra essere il più preoccupante, soprattutto in pianure intensamente coltivate.

Per questo motivo, l'acquifero costiero non confinato della Provincia di Ferrara, situato nella pianura del delta del fiume Po, è stato scelto come area di studio per esaminare i meccanismi che regolano il processo di salinizzazione delle acque sotterranee.

Questo territorio è stato ampiamente studiato negli ultimi decenni e un gran numero di contributi provenienti da discipline diverse permettono di ottenere una solida conoscenza dell'evoluzione geologica e geomorfologica della falda costiera della Provincia di Ferrara. D'altra parte, essendo le acque sotterranee poco sfruttate a causa delle abbondanti risorse idriche superficiali, gli studi sulle falde acquifere locali sono limitati.

Per migliorare la comprensione degli aspetti idrologici e idrochimici dell'acquifero costiero sono stati utilizzati, 11 dei 30 pozzi di monitoraggio delle rete del Servizio Geologico della Regione Emilia Romagna insieme con 38 pozzi di monitoraggio pre-esistenti della Provincia di Ferrara.

Oltre al buon livello di dettaglio con cui questa zona è stato indagata, altri fattori la rendono ideale per condurre lo studio oggetto di questa tesi: (i) la zona costiera di Ferrara è intensamente coltivata sin dalla sua bonifica più recente (metà del 1900), (ii) ancora oggi il sistema di drenaggio è necessario per abbassare la falda e garantire la coltivabilità dei terreni, (iii) l'irrigidimento della rete idrografica causata dalla bonifica ha aumentato la subsidenza del terreno, già naturalmente presente, (iv) l'aumento della differenza tra la quota del piano campagna ed il livello del mare ha favorito l'ingressione marina nella rete idrografica, (v) la salinizzazione del suolo danneggia la produttività agricola, (vi) la diminuzione della disponibilità delle risorse idriche, specialmente nel periodo estivo, rappresenta un rischio per lo sviluppo delle attività turistiche.

L'analisi dei risultati aiuterà le autorità locali a gestire correttamente le risorse idriche costiere e permetterà di individuare possibili azioni di mitigazione del fenomeno della salinizzazione delle acque sotterranee e superficiali.

Va comunque sottolineato che lo studio qui presentato si è focalizzato esclusivamente sugli aspetti fisico-chimici del problema della salinizzazione senza tener conto degli aspetti economici di tale problematica, che sono altrettanto importanti per l'identificazione e l'attuazione delle azioni di mitigazione. Tuttavia, il protocollo di caratterizzazione impiegato in questo studio potrebbe essere applicato con successo in molte altre zone costiere con problemi analoghi a quelli descritti per l'area costiera ferrarese.

Obiettivi della tesi

A causa dell'impatto potenzialmente irreversibile del deterioramento della qualità delle risorse idriche, l'obiettivo primario di questa tesi è stato quello di ottenere una comprensione quantitativa dei processi che hanno causato la salinizzazione delle acque sotterranee nella falda acquifera costiera ferrarese. In secondo luogo si è voluto indagare l'impatto che i cambiamenti climatici potranno avere sul processo di salinizzazione in atto e le eventuali conseguenze che un aumento di salinità possono avere sulla mobilizzazione di contaminanti sia maggiori che in tracce. Alla luce di quanto detto sin qui, lo studio in oggetto si propone di raggiungere i seguenti obiettivi:

Caratterizzazione della falda acquifera costiera della pianura di Ferrara: idrologia, idrochimica ed evoluzione del sistema

La caratterizzazione idrodinamica e idrogeochimica della falda acquifera costiera ferrarese, soggetta a profondi cambiamenti naturali e antropici dall'ultima glaciazione ad oggi, ha permesso di comprendere le cause che hanno portato alla salinizzazione delle acque sotterranee (vedi capitolo 4.1).

Le acque saline e ipersaline sono per lo più associate a sedimenti fini di retro-barriera e ambienti lagunari, legati alla trasgressione Flandriana, mentre le acque dolci e salmastre sono legate a sistemi di dune e spiagge relitte. Le acque ipersaline si trovano nella parte più profonda della falda acquifera e non possono essere associate all'intrusione marina attuale ma testimoniano piuttosto la presenza di acque marine relitte intrappolate in ambienti retro-dunali e lagunari durante le fasi interglaciali dell'Olocene. Dati di campo mostrano come gli elevati tenori di salinità (superiori all'acqua di mare) possano essere attribuiti all'evaporazione diretta e/o alla traspirazione di acqua di mare prima della sua infiltrazione.

La parametrizzazione idrodinamica dell'acquifero ha permesso di individuare la presenza di un gradiente idraulico verticale dovuto al drenaggio delle rete di canali di bonifica presenti nell'area. Di conseguenza le acque saline precedentemente intrappolate nella parte più profonda dell'acquifero da lenti a bassa permeabilità, sono state trasportate verso la parte superficiale della falda e addirittura scaricate nella rete di canali di irrigazione.

L'indagine idrogeochimica ha anche permesso di distinguere tra il ruolo della miscelazione tra acque a diversa salinità e quello dell'interazione acqua/sedimento (scambio ionico, dissoluzione/precipitazione di calcite e dolomite, ossidazione della materia organica, riduzione dei solfati) nell'evoluzione delle acque sotterranee. Le acque più saline infatti sono caratterizzate da scambio cationico e riduzione di SO_4^{2-} , soprattutto dove è presente materia organica fossile (depositi paleo-palustri e strati di torba). L'insieme di tali processi comporta poi l'aumento del contenuto di Ca^{2+} e HCO_3^- nelle acque sotterranee con conseguente precipitazione di dolomite/calcite.

Importanza di tecniche di monitoraggio nella comprensione dei processi di salinizzazione

L'esperienza in campo ha dimostrato che una dettagliata caratterizzazione verticale è l'unico metodo che può restituire una ricostruzione affidabile della distribuzione delle specie disciolte all'interno della falda freatica. Per questo motivo sono state applicate diverse tecniche di monitoraggio per acquisire i principali parametri fisico-chimici in funzione della profondità: diagrafie (OBL), campionamento integrato (IDS) e campionamento multilivello (MLS). I risultati derivanti dall'applicazione delle diverse tecniche di monitoraggio sono stati quindi confrontati per individuare la metodologia più adatta ed efficace (vedi capitolo 4.2).

Il confronto tra la tecnica OBL e la tecnica MLS mostra che, escludendo la distribuzione delle acque saline e ipersaline alla base dell'acquifero, le due metodologie non presentano differenze significative. Ne consegue che il metodo OBL può essere utilizzato con successo per una determinazione preliminare della posizione dell'interfaccia acqua dolce/acqua salata. Tuttavia, il metodo OBL ha fornito una caratterizzazione fuorviante della distribuzione degli ambienti redox all'interno della falda poiché la distribuzione dei dati idrochimici (pH, Eh e O₂) raccolti con la tecnica OBL non concorda con quella della tecnica MLS. Ne consegue che uno studio più dettagliato sui processi geochimici reattivi può essere intrapreso solo attraverso la tecnica MLS, che è comunque preferibile anche quando è richiesto un elevato livello di precisione nel descrivere la distribuzione delle acque ad elevata salinità.

Un confronto diretto tra l'affidabilità delle tecniche di monitoraggio IDS e MLS è stato effettuato derivando due diversi modelli concettuali della distribuzione della salinità sulla base dei monitoraggi effettuati con l'una e con l'altra tecnica.

Il disaccordo nell'interpretazione dei risultati ottenuti con le due tecniche di campionamento è particolarmente evidente nell'analisi del TDS rispetto alla profondità, e del Eh rispetto al pH. Il modello concettuale IDS richiama il fenomeno dell'intrusione marina attuale, poiché le concentrazioni di Cl⁻ non sono mai superiori a quella dell'acqua di mare e per l'assenza di acque ipersaline in tutta l'area di studio. Al contrario, nel modello concettuale MLS la parte inferiore della falda freatica presenta acque ipersaline rendendo necessario considerare processi di salinizzazione diversi dall'intrusione marina attuale, come l'evoluzione geochimica delle acque sotterranee causata dall'evapoconcentrazione o l'interazione acqua/sedimenti.

Le discrepanze tra il monitoraggio effettuato via MLS e IDS risultano particolarmente evidenti specialmente nel caso di specie disciolte sensibili agli ambienti redox, confermando che nella tecnica IDS la miscelazione artificiale all'interno del pozzo può mascherare la stratificazione verticale delle concentrazioni nella falda acquifera.

I risultati dimostrano non solo che la tecnica IDS è decisamente più imprecisa rispetto alla tecnica MLS, ma addirittura che essa potrebbe dare rappresentazioni fuorvianti della realtà. Pertanto, i modelli concettuali ottenute tramite la tecnica IDS non possono neppure essere considerati uno studio preliminare in un acquifero costiero affetto da salinizzazione ma dovrebbero essere evitati con fermezza, soprattutto quando il contrasto di densità tra acque dolci e saline è particolarmente elevato.

Previsione dei trend di salinizzazione della falda acquifera costiera

Attraverso l'utilizzo della modellazione numerica, basata sui rilievi di campagna e sul conseguente modello concettuale, è stato possibile ricostruire e confermare l'ipotesi sull'origine di salinizzazione (vedi capitolo 4.3). La salinizzazione della falda dovuta al richiamo verso l'alto di acque ipersaline relitte ed il conseguente deterioramento della qualità anche delle acque superficiali, sono stati simulati tramite l'implementazione e la calibrazione di un modello di flusso tridimensionale (MODFLOW-2000) accoppiato ad un modello di trasporto non reattivo a densità variabile (SEAWAT).

Le simulazioni hanno chiaramente indicato che il principale driver del processo di salinizzazione è l'interazioni tra la falda freatica costiera e la rete di canali che richiamano verso l'alto le acque salate relitte. Questo processo, che è il risultato di un drenaggio avvenuto per secoli e che continua ancora oggi, influisce sulla qualità delle acque superficiali mettendo a rischio il loro futuro utilizzo a scopo agricolo e sottoponendo ad una crescente pressione gli ecosistemi costieri.

Per comprendere meglio l'evoluzione di tale fenomeno in un prossimo futuro, quando anche gli effetti dei cambiamenti climatici contribuiranno ad alterare i labili equilibri che governano gli scambi idrici tra acque sotterranee ed acque superficiali nella bassa pianura ferrarese, è stato implementato un modello numerico bidimensionale che tenesse conto di: (i) aumento dell'evapotraspirazione indotto dall'aumento della temperatura; (ii) aumento della frequenza di eventi di pioggia estremi; (iii) comparsa di condizioni di estrema siccità; (iv) e aumento del livello medio marino.

I risultati mostrano che in primavera e estate i canali di irrigazione ricaricano la falda diminuendo la falda salinità superficiale, anche nel caso di un aumento della temperatura (e quindi dell'evapotraspirazione). Al contrario, durante la stagione fredda i canali non sono più utilizzati per l'irrigazione e, rimanendo vuoti, portando ad una inversione di flusso che provoca un aumento della salinità nella falda superficiale dovuta al movimento verso l'alto dell'acqua ipersalina contenuta nei sedimenti di prodelta. Questo flusso verso l'alto salinizza lentamente i corpi d'acqua superficiali connessi con la falda acquifera tanto più quanto più è elevata la differenza di carico idraulico tra i due corpi idrici. Ne deriva che il previsto aumento de livello del mare influirà negativamente sui processi di salinizzazione, molto più di quanto non facciano l'aumento della temperatura o degli eventi di precipitazione estremi.

L'influenza della salinizzazione sui trend di concentrazione dell'ammonio e degli elementi nell'acquifero costiero

Dato che i cambiamenti climatici possono aumentare il tasso di salinizzazione della falda, per valutare se il cambiamento nelle attuali condizioni chimico-fisiche e idrodinamiche può anche indurre la mobilizzazione di elementi geogenici, sono stati studiati il contributo dell'interazione acqua/sedimento e l'influenza antropica sulla qualità delle acque sotterranee,

focalizzando l'attenzione sull'azoto (vedi capitolo 4.4) e sugli elementi in traccia (vedi capitolo 4.5).

Per capire se i processi di salinizzazione possono svolgere un ruolo nella mobilitazione delle specie azotate, è stata condotta una caratterizzazione dettagliata riguardante la distribuzione spaziale e le possibili fonti di nitrati (NO_3^-) e ammonio (NH_4^+) nell'acquifero costiero ferrarese. L' NH_4^+ è la specie di azoto inorganico prevalente nelle acque sotterranee. Mentre NO_3^- è presente nella porzione superiore dell'acquifero dove esistono condizioni ossidanti, la concentrazione di NH_4^+ aumenta con la profondità e la salinità. Concentrazioni molto elevate di NH_4^+ si trovano in coincidenza con sedimenti torbosi presenti alla base dell'acquifero dove sussistono condizioni anossiche e nell'aquitard sottostante. I risultati di questo studio mostrano che l' NH_4^+ deriva principalmente dalla mineralizzazione della sostanza organica presente nei sedimenti fini depositati in ambienti paleo-palustri.

L'effetto dell'elevata salinità sulla mobilità degli elementi in traccia (TE), è stato studiato mediante l'analisi sia di campioni di falda sia di carote di sedimento, a varie profondità. La concentrazione totale di TE è maggiore nei sedimenti fini, ed in particolare nella frazione argillosa, mentre le concentrazioni di TE in falda aumentano con la forza ionica della soluzione e cioè con la profondità dal momento che la parte basale dell'acquifero presenta acque a maggior tenore di salinità. L'elevato contenuto di materia organica impone condizioni riducenti lungo tutto il profilo falda, cosa che promuove ulteriormente la mobilizzazione di TE. Le uniche eccezioni sono V e As, probabilmente rilasciati dalla lisciviazione dei fertilizzanti nella parte superiore della falda e da strati torbosi sepolti nella parte inferiore della falda acquifera. Pertanto, i risultati di questo studio mettono in evidenza la necessità di distinguere tra il rilascio di TE a causa dell'alterazione dell'equilibrio acqua/ suolo indotta dalla salinizzazione delle acque sotterranee ed il rilascio di TE in falda a causa di attività antropiche.

Implicazioni e prospettive

Il presente studio ha impiegato diverse discipline delle Scienze della Terra per indagare i fenomeni di salinizzazione dell'acquifero costiero ferrarese. Nessuna delle metodologie impiegate sarebbe stata in grado di garantire la completa comprensione del sistema idrogeologico in esame se applicata separatamente.

Discriminare tra processi di salinizzazione passati e attuali è spesso difficile, se non impossibile, soprattutto quando sono disponibili solamente i dati di salinità. La presenza di acque ipersaline nella falda acquifera costiera ferrarese dimostra che l'attuale situazione idrogeologica testimonia la presenza di acque relitte originatesi in un ambiente totalmente diverso da quello odierno. Ne deriva che l'interpretazione delle osservazioni attuali deve tener conto che la qualità dell'acqua continua ad evolversi dal passato, adattandosi alle condizioni al contorno contemporanee. La conoscenza della storia geologica della zona oggetto di indagine è quindi essenziale per riconoscere il potenziale contributo di processi idrologici passati alla situazione attuale.

Inoltre, la scelta di un metodo di monitoraggio e campionamento affidabile è risultata di vitale importanza per la corretta identificazione delle proprietà fisiche dell'acquifero e della distribuzione della qualità delle acque sotterranee. Contare su appropriate tecniche di monitoraggio, come ad esempio il campionamento multilivello, è quindi importante tanto quanto selezione le giuste tecniche di analisi e di modellazione. Il campionamento multilivello non richiede competenze altamente specializzate o attrezzature particolarmente costose, tuttavia ancora oggi fatica ad imporsi negli studi sui processi di salinizzazione.

Questo studio, dimostrando in modo tangibile, come gravemente fuorviante potrebbe essere un modello concettuale più semplice, costruito sulla base di tecniche di monitoraggio inaffidabili, vuole essere un monito per i gestori delle risorse idriche che devono fare scelte difficili per la pianificazione della futura gestione e protezione delle acque sotterranee.

Infine, anche se i dati di campo sono indispensabili per comprendere il sistema idrogeologico in esame, i modelli numerici possono fornire un valido aiuto per testare le ipotesi del modello concettuale. Con il giusto approccio, l'uso congiunto di attività di campo e simulazioni può portare ad una migliore comprensione dei fenomeni ed a nuove intuizioni. Ad esempio, gli scenari numerici permettono di quantificare i possibili effetti dei cambiamenti climatici sulla salinizzazione delle acque sotterranee e le sue conseguenze sulla qualità delle risorse idriche, e potrebbero essere utili per trovare strategie di mitigazione per il futuro.

1. INTRODUCTION

1.1 Background and motivation

In coastal areas groundwater has gained increasing attention as a source of water supply, owing to its relatively low vulnerability to pollution in comparison to surface water as well as its relatively large storage capacity (Dillon, 2005). However, in the absence of sustainable water resource management schemes, uncontrolled land-use activities and over-exploitations can lead to significant and long-lasting deteriorations of water resources and groundwater-dependent ecosystems (Candela et al., 2009; Grassi et al., 2007; Park et al., 2005). For these reasons, in the last decades the research on coastal aquifers has intensified especially with regards to salinization processes (Barlow and Reichard, 2010; Custodio, 2010; Post and Abarca, 2010; Werner et al., 2013). In these areas the saltwater intrusion is a well-known and studied problem, like the Polders in the Netherlands (Oude Essink et al., 2010) or in the south-eastern Florida (Langevin and Zygnerski, 2013) and the Po river lowland (Giambastiani et al., 2007).

The recognition of groundwater salinization origin in coastal aquifers is not straightforward. Salinization into coastal aquifers may occur from both natural and anthropogenic sources and in many cases salinity problems arise from more than one salt source (Cartwright et al., 2004; Fakir et al., 2002; Lenahan and Bristow, 2010; Sanchez Martos et al., 2002). In some coastal area, the issue of saline groundwater origins involves, beyond actual seawater, relic seawater and hyper-saline waters (Fass et al., 2007; Ridd and Stieglitz, 2002; Wood et al., 2003). In these cases, it is vital to distinguish between modern and ancient saltwater intrusion to build a robust conceptual model of groundwater salinization through which a sustainable management program can be designed (Werner and Gallagher, 2006). The most relevant salt sources/processes recognized worldwide are: evaporation, evaporite leaching, mobilization of salts stored in the unsaturated zone, infiltration of non-marine polluted surface waters, slow-moving saline/salt waters of marine origin, highly mineralised waters from geothermal fields (Fidelibus et al., 2011), sea spray, hyper-filtration, agricultural practices (return flow, use of fertilizers and irrigation with treated wastewater), cycling wetting and drying. Whatever the salt source, its identification is often puzzled by soil-water interactions amplified by the increased water ionic strength (de Montety et al., 2008) or by mixing processes enhanced by human activities as over-exploitation, land reclamation and construction of navigation channels along rivers or artificial canals (Barlow and Reichard, 2010; Custodio, 2010; Kass et al., 2005; Yamanaka and Kumagai, 2006).

A key issue to understand salinization processes is the correct characterization of vertical variability of aquifer properties governing groundwater quality (de Louw et al., 2010; 2011; Netzer et al., 2011). A variability in vertical chemical composition of groundwater has been described both among different hydrological units of the same aquifer (Nativ and Weisbrod, 1994) and over small sections of a given hydrological unit (Dhar et al., 2008). Coastal aquifers often consist of layered sequences with varying hydraulic properties (Bear et al., 1999) that

can complicate monitoring of fresh–saltwater interface because of heterogeneity of the aquifer matrix (Kim et al., 2008). Therefore, coastal monitoring wells may act as vertical short circuits between layers (Werner et al., 2013), inducing local vertical flow due to connection between higher and lower hydraulic head zones (Elci et al., 2003). A common consequence is that ambient flow within long-screen wells may cause solute transport (Konikow and Hornberger, 2006), even in homogeneous aquifers with small vertical hydraulic gradients (Britt, 2005) and it may also compromise hydraulic head measurements (Shalev et al., 2009). Open borehole logging (OBL) is often employed to identify fresh-saltwater interfaces in coastal aquifers (Kim et al., 2008) and to characterize the redox zones within contaminant plumes (Jorstad et al., 2004). Even if this method of obtaining depth dependent groundwater quality data is plain, inexpensive and fast, the OBL technique has some limitations, most notably in coastal zones where measured values (salinity or any other water property) may be well representative of the stratified water column accumulated within the monitoring well, but not necessarily of the surrounding porous media (Balugani and Antonellini, 2010; Kurtzman et al., 2011; Shalev et al., 2009). Similarly, Integrated Depth Sampling (IDS) provides water samples representing an undefined integration of groundwater quality over the entire screen length (Robbins and Hayden-Martin, 1991): thus, it is largely deficient for the purposes of understanding salinization processes, since in coastal aquifer groundwater stratification is the rule rather than the exception.

On the contrary, Multi-Level Sampling (MLS) is an invaluable method that, by sampling at multiple intervals of an aquifer, allows the reconstruction of three-dimensional distribution of groundwater quality within a coastal aquifer system (Mastrocicco et al., 2012c). MLS is routinely applied in contaminated sites to map contaminant spreading and to quantify biogeochemical reaction pathways (Colombani et al., 2009; Henderson et al., 2009; Mastrocicco et al., 2011b; Prommer et al., 2006), but it is less frequently used in monitoring salinization in coastal areas because of high costs and time involved (Einarson and Cherry, 2002). The costs, however, cannot obscure the need for a dedicated depth-dependent groundwater monitoring, which is necessary to properly estimate the chemical composition of groundwater in coastal areas and to enhance the predictability of regional scale management models that will inevitably be required in the near future.

Depth-dependent aquifer characterization is essential to indentify vertical flow, which, beside salinizing the whole aquifer body, could enhance the mobility of geogenic and anthropogenic contaminants dissolved in groundwater, posing risk to surface water (Li et al., 2014) and to crop root uptake (Li et al., 2010). For instance, high-nitrogen loading in surface and ground waters is getting an increasing attention in order to fulfil the water quality objectives required by the Water Framework Directive (Directive 2000/60/EC, 2000). Nitrogen (N) enrichment is believed to be responsible for health hazards (Gelberg et al., 1999; Gulis et al., 2002) and deterioration of water quality, such as eutrophication (Jayasingha et al., 2011) and algal growth (Linderfelt and Turner, 2001). Increasing N content in surface and ground waters has been commonly explained evoking anthropogenic sources such as agricultural and industrial activities and sewage wastes (Rodvang and Simpkins, 2001).

Many studies have focused on NO_3^- groundwater contamination in agricultural areas (Bohlke et al., 2002; Mastrocicco et al., 2011a; Puckett et al., 2002) or in presence of anthropogenic sources (Aravena and Robertson, 1998); other studies have reported ammonium (NH_4^+) contamination in groundwater due to rich wastewater spillage or landfill leachate plumes (Brun et al., 2002; Christensen et al., 2001). Less attention has been given to natural sources of N in ground waters. Thus, identification of potential sources of N and assessment of its speciation in aquifer is still needed. Elevated NH_4^+ contents of natural origin have been reported in aquifers in different parts of the world: U.S. (Glessner and Roy, 2009; Hinkle et al., 2007), Mexico (Ortega-Guerrero, 2003), Asia (Jang and Liu, 2005; Jiao et al., 2010), Australia (Linderfelt and Turner, 2001) and Europe (Lorite-Herrera et al., 2009). Potential natural sources of NH_4^+ are mostly related to contribution of water/sediment interaction, such as mineralization of sedimentary organic matter rich in organic N (Lorite-Herrera et al., 2009), and release of NH_4^+ from sediments, governed by cation exchange capacity under anoxic conditions (Appelo and Postma, 2005; Lewandowski and Nützmann, 2010), especially in association with saline groundwater (Seitzinger et al., 1991).

Another topic where the vertical discretization is unavoidable is the study of trace element (TE) distribution of in groundwater with variable salinity and their associated sediments. TE can derive from anthropogenic sources like agricultural, industrial and mining activities (Buggy and Tobin, 2008; Du Laing et al., 2009), but they can also be related to weathering of host formations, or by cation or anion exchange reactions promoted by intrusion of saline waters (Teuchies et al., 2013). Geogenic metal contamination is of upcoming concern, especially in coastal areas where the ionic strength of groundwater can be very high, thus promoting substantial mobilization of TE (Acosta et al., 2011; Wang et al., 2012). In fact, many authors pointed out a potential significant threat related to the elevated trace and rare metals concentrations found in floodplain saline soils (Cidu et al., 2013; DeLaune et al., 2008; Devai et al., 2005; Du Laing et al., 2008). A peculiar case are the low lying areas, which represent a possibly extended problem throughout the world in the midterm future, with the forecasted sea level rise induced by climate changes (Werner et al., 2013). In these environments, the land reclamation usually induces upconing of the basal saline and hyperhaline groundwater (de Louw et al., 2013a; Giambastiani et al., 2013; Mollema et al., 2013). Thus, the ubiquitous presence of metals obliges to accurately prepare risk assessment studies especially in floodplains used for agriculture (Hinsby et al., 2008; Vandecasteele et al., 2006).

With the recent refinement of climate change projections, namely sea level rise (SLR) and changes in recharge and evapotranspiration patterns, the number of studies investigating the effects of raised pressures on coastal groundwater systems has increased (Ranjan et al., 2006; Werner et al., 2013). The IPCC 2014 reports (2014a; 2014b) predicted that climate change will have a range of impacts on water resources: annual runoff will decrease in southern Europe by 0 to 23% in 2020s and by 6 to 36% in 2070s; summer low flow may decrease down to 80% in some rivers in southern Europe; storage changes in soil moisture and recharge of groundwater will be largely reduced in valleys and lowlands; increasing drought risk in the Mediterranean might be amplified by water withdrawal leading to a strong competition for available water resources and for reduction of available drinking water (García-Ruiz et al.,

2011). These problems may especially affect coastal areas where large socio-economic and environmental stresses are already observed. Several studies attempted to quantify the effect of SLR on salt water intrusion into a coastal aquifer. Werner and Simmons (2009) identified the major hydrogeologic controls on the impact of SLR on salt water intrusion in unconfined coastal aquifers by using a steady-state analysis with an analytical solution. They differentiated between flux-controlled and head-controlled systems and showed that SLR is more problematic for head-controlled systems because inland water levels do not rise with rising sea level. Chang et al. (2011) also found that for flux-controlled confined aquifers SLR may not have an impact on fresh water volumes. Watson et al. (2010) investigated the migration aspect and response time of salt water movement, concluding that in certain condition several centuries may be required for the salt water interface to reach equilibrium after SLR. Other studies focused on the effect of SLR on specific coastal settings. Just considering Europe, vulnerability of low-lying coastal areas to SLR has been addressed by Lebbe et al. (2008) and by Vandenbohede et al. (2008) for the Belgian coastal plain, by Oude Essink et al. (2010) for the Netherlands, by Feseker (2007) for North-western Germany, by Fujinawa et al. (2009) for the eastern Mediterranean coastal region of Turkey, by Giambastiani et al. (2007) and by Colombani et al. (2015a) for the unconfined coastal aquifers of Ravenna and Ferrara, Italy. Most of these studies point out that coastal aquifer salinization often directly endanger surface water resources. Recent studies have looked at quantitative interactions between surface and ground waters near the coast at large scales (Oude Essink et al., 2010; Vandenbohede et al., 2008), but less has been done to clarify the small scale interactions between groundwater and irrigation canals and drainage ditches. Only recently a few detailed case studies have been published, in which the actual flow and salt transport processes occurring in drained agricultural lowlands are quantified and modelled (de Louw et al., 2010; 2011; 2013).

Once a reliable conceptual model of the stresses acting on a territory has been built, a valuable approach to understand salinization mechanisms (both from seawater intrusion and saline seepage), their effect on the mobilization of geogenic contaminants, and the impacts that different climate change scenarios will have on these phenomena, is the implementation of predictive density-dependent groundwater flow and transport numerical models, like SEAWAT (Guo and Langevin, 2002; Langevin et al., 2007) and MODFLOW-2000 (Hill et al., 2000); such models are based on the commonly used groundwater code, MODFLOW, developed by the U.S. Geological Survey (Harbaugh et al., 2005; McDonald and Harbaugh, 1988). By means of such a comprehensive tool, based on field hydrodynamic and hydrogeochemical evidences, water managers will be enabled to better manage the surface/groundwater continuum, and to put in place prevention and/or mitigation measures to avoid water resources deterioration.

1.2 Significance of the selected test site

The areas mostly prone to groundwater deterioration are the densely populated coastal plains, which more than other areas are exposed to anthropic perturbation and aftermath of climatic change. Among the issues that these areas have to face, the salinization of both surface and groundwater resources seem to be the more worrisome, especially in lowlands intensively farmed.

For this reason, the unconfined coastal aquifer of the Ferrara Province (Northern Italy), located in the Po River Delta lowland was selected to examine the extent of groundwater salinization, the mechanisms governing the salinization process, the response of the salinization rate to the expected impacts of climate change and the role of salinization on the mobilization of geogenic contaminants.

This territory has been widely studied in the last decades, and a large number of contributes from different disciplines allows achieving a robust knowledge of the geological and geomorphological evolution of the coastal aquifer of the Ferrara Province.

However, being the groundwater beneath the Po River Delta poorly exploited due to the abundant surface water resources, studies on the local aquifers are limited; thus, groundwater resources still need to be properly characterized and known in order to better manage the surface/groundwater continuum. To improve the understanding of the hydrological and hydrochemical aspects of the Ferrara coastal aquifer, since 2009 the Geological Survey of the Emilia Romagna Region developed a specific network of 30 monitoring wells as a mean of characterizing the saltwater intrusion along the Northern Adriatic coastal aquifer; 11 of these monitoring wells, falling within the coastal area of the Ferrara Province, together with 38 pre-existing monitoring wells, have been used to carry out the field activities required to improve the conceptual model of the study area.

Apart from the good level of detail with which this area has been investigated, other factors make it ideal for achieving the objective of the thesis: (i) the Ferrara coastal area is intensively farmed (Fig. 1.1) since its reclamation (late 1900), (ii) nowadays the drainage system is necessary to lower the water table because of the agricultural requirements, (iii) the stiffening of the hydrographic network due to reclamation activities has augmented land subsidence, (iv) the increasing difference in the elevation of the ground level and the sea level enhances seawater encroachment along the rivers, (v) the occurrence of present seawater intrusion and saline relict groundwater in the deepest part of the coastal aquifer has induced groundwater and soil salinization harming the agricultural productivity, (vi) the decrease in the availability of freshwater resources, especially in the summer period, poses a risk in the development of the tourist activities. All these factors make the area of the Ferrara Province ideal for conducting the study for the thesis.

The analysis of the results will help local authorities to properly manage coastal fresh water resources under increasing pressures, and eventually to identify reasonable countermeasures to decrease the salt load for the future. This thesis, however, only deals with the physical aspects of the territory and does not take into account the economic aspects, which are as

important as the physical ones in the identification and implementation of sustainable adaptation initiatives. Nevertheless, the characterization protocol employed in this study could be successfully applied in many other similar coastal low lying areas worldwide, suffering from the same issues that are stressing the Ferrara coastal aquifer.



Figure 1.1 – Wheat fields in the Ferrara lowland (www.estense.com)

1.3 Objectives of the thesis

Because of the potentially irreversible impact of groundwater quality deterioration in the Ferrara coastal aquifer, answers concerning the assessment of the extent of the salinization problem, the understanding of the mechanisms governing salinization processes, and the sustainability of the current water resources management are urgent.

In this light, the present thesis aims to achieve the following objectives:

Characterization of the lowland coastal aquifer of Ferrara: hydrology, hydrochemistry and evolution of the system

The actual hydrogeochemistry and the geological evolution of the unconfined coastal aquifer of Ferrara have been addressed in order to understand the drivers of groundwater salinization. Physical aquifer parameterization was performed to infer the presence of a vertical hydraulic gradient due to the drainage system. Seepage of relict seawater, trapped within low permeability sediments during the Holocene transgression, was found to be responsible for groundwater salinization. The hydrogeochemical investigation allows also distinguishing between the role of seepage and water-sediment interactions (such as NaCl solution, ion-exchange, calcite and dolomite dissolution/precipitation, oxidation of organic matter, and sulphate bacterial reduction) in the evolution of groundwater chemistry.

The importance of data acquisition techniques in saltwater intrusion monitoring

A detailed vertical characterization of the Ferrara coastal aquifer is unavoidable to properly monitor salinity distribution. Physical-chemical depth-dependent logs were obtained by different techniques: Open-Borehole Logging (OBL), Integrated-Depth Sampling (IDS), and Multi-Level Sampling (MLS) via straddle packers. The OBL led to a satisfactory reconstruction of the extent of the fresh-saltwater interface, but provided a misleading characterization of the distribution of redox environments within the aquifer. The IDS conceptual model recalls the phenomenon of actual seawater intrusion, with Cl⁻ concentration never exceeding that of seawater and the absence of hypersaline groundwater all over the study area. On the contrary, good fits between sedimentological, stratigraphical and physical-chemical data were obtained using the MLS. In the MLS-derived conceptual model the lower portion of the unconfined aquifer shows hypersaline groundwater, leading to necessarily consider salinization processes other than seawater intrusion, like the water/sediment interaction or the geochemical evolution of groundwater due to evapo-concentration. Results demonstrate the need to use MLS in reconstructing a reliable conceptual model, especially in areas where the density contrast between fresh and saline groundwater is large.

Predicting salinization trends in the lowland coastal aquifer

A conceptual model based on detailed topography and bathymetry, stratigraphical information from analysis of well logs, well driller's reports and pumping tests was developed to quantify the possible impacts of climate change on the whole coastal groundwater system in the Ferrara Province. On the basis of such a conceptual model, a three-dimensional variable-density groundwater flow model coupled with solute transport was developed; it was calibrated using highly parameterized inversion techniques with MODFLOW-2000 to ensure that the model is a reasonable representation of the physical

system. The calibrated model was employed to constrain a two-dimensional numerical simulation, using SEAWAT, capable of investigating the interactions between the coastal unconfined aquifer and the canals network, and to quantify the possible future effects of climate change on groundwater salinization with a multiple scenario approach: (i) increase in evapotranspiration induced by temperature increase; (ii) increase in the frequency of extreme high rainfall events; (iii) extreme drought conditions; (iv) and canal dewatering due to salinization of the water courses. The results show that the Ferrara coastal area will experience a significant salinization and that the major cause is autonomous salinization via seepage of saline groundwater.

Ammonium occurrence in a salinized lowland coastal aquifer

Impacts induced by climate change may consist in the modification of water/sediment interaction. A detailed characterization concerning the spatial distribution and the possible sources of nitrate and ammonium concentrations in the Ferrara coastal aquifer was completed to understand if salinization processes may play a role in the mobilization of nitrogen species. Ammonium is the prevalent nitrogen inorganic species in groundwater, and its concentration increases with depth and salinity. Very high ammonium concentrations are found in coincidence with peaty sediments in the salinized anoxic aquifer and in the low-lying aquitard. The results from this study show that the elevated ammonium concentration derives from the mineralization of organic matter present in fine sediments deposited in paleo-marsh environments.

Trace elements mobility in a saline coastal aquifer

The effect of elevated salinity on the mobility of trace elements (TE) was studied. The use of intensive depth profiles gave insights into groundwater and sediment matrix interactions. The total concentration of TE within the aquifer matrix was higher in the fine sediments, since usually TE concentrate in the clay fraction, while groundwater concentrations generally increased with the ionic strength of the solution. Still, some TE did not follow this trend, being probably released by fertilizers leaching. Thus, the results from this study highlight the need to distinguish between the release of TE due to alteration of water/soil interaction equilibrium induced by groundwater salinization and the release of TE in groundwater due to anthropogenic activities.

2. SITE DESCRIPTION

2.1 Study area

The study area is situated within the Province of Ferrara (Northern Italy) and covers 700 km². This coastal floodplain is bounded to the North by one of the Po River branches, the Po di Goro, and to the South by the brackish water marshes of the Comacchio Lagoons (Fig. 2.1). Most of the territory is a recently reclaimed land with flat topography below sea level, and with an altitude ranging from 12 to -11 m above sea level (a.s.l.); the only topographic heights consist of dune systems, paleodunes and river banks.

The climate is temperate, characterized by cold winters and warm summers with modest diurnal (10-12 °C) and annual temperature ranges (20-25 °C). Rainfall is on average 670 mm/year, evenly distributed throughout the year. Aquifer recharge from precipitation surplus is minimal due to a reference evapotranspiration rate of about 650 mm/year: it occurs mainly during winter months (Mollema et al., 2012).

The area is intensively farmed since its reclamation (late 1900), and the primary land use is horticultural crops (generally carrots, asparagus, strawberries, melons, watermelons, etc.). Tourist activities are also developed along the coast, especially during summer periods (June-September).

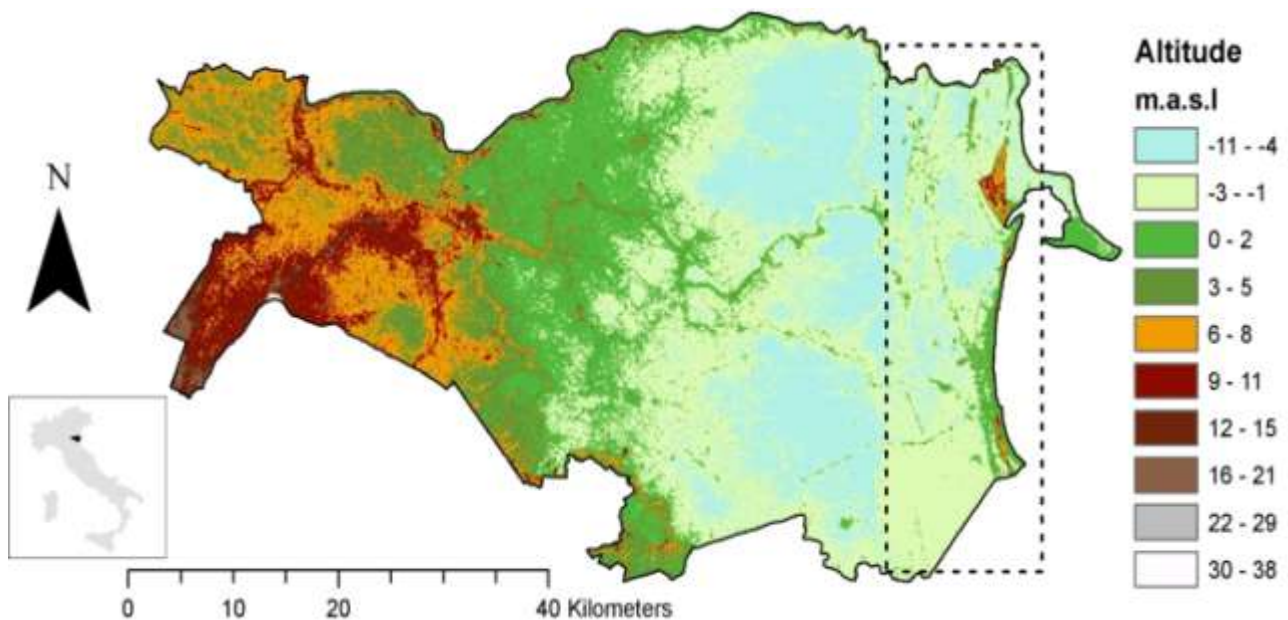


Figure 2.1 - Ferrara Province topography map and location of the coastal lowland study area (dashed rectangle).

Several natural and anthropogenic features threaten this area: saltwater intrusion in the phreatic aquifer and seawater encroachment along the rivers (Giambastiani et al., 2007); natural (Carminati et al., 2005) and anthropogenic land subsidence (Teatini et al., 2006); soil salinization; high demand of water during the peak tourist season; insufficient aquifer recharge and sea level rise (Antonellini et al., 2008).

2.2 Morphological evolution during the last glacial period

The Quaternary evolution of the Po Delta plain is controlled by eustatic and climatic fluctuations (Stefani and Vincenzi, 2005). The stratigraphic architecture shows consistent patterns with changing sea level position recording the depositional evolution from lowstand continental accumulation to marine transgression and highstand progradation.

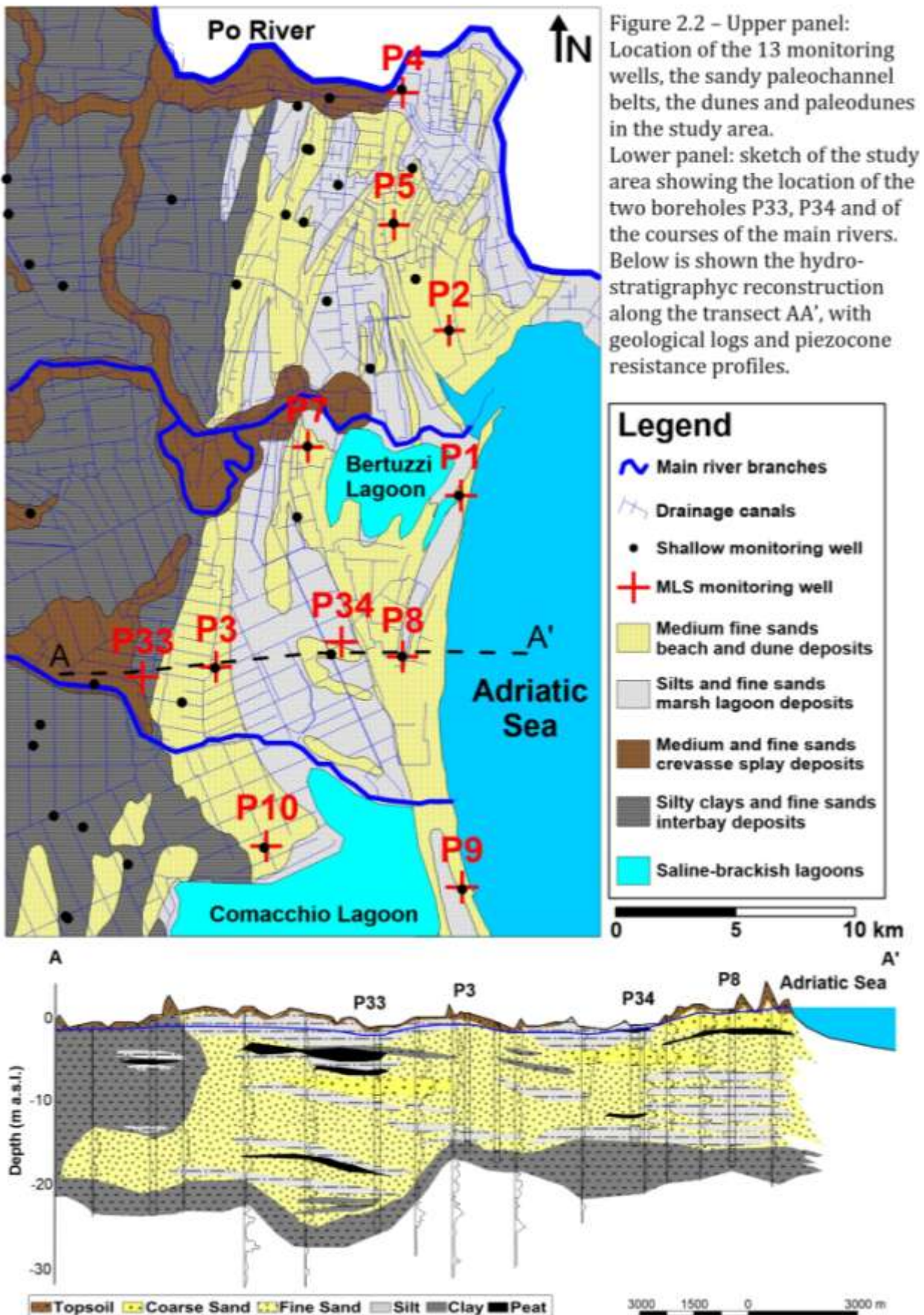
The last glacial lowstand, when the sea level dropped 120 m below the present level and the paleoshoreline shifted 250 km South-East of its current position, resulted in extensive and repeated basinward shifts of facies, which can be observed across closely spaced unconformity surfaces associated to alluvial plain sedimentation in the modern coastal area of Ferrara (Amorosi et al., 2003).

During the Flandrian transgressive phase (18000-5500 yr BP), these deposits were followed by a retrogradational stacking pattern of coastal plain and littoral facies, reflecting the landward migration of a barrier-lagoon-estuary system. Back-stepping fluvial and brackish marsh deposits with widespread organic clay intercalations and peat horizons are followed by delta-estuarine sand bodies.

At the maximum transgression (6000-5500 yr BP) the paleoshoreline was located 20-30 km west of its present position (Amorosi et al., 2003). During the early highstand period, large sand spits and barrier islands grew, progressively turning the previous bays into confined lagoons (Amorosi et al., 2004). Afterwards, the depositional dynamics were significantly modified by both climatic change (warmer conditions starting from 2800-2700 yr BP) and anthropic events (infrastructures, reclamation works and fluvial diversions) causing coastal progradation and a consequent regressive upward succession of the deposits (Fig. 2.2).

Coastline migration and different phases in the Po Delta progradation resulted in a series of coastal sand ridges (paleodunes) and paleo marsh lagoons, corresponding to the alternation of current topographic highs and lows (Simeoni and Corbau, 2009).

SITE DESCRIPTION



2.3 Recent anthropogenic activity

Since the Middle Ages, the need to acquire new areas to be allocated to agricultural activities led to a succession of remediation works (Fig. 2.3), intensified from 1850s to 1960s.

The resulting surface water system is very complex, since it is constituted by numerous natural and non-natural water bodies (Fig. 2.2): the course of the Po River, its tributaries and an extended hydrological network consisting of WE oriented channels used for irrigation. These last derive water by gravity directly from the Po River and drainage ditches connected to pumping stations that maintain this lowland dry, lastly discharging water to the sea (Antonellini et al., 2008). This induced the stiffening of the hydrographic geometry and consequently increased the natural subsidence rate (Teatini et al., 2005), which has dropped most of the territory below sea level, modifying river and groundwater flow regimes.

Nowadays, the drainage system is necessary to maintain the surface water level at about -0.5 m a.s.l. because of the agricultural requirements and to guarantee water discharge toward the sea to keep this lowland dry (Fig. 2.4).



Figure 2.3 – Waterworks in the Ferrara Province at the beginning of the XX century (www.bonificaferrara.it).



Figure 2.4 - “Valle Lepri” dewatering station in the Ferrara Province lowland (www.bonificaferrara.it).

2.4 Hydrogeological setting

The complex depositional evolution of the Po Delta system has led to complex aquifer geometry. The sedimentary sequence is characterized by transgressive bay and barrier deposits at the base, and prograding sandy deltaic lobes and strand plains at the top. From East to West, the majority of the sedimentary units consists of a wedge of permeable sand sediments deposited in shallow sea with intercalation of peat and silty layers, littoral sands formed in the foreshore and in the adjacent beach, and sand dune systems (Simeoni and Corbau, 2009).

The coastal aquifer in the study area is generally unconfined; in the westernmost area thin layers of fine continental alluvial deposits (mostly silt and clay) overlay littoral sands (Amorosi et al., 2002) making the aquifer semi-confined. The unconfined coastal aquifer is mainly located within the littoral sands and shallow marine wedge deposits. Fine-grained deposits of silt and clay at the bottom of sand deposits constitute a 10 m thick confining unit. The aquifer thickness decreases inland and ranges between 2 and 24 m, while the thickness is 15-20 m.

The aquifer hydraulic conductivity is variable, depending on the sorting of aquifer materials and ranges from 1×10^{-6} m/s in depressed areas to 1×10^{-3} m/s in the coastal dunes (Mastrocicco et al., 2012c).

SITE DESCRIPTION

The horizontal hydraulic gradient of the shallow unconfined aquifer (0.1-0.5 ‰) is mainly controlled by canals and drains system; the horizontal flow velocity is generally very low, about 7-10 m/y (Mastrocicco et al., 2013b). On the contrary, quite high vertical hydraulic gradients have been measured in this aquifer due to the hydraulic head difference between groundwater and surface waters (about 1 m) that causes a permanent upward groundwater seepage flux even if in the study area the unconfined aquifer is not stressed by pumping wells (Giambastiani et al., 2013).



Figure 2.5 - Excerpt of the coastal territory of the Duchy of Ferrara in the XVI century (www.ilmuseodimirabello.com)

SITE DESCRIPTION

The unconfined aquifer in the study area is affected by relict saline and hypersaline groundwater due to the presence of vast coastal lagoons originally connected to the sea (Fig. 2.5); these lagoons, keeping a high degree of salinity in pore-water, were reclaimed to acquire new land for agricultural practice. Even nowadays, the upconing of such highly saline groundwater (Giambastiani et al., 2013) could threaten the agricultural practices (Mastrocicco et al., 2012a). In fact, in this area, fresh groundwater lenses are created by infiltration of rainwater or canals leakage in permeable sandy sediments. The freshwater thickness allows plant growth, thus strongly influencing both agriculture (Mastrocicco et al., 2013a) and natural vegetation (Antonellini and Mollema, 2010). Given this active exchange between groundwater and the surface water network (Colombani et al., 2015a), the need to drain the agricultural land to keep it dry may concurrently induce salinization of surface water due to saline groundwater upconing. Fortunately, the upconing is often hindered by the vertical superimposition of low permeability lenses on permeable layers (Fig. 2.2).

3. MATERIALS AND METHODS

3.1 Field activities

This section describes the methodology used to characterize the unconfined aquifer of the Ferrara province, in particular the methodology developed via straddle low pressure packers to simultaneously characterize vertical hydraulic gradients, hydraulic conductivity, and groundwater quality with the aim of identifying the aquifer dynamics.

3.1.1 Monitoring wells installation

Since 2009, the Geological Survey of the Emilia-Romagna Region (Northern Italy) has developed a regional monitoring network to monitor saltwater intrusion in the coastal aquifer facing the Adriatic Sea. A distributed network of 59 monitoring wells (Fig. 2.2) was installed to monitor water table fluctuations and groundwater quality of the shallow unconfined aquifer. 46 standard PVC monitoring wells (2.5 cm inner diameter) were drilled manually with a Ejielkamp Agrisearch auger equipment up to depths between 1.1 and 6 m below ground level (b.g.l.), depending on the water table depth. Monitoring wells' location was selected on the base of the soil characteristic in order to sample the different soil types of the Ferrara Province. These monitoring wells are located in agricultural fields, in which crop type, preceding crop, irrigation amount, type and amount of applied fertilizers are well known (Mastrocicco et al., 2011c). In addition to the shallow monitoring network, 13 deeper boreholes (5 cm inner diameter) were drilled to get insight of groundwater salinization and inorganic N concentration in the unconfined aquifer. These wells were screened from 1 m below ground level (b.g.l.) to a maximum of 22 m b.g.l. to fully penetrate the aquifer. To prevent cross contamination between sampling points and short-circuits during pumping tests, the screens were not surrounded by a siliceous gravel pack; a geotextile sock was instead used to minimize clogging. The monitoring wells were sealed at the top with a mixture of cement and bentonite to prevent surface-water infiltration. In particular, the monitoring wells P3, P8, P33, and P34 are located along a flow line and are aligned along fore-stepping direction of Holocene Po Delta system (Fig. 2.2). With respect to the geomorphologic features (map in Figure 2.2), P8 and P34 are located in an area of marsh lagoonal deposits characterized by silts and fine sands, P3 is found on a palaeo-dune characterized by medium to fine sand deposits, while P33 is placed on silty clays and silt-very fine sands, typical of bay deposits.

Core samples were also collected in P33 and P34 (Fig. 2.2) every meter or when a change in stratigraphy was recognized during drilling operations. Samples were stored in a cool box at 4 °C and immediately transported to the laboratory for sediment analysis.

3.1.2 Continuous monitoring of piezometric heads and surface waters levels

Groundwater levels were measured twice in the 46 shallow monitoring wells (Fig. 2.2), once in summer and once in winter, via a PASI phreatimeter. In the 13 deep monitoring wells, heads were measured every 4 months from 2009 to nowadays.

In order to define groundwater temporal variations due to surface water/groundwater interaction and due to tidal fluctuations, two data-loggers LTC M10 Levelogger Solinst® were inserted at -4.5 m and -8 m a.s.l. inside the monitoring well P8, using Teflon packer rings to insulate each aquifer portion, from July to December 2012. The data-loggers were set up for continuous barometric compensated level measurement and electrical conductivity (one record per hour).

To define the physical boundary conditions of the Ferrara coastal aquifer, surface waters were monitored over the whole period of the study.

The online data from Porto Garibaldi tide gauge (www.provincia.fe.it), positioned in proximity of the monitoring well P8, were used to compare groundwater fluctuations with tidal variations. The Valli di Comacchio and Valle Bertuzzi water level gauges (www.provincia.fe.it) provide stage data for the two major marsh lagoons of these territories. The average stages of the Lago delle Nazioni, Po River and irrigation canals were supplied by the Consorzio di Bonifica Pianura di Ferrara.

To understand in detail the interaction between the irrigation canals and the shallow aquifer, a datalogger LTC M10, programmed to record every 30 minutes, was inserted in the “Canale della Gronda” (Fig. 4.24) to monitor hydrometric level variation and EC from July to December 2012. The water level and EC variations in the drain ditch and in the canal were also monitored every two weeks with a hand meter and a Hanna® HIcell-21 portable conductivity meter.

3.1.3 Depth profiles acquisition

Three different methodologies were employed to reconstruct the distribution of the dissolved species in groundwater over the whole profile of the unconfined aquifer: the Open Borehole Logging (OBL), the Integrated Depth Sampling (IDS) and the Multi-Level Sampling (MLS).

In order to obtain the OBL profiles, a Hydrolab MS-5 (OTT, Germany) water quality probe was lowered manually into the monitoring wells to simultaneously record temperature, electrical conductivity (EC), dissolved oxygen (DO), redox potential (Eh), pH and salinity. The Hydrolab MS-5 water quality probe consists of six sensors and a data transmitter mounted inside a 4.4 cm diameter housing, with a 30 m long underwater cable and an YSI interface (YSI, California) at the ground surface. Eh was corrected to the standard H⁺ electrode potential. After a 5 min wait, the six parameters were simultaneously acquired every 1 m depth. The hydrochemical logs were made under natural conditions, without purging the monitoring wells before the tests.

MATERIALS AND METHODS

For the IDS measurements a Proactive® electrical submersible pump with flow controller was placed in the middle of the screened interval for each monitoring wells and a minimum of four volumes were purged maintaining a flow rate of 0.1-0.5 l/min to minimize the piezometric lowering.

For the MLS measurements a Solinst® 800L straddle packers system was used to isolate a window of 0.2 m within the fully penetrating wells. After the selected port and the tubing were purged for 3 volumes (approximately 15 l), a groundwater sample was collected at each depth interval via a low-flow technique using an inertial pump.

The groundwater samples, both for the IDS and the MLS measurements, were collected after the stabilization of physical-chemical parameters monitored via a Hydrolab flow-through cell connected to the Hydrolab® MS-5 OTT Corr-Tech® probe able to acquire in situ T, pH, EC, Eh and DO. Groundwater samples for major ions were then filtered through 0.22 µm Dionex polypropylene filters, stored in vials with no head space, kept refrigerated in a cool box at 4 °C and immediately transported to the laboratory to be analyzed. Groundwater samples intended for TE analysis were filtered through 0.45 µm polypropylene filters and collected in acid-washed and deionized-water-rinsed HDPE or amber borosilicate glass bottles preserved with ultrapure acid. Teflon sealed glass vials with no headspace were used to sample for dissolved H₂S.

To compare data obtained by OBL and MLS techniques, the absolute residuals (the absolute value observed using MLS minus the absolute value observed using OBL at the same depth) and the linear regression coefficient (R^2) with respect to the line $Y_{OBL} = X_{MSL}$ was calculated for each parameter analyzed.



Figure 3.1 - Multilevel Sampler set up and installation

To infer the chemical boundary conditions of the Ferrara coastal aquifer, surface waters were also sampled: the Po di Gnocca near the monitoring well P4, Po di Volano near the monitoring well P1 and Canale Circondariale near the monitoring well P10, were sampled in four surveys from 2010 to 2014; the seawater samples were collected at the shoreline in seven surveys from 2010 to 2014 near the monitoring wells P1, P8 and P9.

Informations concerning the main surface bodies of this area (Valli di Comacchio, Valle Betuzzi and Lago delle Nazioni) were also available from the monitoring programs of ARPA and Ferrara Province.

Finally, the bulk (wet and dry) atmospheric deposition was sampled in four campaigns from 2010 to 2014 using a HDPE bottle and a 20 cm diameter funnel equipped with a 100 μm Nitex[®] net to avoid external contamination. Samplers were installed near the monitoring wells P1 and P8 at a height of 1.5 m above the ground.

3.1.4 Constant rate pumping tests

Constant rate pumping tests were carried out every meter in the 13 deep monitoring wells in order to define physical parameters of the aquifer and to quantify flux dynamic under drainage situation. Tests started at the bottom of the well and, after each test, the packer was lifted 1 m and the test was repeated until the entire well was tested.

To perform constant rate pumping tests, two inflatable Solinst[®] 800L straddle packers were used to isolate a window of 0.2 m within the fully penetrating monitoring wells. The original arrangement was modified by replacing the straddle pipe, within the sampling window, with a LTC M10 Levellogger Solinst[®] to monitor head, temperature (T) and electrical conductivity (EC) every 1 second. The accuracy of the Levellogger employed in this occasion is ± 0.01 m for a maximum pressure range of 10 m; below this depth the measurements are less reliable.

The system is set at the chosen depth within the monitoring well and the packers are inflated by a portable air compressor until they stick to the well screen. Before starting the pumping test, the inflated packers system is left to stand for at least 20 minutes (or longer in finer sediments) until the piezometric equilibrium is reached and the point head measurement is recorded. Afterwards a constant pumping rate test is performed using an in line submergible centrifuge pump able to deliver 20 l/min, and a flow controller to regulate the flow and to perform the constant rate pumping tests.

Hydraulic conductivity (k) values (m/s) were derived from the equation (Bureau of Reclamation, 2001):

$$k = \frac{Q}{C_s r \Delta h} \quad (1)$$

where Q is the steady flow in the well (m^3/s); C_s (-) is the conductivity coefficient for semi-spherical flow in saturated materials through partially penetrating cylindrical test wells and for these condition is equal to 28 based on graphs defined in Bureau of Reclamation study

(2001), r (m) is the radius of the test well, Δh (-) is the head hydraulic gradient between static head and steady state head under pumping condition.

Since the Levellogger LTC simultaneously acquires the piezometric drawdown induced by pumping and any variations in T and EC within the aquifer window isolated by the packers, the equivalent freshwater head (h_f) and vertical flow values (q_z) can be respectively derived using the equations (2) and (3) that take into account variable density and salinity values (Post et al., 2007):

$$h_f = \frac{\rho_i}{\rho_f} h_i - \frac{\rho_i - \rho_f}{\rho_f} z_i \quad (2)$$

where h_i (m) is the hydraulic head measured at point i , z_i (m) is the elevation head and indicates the depth of the well screen, ρ_i and ρ_f (kg/m^3) are respectively the density of the water in the sampling window and the density of freshwater; and

$$q_z = -K_{av} \left[\frac{\Delta h_f}{\Delta z} + \left(\frac{\rho_a - \rho_f}{\rho_f} \right) \right] \quad (3)$$

where K_{av} (m/s) is the average k_v calculated between two sampling windows ($i = 1$ and 2), ρ_a (kg/m^3) is the average density of the groundwater between the two sampling points, and $\Delta h_f = h_{f,2} - h_{f,1}$ (m) and $\Delta z = z_2 - z_1$ (m) are respectively the difference in freshwater head and elevation head of two consecutive measures.

Finally, the pore water velocity along each monitoring well was calculated following Darcy's law in the form of freshwater heads:

$$v = \frac{k_f \times \vec{i}}{n_e} \quad (4)$$

where v is the average pore water velocity (m/y), \vec{i} is the freshwater hydraulic head gradient (-), n_e is the effective porosity (-) and k_f is the fresh water hydraulic conductivity (m/y). By assuming that salinity variations have a negligible effect on the groundwater kinematic viscosity, viscosity k_f values can be considered similar to field-measured values of k (Post et al., 2007). In order to compute velocity values, k values were obtained by equation (1) while effective porosity values (n_e and n_{ev}) were calculated for each core sample by equation (3) using both the measured total porosity (n) and the calculated total porosity (n_v) by Vukovic and Soro (1992). For the shallow coastal aquifer, a regional \vec{i} influenced by the dewatering stations equal to 0.4‰ was applied.

3.2 Analytical methods

This section describes the laboratory procedures used to analyze water and sediments samples with the aim of identifying the spatial distribution of saline groundwater, major ions and selected contaminants in the Ferrara coastal aquifer.

3.2.1 Sedimentological characterization

Particle size curves were obtained using a sedimentation balance for the coarse fraction and an X-ray diffraction sedigraph 5100 Micromeritics for the finer fraction; the two regions of the particle size curve were connected using the computer code SEDIMCOL (Brambati et al., 1973).

The median of the average grain radius (expressed in φ), the 10th and 60th percentile of the cumulative curve (d_{10} and d_{60} expressed in φ) and the sorting were calculated to describe grain size distribution analysis. Grain size distribution was then used to calculate hydraulic conductivity by pedotransfer formulae (K_{ped}), such as Breyer and Shepherd formula (Vukovic and Soro, 1992), which are appropriate for materials with heterogeneous distributions and poorly sorted grains. Calculated K_{ped} were compared with the results of the constant rate pumping tests (see paragraph 3.1.4) carried out in the same monitoring wells to validate the methodology.

Organic matter content (SOM) of the sediments was measured by dry combustion (Tiessen and Moir, 1993), then converted to total organic carbon (TOC) using the conversion factor of 0.58 (Danielson and Sutherland, 1986). The water content was measured gravimetrically in saturated condition after heating for 24 hours at 105°C (Danielson and Sutherland, 1986).

Laboratory porosity measurements (n) on core samples are often affected by errors, as many sampling methods alter the structure, packing and compaction of the sediment sample (Vienken and Dietrich, 2011). Hence porosity values were also computed using the following empirical equation (Vukovic and Soro, 1992):

$$n_v = 0.225(1 + 0.83\eta) \tag{5}$$

where η stand for uniformity coefficient, defined as $d_{60}[\varphi]/d_{10}[\varphi]$.

The effective porosity (n_e) was estimated with the formula (Worthington, 1998):

$$n_e = n - CBW \tag{6}$$

where CBW is the clay-bounded water, which comprises electrochemically bound water from clay surfaces and interlayers. The CWB varies in volume according to the clay-type and the salinity of the formation water, and can be estimated from (Hill et al., 1979):

$$CBW = n \times (0.6425 \times \sqrt{S} + 0.22) \times CEC \quad (7)$$

where S is the salinity (g/l) and CEC is the Cation Exchange Capacity (meq/ml of pore space).

3.2.2 Chemical analysis of water samples

Major ions in groundwater were analyzed using an isocratic dual pump ion chromatography ICS-1000 Dionex, equipped with an AS9-HC 4 x 250 mm high capacity column and an ASRS-ULTRA 4mm self-suppressor for anions. An AS-40 Dionex auto-sampler was employed to run the analyses; Quality Control (QC) samples were run every 10 samples and the standard deviation for all QC samples run was better than 4%. The sum of the resulting anions and cations was referred to as Total Dissolved Solids (TDS).

The EC data from the field depth profiles were also converted to total dissolved solids (TDS) using a linear relationship obtained from Mastrocicco et al. (2012c), where 0.873 is found to be the local slope between groundwater EC (dS/m) and groundwater TDS (g/L). This slope differs from the typical value of 0.64 since the local groundwater ionic composition is quite complex (Giambastiani et al., 2013).

Trace elements (TE) in groundwater (B, Al, P, Fe, Sr, Sc, Ti, Mn, V, Cr, Co, Ni, Cu, Zn, Ga, As, Rb, Ba, Hg, Pb, U) were analysed using an X Series Thermo-Scientific spectrometer (ICP-MS). Specific amounts of Rh, In and Re were added to the analysed solutions as internal standards, in order to correct for instrumental drift. Accuracy and precision, based on replicated analyses of samples and standards, are better than 10% for all elements, well above the detection limit.

The H₂S was analysed with LCK 653 cuvette tests and a CADAS 100 UV/Vis spectrophotometer (Hach-Lange, UK).

Alkalinity was measured via titration using the kit Alkalitats-Test (Aquamerck®).

Saturation index (SI) of gypsum, calcite and dolomite were also calculated using PHREEQC software (Parkhurst, 1995).

Plots of selected species concentrations of all water samples were built and the relationships between the groundwater samples, the seawater (Adriatic Sea) and freshwater (irrigation canals surrounding the monitoring wells) end-members were analyzed.

3.2.3 Geochemical analysis of soil samples

NH₄⁺ was determined in sediments both with ion chromatography and a double beam Jasco V-550 UV/VIS spectrophotometer (Bower and Holm Hansen, 1980). The two different analytical techniques employed returned similar NH₄⁺ concentrations with a correlation coefficient (R²) of 0.971. KCl 1 M was used to extract NH₄⁺ from the sediment samples, using the sediment to water weight ratio of 1:10. Sediment and water were mixed and sealed in baker, then shaken for one hour, and centrifuged at 3500 rpm for one hour at 25 °C to separate the sediment from

the solution. Total leachable nitrogen (TLN) was extracted from the sediment samples by using Milly-Q (Millipore, USA) water and the sediment to water weight ratio of 1:10; leachates were analysed with LCK 238 LatoN cuvette tests and a CADAS 100 UV/Vis spectrophotometer (Hach-Lange, UK).

Major oxides (SiO₂, TiO₂, Al₂O₃, Fe₂O₃, MnO, MgO, CaO, Na₂O, K₂O and P₂O₅ expressed in weight percent) and TE (Sc, V, Cr, Co, Ni, Cu, Zn, As, Rb, Sr, Zr, Ba, La, Ce, Pb, Th and S expressed in ppm), were analysed by X-ray fluorescence (XRF) on powder pellets, using a wavelength-dispersive automated Panalytical Axios 4000 spectrometer. Accuracy and precision based on systematic re-analysis of standards were better than 3% for major oxides; while accuracy and precision were below 10% for TE (above 10 ppm). Detection limits for TE results are 3 ppm. As reference standards, the E.P.A. Reference Standard SS-1 (a Type B naturally contaminated soil) and the E.P.A. Reference Standard SS-2 (a Type C naturally contaminated soil) were also analysed to cross-check and validate the results.

Calcite and dolomite content in soil was determined with a Chittick gasometrical apparatus.

Pyrite content and pyrite-bound Fe were then calculated from the total S content:

$$\text{FeS}_2 = 0.5 * \frac{M_{\text{FeS}_2}}{M_s} * S \quad \text{and} \quad \text{Fe}_{\text{py}} = 0.5 * \frac{M_{\text{Fe}}}{M_s} * S \quad (8)$$

where FeS₂ is pyrite content, Fe_{py} is pyrite-bound Fe, M_i is the molar mass of compound *i*, and S is total sulphur. These formula work well as long as total reactive Fe is higher than total S, taking into account stoichiometry, which holds for nearly all samples except for the peaty sediments, where some kind of overestimation could be expected.

Total reactive Fe was then calculated using the following empirical formula, based on the XRF analyses:

$$\text{Fe}_{\text{TR}} = 2 * \frac{M_{\text{Fe}}}{M_{\text{Fe}_2\text{O}_3}} * [\text{Fe}_2\text{O}_3 - (0.225\text{Al}_2\text{O}_3 - 0.91\%)] \quad (9)$$

where Fe_{TR} is total reactive Fe, and Fe₂O₃ and Al₂O₃ are total Fe content and total Al content respectively. This formula assumes that silicate-bound Fe₂O₃ amounts to about 22.5% of total Al₂O₃ content and that total reactive Fe could be viewed as enrichment on top of the silicate-bound Fe (Dellwig et al., 2001; 2002).

By subtracting pyrite-bound Fe, the non-pyrite bound reactive Fe (Fe_{react}) can be calculated:

$$\text{Fe}_{\text{React}} = \text{Fe}_{\text{TR}} - \text{Fe}_{\text{py}} \quad (10)$$

The potential reduction capacity (PRC) takes into account sediment organic matter (SOM) and pyrite as major reductants (Hartog et al., 2002):

$$\text{PRC} = 10000 * \left[15 * \frac{\text{FeS}_2}{M_{\text{FeS}_2}} + 2 * \text{SOM}/M_c \right] \quad (11)$$

where the factor 10,000 is a dimensionless constant for the conversion from % to meq/kg dry mass. The SOM and the grain size distribution analyses in P33 and P34 were taken from a previous work (Mastrocicco et al., 2012c).

Carbonate buffering upon pyrite oxidation (CBPO) takes into account the acid buffering capacity of carbonate following pyrite oxidation by O₂:

$$CBPO = 10000 * \left[15 * \left(\frac{CaCO_3}{M_{CaCO_3}} + \frac{MgCa(CO_3)_2}{M_{MgCa(CO_3)_2}} \right) - 2 * \frac{FeS_2}{M_{FeS_2}} \right] \quad (12)$$

Again, the factor 10,000 is a dimensionless constant for the conversion from % to mmol/kg dry mass and CaCO₃ + MgCa(CO₃)₂ is the carbonate content.

3.3 Numerical modelling activities

On the basis of the conceptual model drawn from field and laboratory activities, density-dependent flow and transport numerical simulations were implemented and calibrated via commonly used codes, such as MODFLOW-2005 (Harbaugh, 2005), SEAWAT 4.0 (Langevin et al., 2007), Hydrus-1D (Šimunek et al., 2008) and PEST (Doherty, 2002).

3.3.1 Site wide steady-state simulation

A non-reactive transport model was used to investigate the freshening and salinization processes of the unconfined aquifer. SEAWAT 4.0 (Langevin et al., 2007) was used to simulate the density driven flow and transport of saline and fresh groundwater. For the saltwater transport, no chemical reactions were considered since this study was planned to investigate physical controls on conservative chemical transport.

The model domain of the study area extends over 753 km², 25 km in the East-West direction and 45 km in the North-South direction. The length of the simulation period was set equal to 100 years, divided into 1000 time steps.

The grid was defined by 125 columns, 225 rows and vertically discretized into 10 layers of variable thickness. The top of the grid is represented by the local ground surface, ranging from 12 m to -10 m a.s.l., obtained by entering the DTM of the Emilia-Romagna Region; the bottom of the grid, representing the top of the underlying aquitard (the silty-clay unit), ranges from -12 m to -20 m a.s.l., as deduced from the stratigraphic logs available in the database of the Emilia-Romagna Geological Survey.

A mean recharge rate of 155 mm/y was assigned to the entire domain, as a function of mean precipitation and mean temperature recorded within the site and calculated with the Thornthwaite method (1948).

The maximum evapotranspiration rate was set to 95 mm/y with an extinction depth of 0.5 m from ground surface, assuming that evapotranspiration is at maximum rate when the groundwater table is close to the surface and becomes null below 0.5 m.

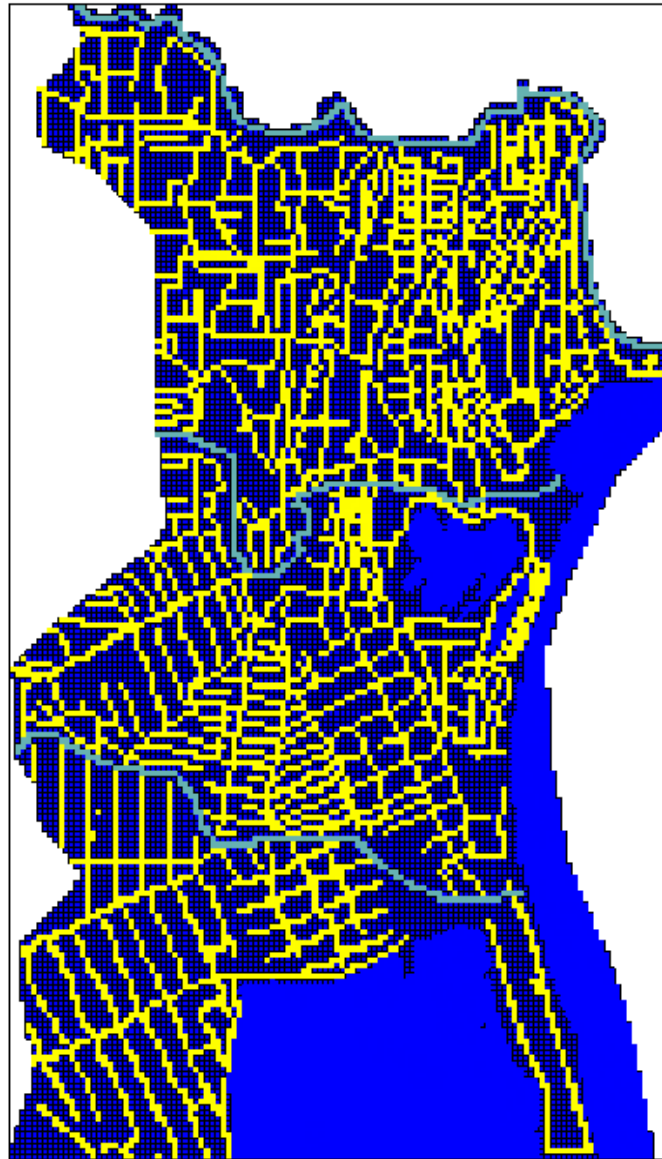


Figure 3.2 - Grid discretization and boundary conditions applied to the model domain: no flow cells (white), constant heads cells (light blue) drain cells (yellow) and river cells (cyan).

The study area was delineated by null flow cells while all other cells are active cells (Fig. 3.2). The General-Head Boundary (GHB) package was used to simulate the Adriatic Sea, Valli di Comacchio and Valle Bertuzzi, by assigning a conductance value of $0.1 \text{ m}^2/\text{s}$ and heads of 0 m for the Adriatic Sea and -0.5 m for the Valli di Comacchio and Valle Bertuzzi.

The River package was employed to simulate the Po River; the weak connection between groundwater and the river was simulated assigning a small hydraulic conductivity to the riverbed, with a conductance of $1e-7 \text{ m}^2/\text{s}$.

The drainage canals network was simulated with the Drain package, assuming an average depth of the canals of 0.8 m from the topographic level and a conductance of $0.03 \text{ m}^2/\text{s}$. This value ensured an excellent connection between the surface water and groundwater bodies: it is the maximum value that can be set, given the size of the cell. The dense network of canals was imported into the model grid from a georeferenced AutoCad DXF file.

The initial pre-calibration estimate of the hydraulic conductivity distribution has been determined from geologic logs and pumping tests (Fig. 3.3). Vertical anisotropy was set to 0.1 for all layers, while effective porosity was taken as 0.25 for the entire model based on grain size analysis. Specific storage and specific yield coefficients for sand and silty-clay sediments (Tab. 3.1) were taken from literature values (Fetter, 2001).

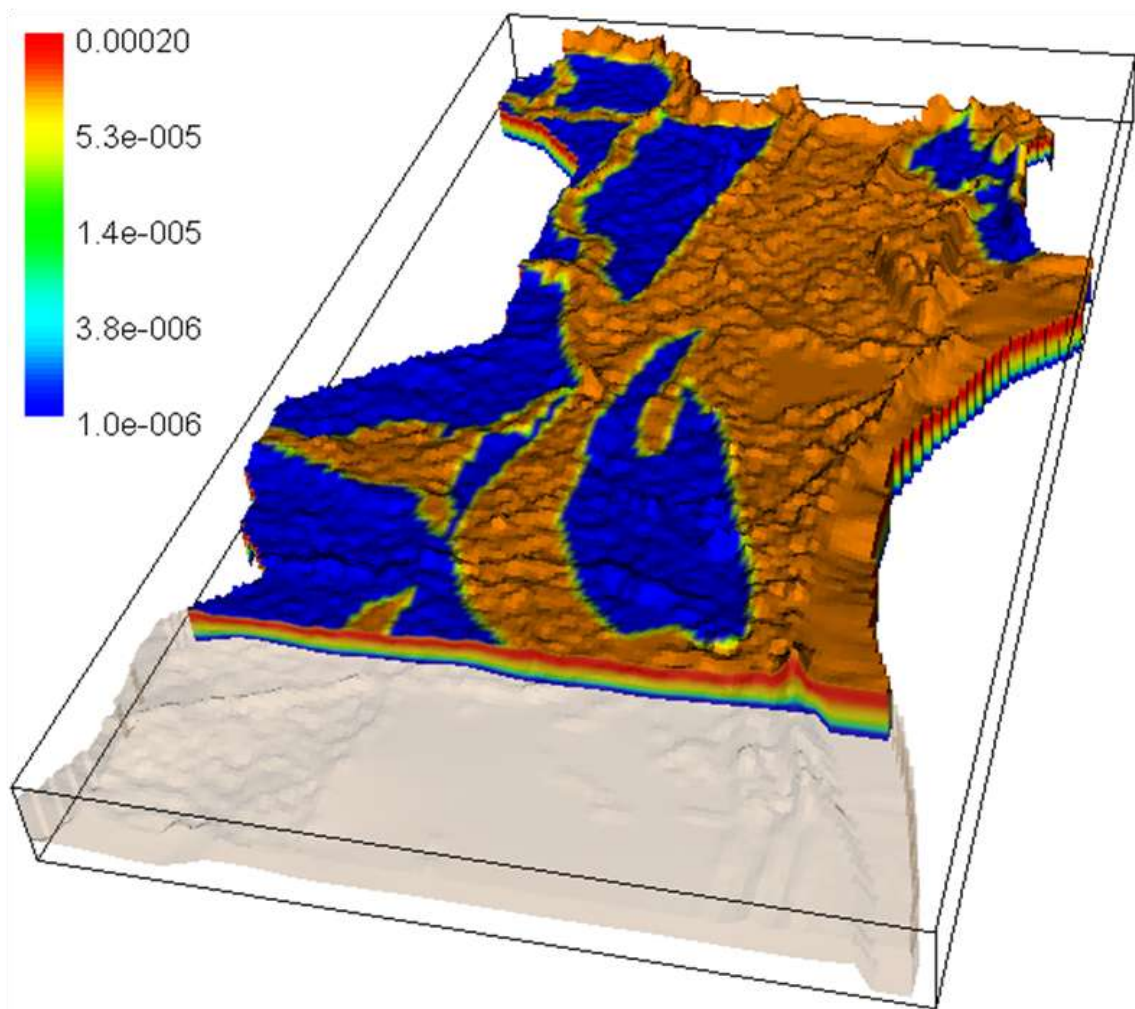


Figure 3.3 - Hydraulic conductivity (m/s) discretization of the model domain based on surface geology and the decreasing hydraulic conductivity pattern found during the multi-level pumping tests.

Table 3.1 - Flow and transport parameters used for the simulations

Parameter name	N° of parameters	Value (units)
Horizontal hydraulic conductivity	9	$2 \times 10^{-4a} - 1 \times 10^{-8a}$ m/s
Vertical anisotropy	1	0.1^b (-)
Effective porosity	1	0.25^b (-)
Specific yield	2	$0.25^b - 0.1^b$ (-)
Specific storage	2	$1 \times 10^{-4b} - 1 \times 10^{-5b}$ (m^{-1})
Vertical dispersivity	1	8.16×10^{-3a} (m)
Longitudinal dispersivity	1	1.02^a (m)
Molecular diffusion coefficient	1	1×10^{-9b} (m^2/s)

^a Parameter values optimized by PEST

^b Parameter values taken from literature values

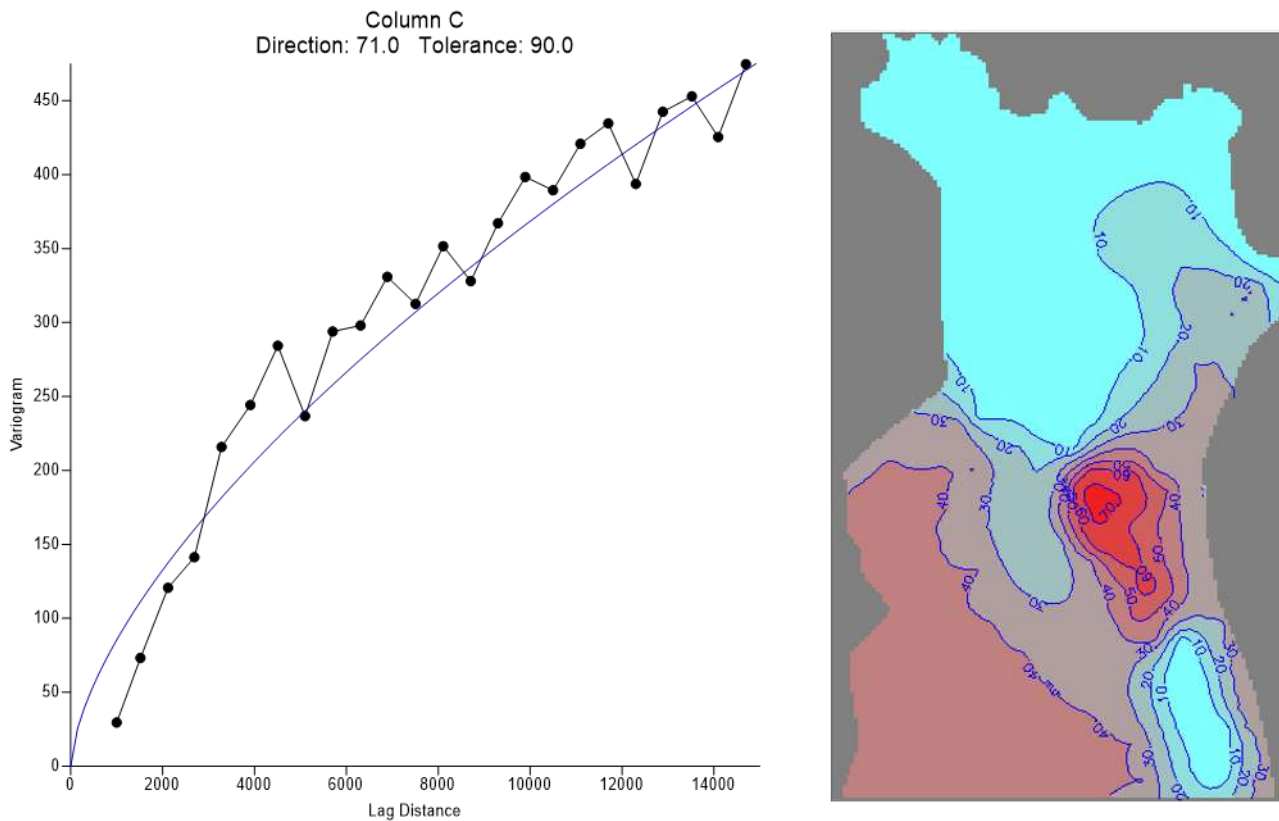


Figure 3.4 - Variogram fitted with a power law function (left plot), and distribution of Specified Concentration in layer 10 derived from the interpolated measured TDS and pilot points (right plot).

The Initial Concentration for transport simulation was set to 35 g/l for the Adriatic Sea, to 25 g/l for the Valli di Comacchio and Valle Bertuzzi, and 35 g/l for the Lago delle Nazioni, while 1 g/l was used in the rest of the model domain. The initial concentration set at layer 10 has been derived from measured TDS at the bottom of the aquifer, while the insertion of pilot points has been deduced from geology: all data are interpolated with the Kriging method using a power law variogram. The pilot points were entered in geologically similar zones to each measured point of the study area (Fig. 3.4).

The power law function had the following parameters obtained via least square optimization: slope 0.77, correlation length 1, power factor 0.635 and anisotropy ratio 2. The pilot points were entered into the model in those areas geologically similar to each measured point of the study area. As can be seen from Figure 3.4, within the bodies of actual and paleo-dunes the TDS concentration is very low due to higher recharge rates. In palaeo back-barrier environments, where the water stagnated and evaporated, the salt concentration is significantly higher. In the northern portion of the model domain, a very low TDS concentration was used for the presence of Po River and its palaeo riverbed environments.

The numerical solver used for the groundwater flow is the Geometric Multigrid Solver (GMG). The TDV-ultimate scheme was used to solve the advective term of the solute transport problem and a constant longitudinal dispersivity of 2 m was employed. The ratios of the horizontal transverse dispersivity to the longitudinal dispersivity, and of the vertical transverse dispersivity to the longitudinal dispersivity were respectively set to 0.1 and to 0.0001. An effective molecular diffusion coefficient of $1e-9$ m²/s was used throughout the model domain to account for solute diffusion in water (Tab. 3.1).

The observed field data used for model calibration, via trial and error technique, were: the outflows from drainage basins (data from the Consorzio di Bonifica Pianura di Ferrara), the hydraulic heads and the TDS concentrations.

3.3.2 Two dimensional transient simulation

Along the transect A-A', perpendicular to the Canale della Gronda (Fig. 4.24), a non-reactive transport model was used to investigate the freshening and salinization processes of the unconfined aquifer.

Groundwater flow simulation was carried out using the MODFLOW-2005 code (Harbaugh, 2005) while SEAWAT 4.0 (Langevin et al., 2007) was used to simulate the interaction between the saltwater upward flow and the freshwater canal, taking into account the effect of density-dependent transport processes. For the saltwater transport, no chemical reactions were considered since this study was planned to investigate physical controls on conservative chemical transport. Groundwater TDS was simulated to track the seasonal vertical variation of the freshwater-saltwater interface.

MATERIALS AND METHODS

The domain of the cross-sectional model consisted of a uniform model grid of 100 columns and 30 layers with dimension 0.3 m in the horizontal direction and 0.5 m in the vertical direction, giving a longitudinal extent of 30 m and a thickness of 15 m (Fig. 3.5).

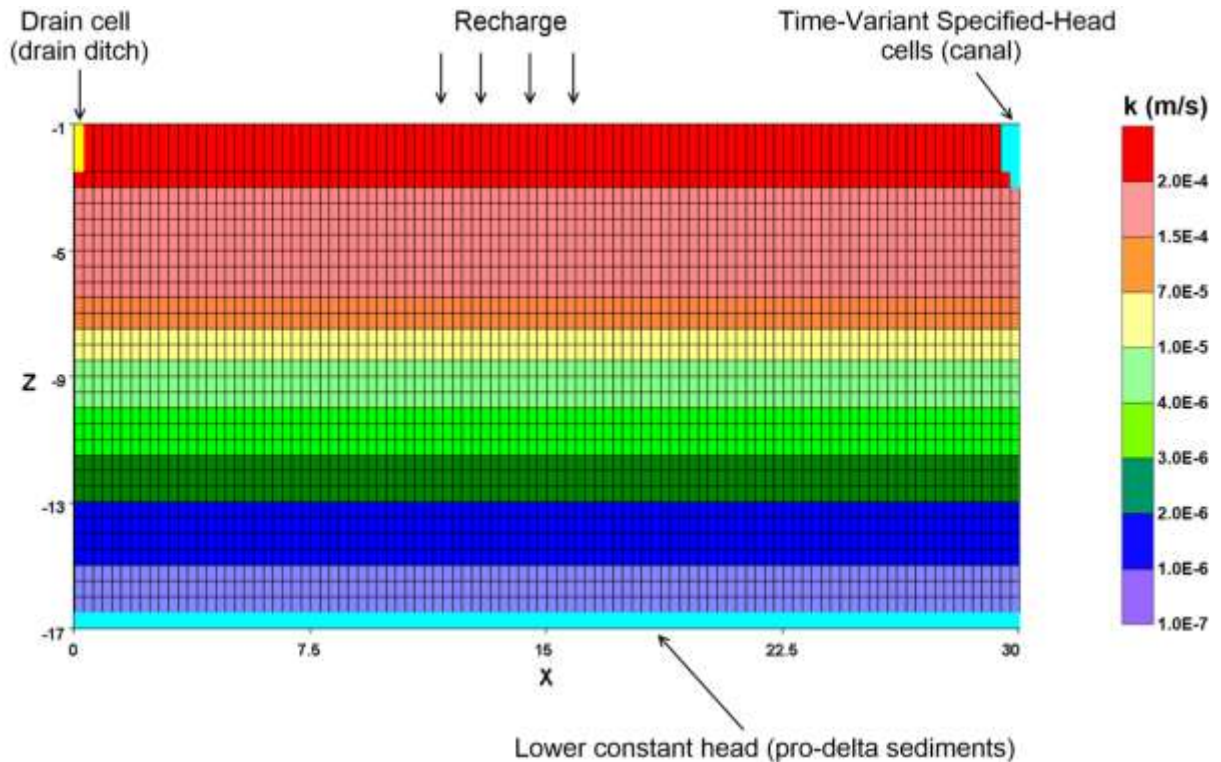


Figure 3.5 - Numerical grid, with the optimized k_h discretization, in yellow the Drain cell, and in light blue the Time-Variant Specified-Head cells pertaining to the canal and to the pro-delta silty clays connected with the Adriatic sea.

Only the first layer was 1 m thick in order to accommodate groundwater table fluctuations: this grid configuration was chosen to avoid cell rewetting, which frequently leads to numerical instabilities and numerical solver's non-convergence. A steady state simulation was initially run to achieve representative heads and TDS distribution within the aquifer in summer 2012. Then the transient simulation time was subdivided into 34 stress periods to simulate the variation of the canal stage and recharge during the simulated period.

The irrigation canal "Canale della Gronda", on the right side of the model, was modelled by time-variant specified head, and the input were extracted from the LTC M10 datalogger, which was installed in the canal at the start of the monitoring period. The Drain Package was used to simulate effects of the agricultural drain (left hand side of the model profile), which removes groundwater from aquifer at a rate proportional to the head difference between the aquifer and the drain. When the hydraulic head in the aquifer is greater than the drain elevation, ground water flows into the drain and is removed from the groundwater model. Recharge from the drain is always zero, regardless of the hydraulic head in the aquifer. The drainage ditch elevation was set at -1.95 m a.s.l. with 1×10^{-4} m²/s of drain hydraulic

conductance; a high conductance was used since the drain ditch was reshaped at the beginning of the 2012.

The Recharge Package was used to simulate the effective precipitation. The daily recharge was calculated using the finite element model Hydrus-1D (Šimunek et al., 2008).

The top soil of the site was discretized in 101 nodes of 2.5 mm each, to form a regular vertical grid of 0.25 m. The soil hydraulic parameters were assigned using default values included in the soil catalogue of Hydrus-1D for loamy sand. Initial water content conditions were measured gravimetrically for the top soil and assumed constant throughout the model profile. Groundwater heads and TDS at two depths (-4 and -8 m a.s.l.) in P8 and within the drain ditch were used for model calibration. TDS profiles were used for model validation.

At the soil surface, variable flux and head conditions were selected to represent the atmospheric boundary. Runoff was assumed negligible due to the flat topography and based on other studies in this area (Mastrocicco et al., 2010). Daily reference evapotranspiration (ET_0) was calculated with the FAO-56 recommended Penman-Monteith equation (Allen et al., 1998). It was assumed that the grass cover at the experimental site resembles the reference surface as defined by Allen et al. (1998). Potential transpiration and evaporation were split using an estimated surface cover fraction of 0.8 (Ritchie, 1972). A meteorological station recording daily rainfall, wind speed, temperature and humidity was located 3.8 km from the site, while solar radiation data were recorded in another station located 8.6 km from the site (www.arpa.emr.it/sim/?osservazioni_e_dati/dexter). The actual root water uptake was simulated using the turf grass dimensionless water stress response function available in the Hydrus-1D database (Feddes et al., 1978), the constant height of 0.12 m and the maximum rooting depth of 0.2 m. The dimensionless constant for the radiation extinction by the canopy was set to 0.463, the interception constant was set to 0.25 mm and the LAI was derived from grass height.

As shown in figure 3.6, Hydrus-1D calculated the daily actual transpiration and evaporation fluxes. Free drainage was selected as lower boundary condition and the cumulative bottom flux expressed as negative flux (recharge towards the aquifer). The daily recharge was subsequently discretized in the 34 stress period used in the SEAWAT model.

The flux across the impermeable clay basement that constitutes the aquiclude between the unconfined aquifer and the confined aquifer, with a conductivity value of approximately 1×10^{-10} m/s, was assumed to be zero. A constant head with value 0 m a.s.l. was needed to properly simulate the observed vertical heads gradients present within the aquifer (Giambastiani et al., 2013), since the bottom part of the unconfined aquifer (the prodelta silty-clays) is hydraulically connected with the Adriatic Sea. Tidal fluctuations were not considered in the simulation since in this area of the Adriatic Sea tide magnitude is known to influence only the near shore monitoring wells (Balugani and Antonellini, 2011).

The temporal TDS variation in the “Canale della Gronda” was simulated by means of Time-Variant concentration cells (Fig. 3.5), while constant concentration cells with a TDS of 65 g/L was set at the bottom of the aquifer. For a conservative solute as chloride, the molecular diffusion coefficient for porous media was taken as equal to 1×10^{-9} m²/s.

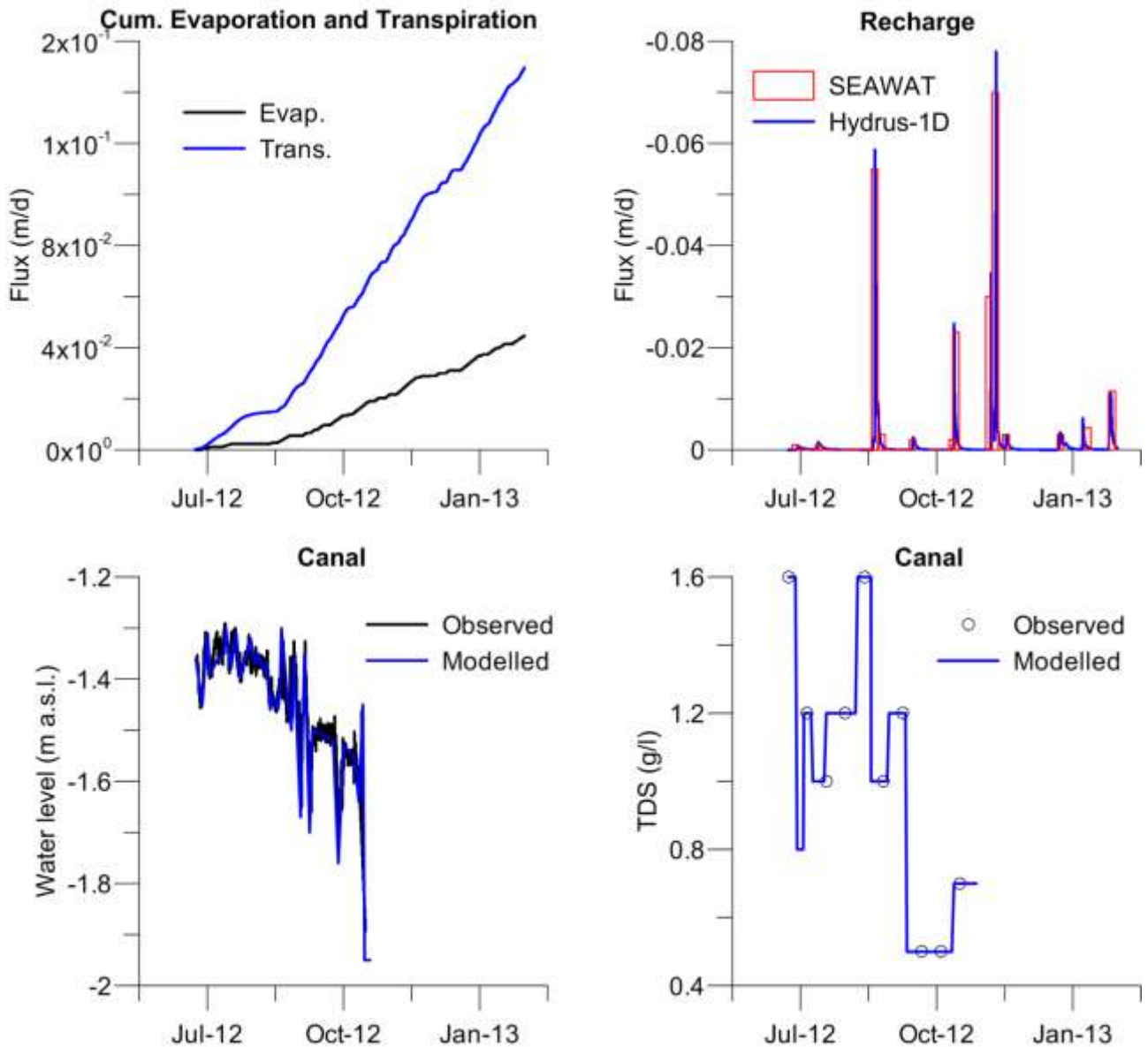


Figure 3.6 - In the upper left hand side plot, the actual cumulative transpiration (blue line) and evaporation rates (black line) computed by Hydrus-1D are shown. In the upper right hand side plot, the recharge rate computed by Hydrus-1D (blue line) and its discretization as input in SEAWAT (red bars) are shown. In the lower left hand side plot, the modelled (blue line) and observed (black line) canal water levels are shown. In the lower right hand side plot, the modelled (blue line) and observed (black open circles) canal TDS values are shown.

Model parameters were estimated by inverse modelling using the numerical code PEST (Doherty, 2002). This process has been performed on the following parameters: k_h , longitudinal dispersivity and vertical dispersivity. The specific storage and yield for transient simulations were judged insensitive in a preliminary sensitivity analysis and thus not included in the model calibration. Prior information on the ratio between horizontal and k_v

values and measured k_h values along the profile were used in order to constrain parameter estimation.

Upper and lower limits of $\pm 200\%$ with respect to the measured k_h values were set as optimization constraints. Upper and lower limits of one order of magnitude with respect to the initial estimate of longitudinal and vertical dispersivity values were set as optimization constraints. The objective function consisted of piezometric heads, drain water table elevations and TDS in both aquifer and drain. Each screen interval was subdivided with the layer proportion to ensure that calculated heads were related to the observed heads. The k_h parameters were log-transformed, while the other parameters were left linear for the inverse modelling.

The calibration of transient state model was performed with the objective of matching modelled with measured hydraulic head and TDS continuously recorded at -4 m and -8 m a.s.l. in the monitoring well P8 and every two weeks in the drain ditch (from 01/07/2012 to 04/12/2012). The model validation was performed using the calculated TDS profiles against the TDS profiles carried out in December 2012 and February 2013 in P8. This was done including other 10 stress periods in the simulation time to reproduce the recharge events from 05/12/2012 to 28/02/2013 (Fig. 3.6). Thus, the validated model consisted of 44 stress periods, 10 more than the calibrated one.

3.3.3 Scenario modelling

Four scenarios were simulated and compared to each other. For the first scenario, a 3% increase in the precipitation amount and increase in evapotranspiration induced by temperature increase of 2°C over the next 40 years (Gualdi et al., 2013; Giorgi and Lionello, 2008) were simulated. In the second scenario the frequency of severe high rainfall events was increased. In the third scenario an extreme drought condition was simulated. The fourth scenario simulated the interruption of canal usage for irrigation purposes.

As regards the first scenario, the average annual precipitations recorded from 2001 to 2012 (676 mm/year) and climatic data used to compute the Penman-Monteith equation were downloaded from the Emilia-Romagna climatic database. The daily climatic data were then mediated over the period 2001-2012 to get mean values for each day of the year. Then, the mean daily values were used as input for a 365 days simulation with Hydrus-1D (keeping the model parameters described in section 2.3) to estimate the actual evapotranspiration and recharge rates. The average annual precipitations were increased by 3% and the induced future actual evapotranspiration (ET_a) was calculated relying on the following equation (Hanson et al., 2012):

$$ET_{a(\text{future})} = \frac{(TDF_{\text{future}})}{(TDF_{\text{current}})} \times ET_{a(\text{current})} \quad (13)$$

where TDF_{future} and TDF_{current} stand for future and current temperature-dependent function, respectively, on the basis of mean monthly air temperature.

Current mean monthly air temperature (T_a) was set equal to 14.8 °C, based on the climate data recorded from 2001 to 2012 and downloaded from the on-line meteorological and climatic database of the Emilia-Romagna region, while future mean monthly air temperature (T) was increased of 2 °C and set equal to 16.8 °C.

In order to calculate TDF values, the following form was applied (Hanson et al., 2012):

$$\text{TDF} = -13.281 + 0.083864(T) - 0.00012375(T)^2 \quad (14)$$

The mean annual recharge rate calculated by Hydrus-1D and used for this scenario was 116 mm/year, while the bottom constant head was raised from 0 m a.s.l. to 0.13 m a.s.l. (and from 0 m a.s.l. to 0.62 m a.s.l. in a second sub-scenario) to account for the predicted sea level rise. Prediction of sea level rise were found in Lambek et al. (2011), where the subsidence rate of 1.5 mm/year summed to a minimum projected Adriatic sea level rise of 1.8 mm/year will produce a net sea level rise for the next 40 years of 0.13 m in the proximity of Po river delta. The maximum projected Adriatic Sea level rise of 14 mm/year plus the subsidence rate of 1.5 mm/year will instead produce a net sea level rise for the next 40 years of 0.62 m. The simulation time of this scenario was subdivided in 8 stress periods of 6 months each. Every stress period was subdivided into 100 time steps, for a total simulation time of 4 years, to achieve pseudo steady-state conditions. In all the stress periods the recharge rate was kept constant while the variable constant head and concentration resembling the canal were turned on and off every 2 stress periods.

In the second scenario the frequency of extreme high rainfall events was increased (triplicate). The average annual recharge amount was assumed to occur during winter and spring periods (six months), instead of being distributed over the entire year. The same sub-scenarios for the predicted sea level rise were run as explained above. The third scenario simulated an extreme drought condition by setting null recharge for the last year of simulation, while maintaining the other boundaries as in the first scenario. The same sub-scenarios for the predicted sea level rise were run also for this third scenario. To account for the large uncertainties connected with the climate forecasts, the first three scenarios were run forcing the input values of plus and minus one standard deviation of the predicted variables.

The fourth scenario simulated the interruption of canal usage for irrigation purposes. Here freshwater recharge from the canal was set equal to zero (canal dewatering) for a total of 6 months in order to simulate an interruption of canal due to degradation of water quality or salinization of water courses. This scenario was run forcing the canal dewatering for a total of 9 and 3 months, to account for different circumstances of salinization of surface water courses. This last simulation was important to understand the effect of no freshwater recharge from canals. The same sub-scenarios for the predicted sea level rise were run also for this fourth scenario.

4. RESULTS AND DISCUSSION

This chapter reports the main results obtained from the three years of field, laboratory and modeling activities spent in the implementation of a reliable conceptual model of the salinization processes and their effects on the hydrogeochemical behaviour of the coastal unconfined aquifer of the Ferrara Province. The majority of the outcomes, targeting the different objectives of this study (see paragraph 1.3), have been published as articles in peer review journals or presented at international conferences (see paragraph 5.4). Excerpts from these articles will be presented in the following paragraphs and, to help the reader, each excerpt will be preceded by a brief explanation that highlights its role within the present study as a whole.

4.1 Characterization of the lowland coastal aquifer of Ferrara: hydrology, hydrochemistry and evolution of the system

The first objective of this study was to delineate the hydrogeochemistry and the geological evolution of the unconfined coastal aquifer of Ferrara to identify the possible drivers of groundwater salinization. Physical aquifer parameterization highlighted the presence of a vertical hydraulic gradient, due to the drainage system, that may induce groundwater salinization via the seepage of relict seawater trapped within low permeability sediments during the Holocene. The hydrogeochemical investigation also allowed distinguishing between the role of seepage and water-sediment interactions in the evolution of groundwater chemistry.

4.1.1 Hydrostratigraphic characterization

Grain size distribution analysis performed on the samples of monitoring wells P33 and P34 (Tab. 4.1) reveals the presence of an heterogeneous aquifer with very poorly-sorted silty clay and peat lenses overlaying a highly permeable well-sorted sandy layer typical of high energy depositional environments, such as coastal environment (dunes and beaches), intercalated with poorly-sorted sandy silt lenses. The sandy and sandy silt layers constituting the aquifer are underlined by an aquitard, in agreement with previous studies (Amorosi et al., 2003).

Porosity values range between 19% and 76%, with an average value of 30%; the highest values are associated with the presence of peat layers, which exhibit high organic matter content, with maximum values of 63%.

The hydraulic conductivity (k), resulting from constant rate pumping tests in the monitoring wells P3, P8, P33 and P34, decreases from 10^{-3} to 10^{-6} m/s from the top to the bottom of the aquifer (Figure 4.1a), due to the presence of silt and fine sand lenses.

RESULTS AND DISCUSSION

Table 4.1 - Core sample analyses of monitoring wells P33 and P34.

	i.d.	Elevation m a.s.l	O. M. %	Sand %	Silt %	Clay %	Median φ	d₁₀ φ	d₆₀ Φ	Sorting φ
	C01	-4.93	2.12	22.28	56.36	21.36	5.90	9.25	5.00	2.28
	C02	-5.70	3.06	2.48	67.47	30.05	6.74	10.13	5.63	2.02
	C03	-6.08	6.15	0.39	46.70	52.91	8.55	11.88	7.63	2.26
	C04	-6.35	17.17	0.31	16.68	83.01	9.49	10.75	9.50	1.56
	C05	-6.70	62.50	6.90	63.10	30.00	7.80	10.10	7.8	2.00
	C06	-7.53	6.59	1.26	70.59	28.15	7.13	11.00	6.00	2.31
	C07	-8.60	6.06	1.46	57.77	40.77	7.95	11.75	6.88	2.48
	C08	-9.40	5.80	80.48	10.74	8.78	3.36	7.50	2.50	1.96
	C09	-10.53	1.59	70.67	23.80	5.53	3.59	7.00	2.50	1.88
	C10	-12.45	0.80	96.52	2.43	1.05	2.25	3.00	2.00	0.47
	C11	-13.65	3.21	26.98	59.16	13.86	5.39	8.75	5.00	2.29
P33	C12	-14.23	1.60	92.72	6.30	0.98	3.12	3.88	3.00	0.56
	C13	-14.80	2.18	62.65	24.10	13.25	4.50	8.88	3.25	2.22
	C14	-16.50	2.30	62.78	28.64	8.58	4.39	7.75	3.50	1.79
	C15	-18.80	3.16	63.18	30.62	6.20	4.05	6.50	3.63	1.37
	C16	-19.40	3.22	76.39	18.09	5.52	3.62	6.25	3.25	1.38
	C17	-20.10	4.07	29.73	44.45	25.82	6.07	9.75	5.50	2.59
	C18	-20.90	37.27	4.25	51.18	44.57	7.91	10.63	7.25	2.10
	C19	-21.60	6.48	50.36	34.67	14.97	5.02	9.25	3.75	2.23
	C20	-23.15	6.22	12.26	59.50	28.24	6.82	10.63	6.00	2.45
	C21	-23.90	4.94	55.83	38.92	5.25	4.26	6.38	3.75	1.27
	C22	-25.20	5.71	5.59	65.83	28.58	6.95	7.13	5.75	2.42
	C23	-25.90	5.45	0.45	29.68	69.87	9.28	12.13	8.50	2.09
	C01	-3.80	7.81	1.44	42.85	55.71	8.56	11.75	7.75	2.33
	C02	-4.60	7.68	7.38	50.52	42.10	7.66	11.13	6.63	2.62
	C03	-6.50	1.65	92.69	5.85	1.46	2.80	3.63	2.75	0.58
	C04	-7.50	1.09	96.64	2.73	0.63	2.18	2.88	2.00	0.46
P34	C05	-8.50	1.34	94.56	4.00	1.44	2.09	3.00	2	0.69
	C06	-12.50	5.04	64.68	29.63	5.69	4.03	6.63	3.50	1.40
	C07	-14.10	10.61	55.58	34.08	10.34	4.61	8.13	3.63	1.99
	C08	-15.50	4.87	71.51	23.55	4.94	3.99	6.38	3.50	1.26
	C09	-16.50	6.67	13.76	48.86	37.38	6.75	10.25	5.25	2.47

RESULTS AND DISCUSSION

These lenses pertain to prodelta depositional environment, which is characterized by a lower formation energy than the sand dune system: the lower energy leads to finer grain size distribution and consequently to less permeable sediments in the former environment compared to the latter. The comparison between k values derived by constant rate pumping tests, calculated by equation (1) (paragraph 3.1.4), and those determined by pedotransfer formulae shows a poor agreement along the monitoring well profiles (Figure 4.1b).

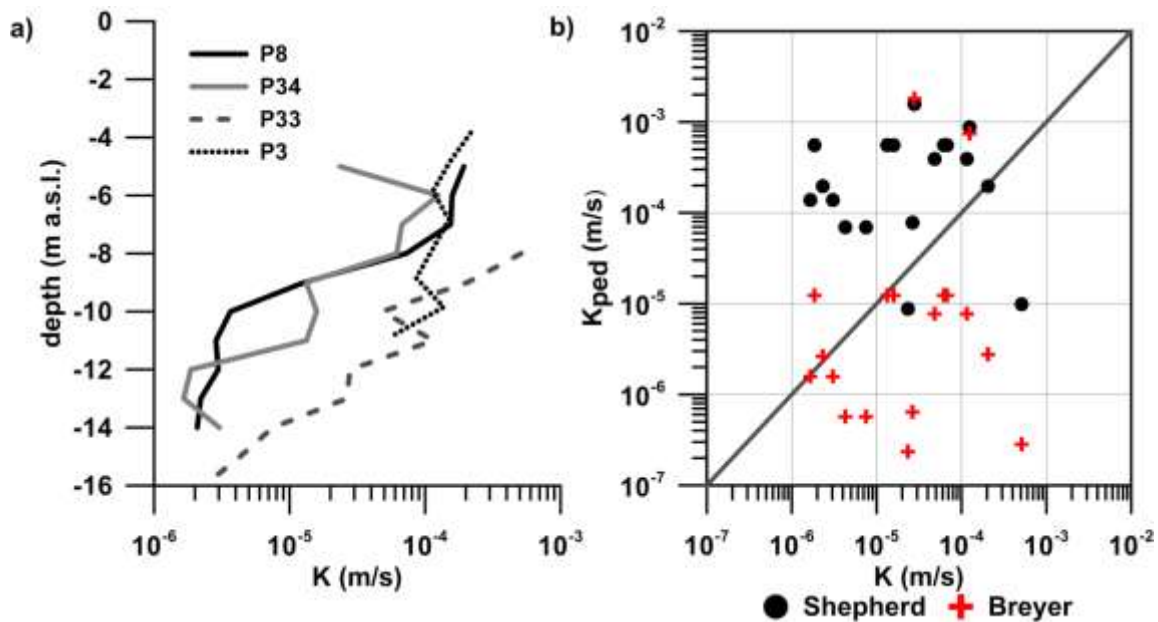


Figure 4.1 - (a) Profiles of hydraulic conductivity measured by constant rate pumping tests in the four monitoring wells and (b) Scatter plot of K values calculated by pedotransfer formula (K_{ped}) and K values resulting from permeability tests in P33 and P34.

The best linear fit between pedotransfer formulae and measured k values gives R^2 of 0.67 (for Breyer in P34) with a correlation coefficient of 0.81. This low correlation is mostly due to peat sediments, where discrepancies of more than 1 order of magnitude occur, since grain size characterization is particularly challenging due to the organic nature of these sediments. In addition, it has to be considered that pedotransfer formulae are empirical relations and introduce high uncertainty; in fact, Vukovic and Soro (1992) noted that the applications of different empirical formula to the same porous medium can yield k values differing by a factor of 10 or even 20. Secondly, there are scale issues: hydraulic parameters acquired by constant rate pumping tests are considered to be average values of large volumes of aquifer (Leven and Dietrich, 2006), while the hydraulic parameters gained from the application of the pedotransfer formulae to sediment samples are point values: this scale issue could also be responsible for the observed discrepancies between k values.

RESULTS AND DISCUSSION

Tables 4.2 summarize the parameters measured (k) and those derived from empirical formulas (n_e) used to calculate the mean groundwater flow velocities in monitoring wells P33 and P34. Peclet number (Bear, 1972) is always below 1 and therefore the flow is dominated by diffusion-driven processes, or at least the role of diffusion is comparable to that of mechanical dispersion (Appelo and Postma, 2005).

The estimated flow velocities show that seawater intrusion is proceeding inland at a very slow rate due to the effects of the dewatering stations draining the recently reclaimed area of the Ferrara Province. Mastrocicco et al. (2012c) have showed that for this shallow coastal aquifer the regional freshwater hydraulic head gradient is equal to 0.4‰ and horizontal flow velocities are very slow, meaning that lateral seawater intrusion is proceeding inland at a very slow rate, especially at distance of 2-10 km from the coastline.

Table 4.2 - Values of measured total porosity (n), calculated total porosity by Vukovic and Soro (1992) (n_v), respective effective porosity (n_e , n_{ev}) and pore-water velocity (v and v_v), and measured hydraulic conductivity (k) in monitoring wells P33 and P34.

i.d.	Elevation m a.s.l	n	n_v	n_e	n_{ev}	k m/s	v m/y	v_v m/y
C05	-6.70	0.76	0.37	0.11	0.05	$1.1e^{-4}$	12.8	26.5
C08	-9.40	0.33	0.29	0.27	0.24	$2.1e^{-4}$	9.5	10.9
C09	-10.53	0.18	0.29	0.16	0.26	$4.8e^{-5}$	3.8	2.3
C10	-12.45	0.27	0.35	0.26	0.34	$1.2e^{-4}$	5.6	4.3
P33 C11	-13.65	0.24	0.33	0.19	0.27	$2.8e^{-5}$	1.9	1.3
C12	-14.23	0.25	0.37	0.24	0.35	$2.6e^{-5}$	1.4	0.9
C13	-14.80	0.19	0.29	0.15	0.24	$7.5e^{-6}$	0.6	0.4
C14	-16.50	0.20	0.31	0.17	0.26	$4.3e^{-6}$	0.3	0.2
C15	-18.80	0.21	0.33	0.18	0.28	$2.3e^{-6}$	0.2	0.1
C03	-6.50	0.26	0.37	0.24	0.34	$6.7e^{-5}$	3.6	2.5
C04	-7.50	0.25	0.35	0.24	0.34	$6.2e^{-5}$	3.3	2.3
P34 C05	-8.50	0.24	0.35	0.23	0.33	$1.3e^{-5}$	0.7	0.5
C06	-12.50	0.25	0.32	0.21	0.27	$1.9e^{-6}$	0.1	0.1
C08	-15.50	0.23	0.33	0.19	0.27	$3.0e^{-6}$	0.2	0.1

RESULTS AND DISCUSSION

This confirms that groundwater salinization in the deep portion of the aquifer should mostly be due to local salt sources and to water/sediment interaction, rather than present seawater intrusion. In fact, considering the geomorphologic evolution of the area during the last transgressive period that was characterized by landward migration of a barrier-lagoon-estuary system, it is probable that the aquifer could contain significant soluble salt amounts or trapped fluids.

Figure 4.2 shows freshwater heads (green colour) and the vertical flow (red colour) in monitoring wells P3, P8, P33 and P34, along with their stratigraphy. An upward vertical flow is induced by the drainage system, being in some cases quite significant (0.17 m/d in P33). In some cases this upward flow is contrasted by small lenses of silt and clay that confine the aquifer at the top and prevent the complete salinization of the shallow aquifer. This feature is very important, since the reclaimed land is mainly used for agricultural purposes and soil salinization could cause severe problems to crops sensitive to salinity stress (Gattacceca et al., 2009; Zalidis et al., 2002). Recharge flows (negative values in Figure 4.2) are present in P3 and in the upper part of P8, both located in the paleodunes (Figure 2.2) that allow surface water infiltration.

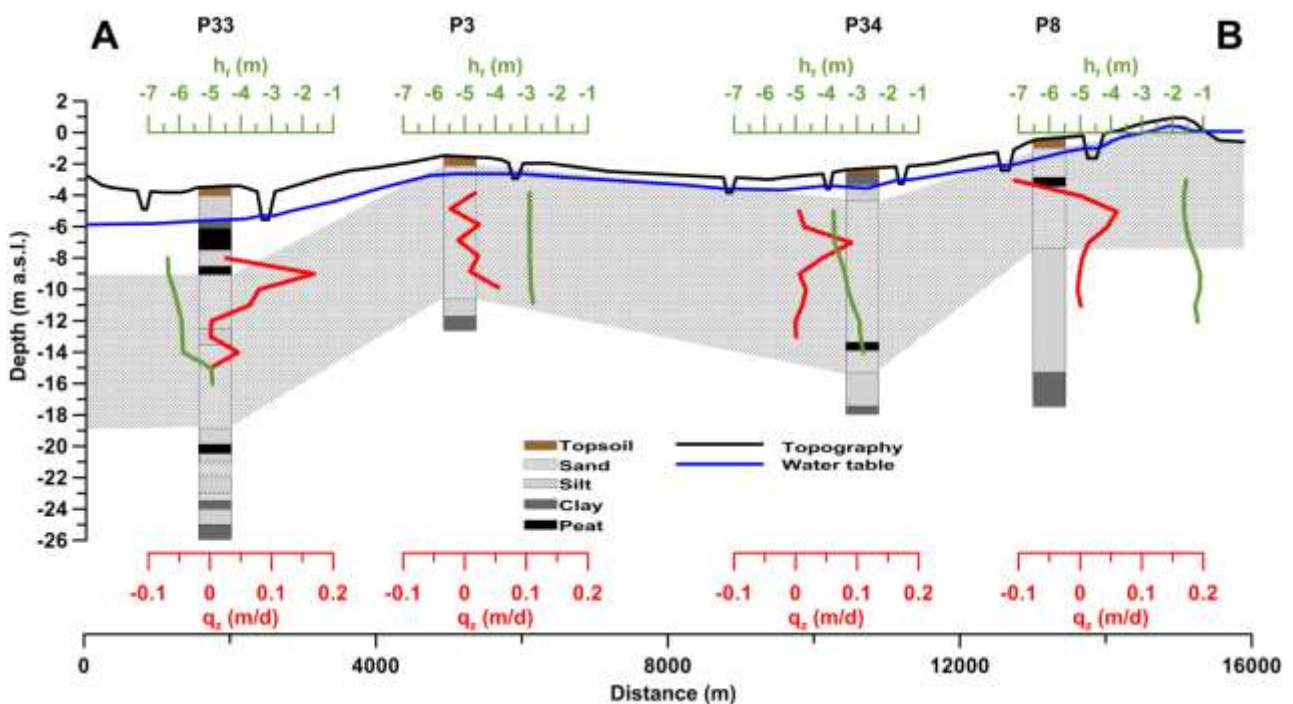


Figure 4.2 - Transect A-A' across the coastal aquifer (see Figure 2.2 for location) showing freshwater head (h_f in green colour) and seepage (q_z in red colour). Note: positive value means flow from the bottom toward the surface, while negative values indicate downward flow (recharge).

4.1.2 Hydrochemical characterization

The base-exchange index for dolomitic system (BEX_D) was used to characterize the status of salinization or freshening of the coastal aquifer (Stuyfzand, 2008).

The most common water types found in the aquifer are $CaHCO_3$, $NaHCO_3$, and $NaCl$. $CaHCO_3$ and $NaHCO_3$ consist of fresh to fresh-brackish waters with low salinity. The BEX_D is positive in both cases, indicating freshening processes. In fact, these two water types are found in the shallowest portion of the aquifer, in proximity of canals (P8) that contribute to dilute groundwater, and topographic heights, such as paleo-dunes (P3). $NaHCO_3$ is also found in the transition zone between fresh and salt water and contains higher Na^+ (31%) than freshwater of the irrigation canals. $NaCl$ is the most abundant subtype found in the aquifer (88%) and consists mainly of brackish, salt and hypersaline waters according to the classification of Vandenbohede and Lebbe (2012).

The anions of these three major water types (HCO_3^- , Cl^- and SO_4^{2-}) are plotted against TDS in Figure 4.3. Salinity clearly correlates with Cl^- in a linear regression with an R^2 of 0.99. HCO_3^- remains in all samples between 6 and 36 meq/l and does not increase with salinity. HCO_3^- is the dominant anion in freshwater, while Cl^- becomes the most frequent in brackish, saline and hypersaline waters. SO_4^{2-} is generally high and increases with TDS; low concentrations of SO_4^{2-} are recorded only in low and very high TDS samples. Possible explanations of low Cl^- and high SO_4^{2-} content are pyrite oxidation or gypsum dissolution (Mollema et al., 2013).

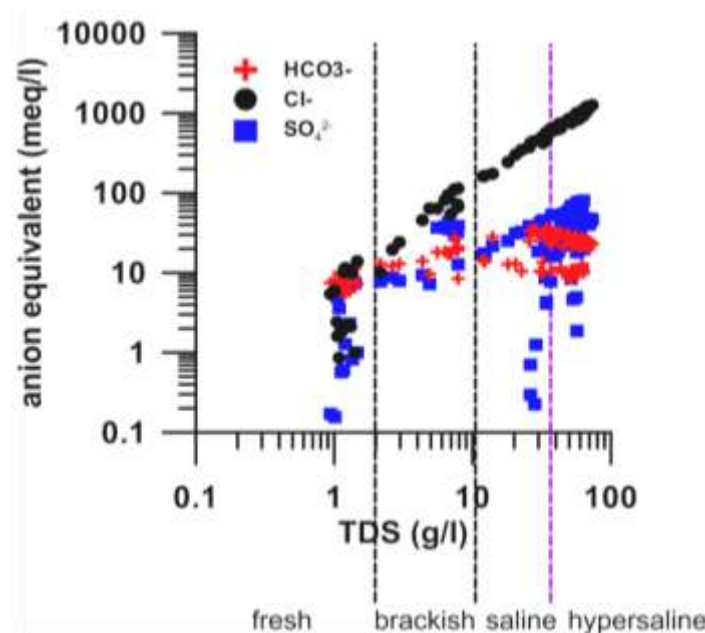


Figure 4.3 - Salinity (TDS in g/l) and concentration of the anions of major salts. The purple line indicates the TDS concentration of the current Adriatic Sea water.

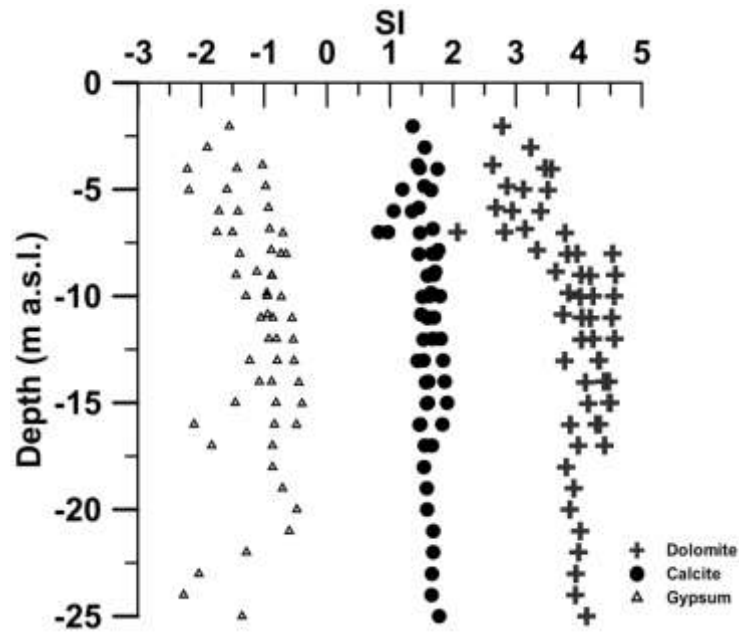


Figure 4.4 - Saturation index for gypsum, calcite and dolomite along the aquifer depth calculated with PHREEQC.

In order to verify if gypsum dissolution could occur, the related saturation index (SI) has been calculated (Fig. 4.4). Negative saturation index (SI) values of gypsum for all samples (Fig. 4.4) suggest that the occurrence of gypsum as the major source of SO_4^{2-} in groundwater is not likely. The most probable source of high SO_4^{2-} detected in brackish groundwater is the temporary oxidation of pyrite Fe_2S or amorphous FeS due to water fluctuation and temporary exposure to O_2 -rich waters that have characterized the geomorphologic evolution of this area. Furthermore, Vandenbohede and Lebbe (2012) and Stuyfzand and Stuurman (2008) have shown that brackish and salt relict Holocene transgression waters, which must have infiltrated in low energy areas protected from direct incursions by the sea, allowing abundant contact with clay and peat, are characterized by high alkalinity combined with extremes in SO_4^{2-} reduction due to the oxidation of organic matter. Many samples in the dataset have high HCO_3^- concentration and SO_4^{2-} concentration significantly lower than the freshwater-saltwater mixing line, indicating the presence of brackish and salt relict transgression waters in the aquifer. This hypothesis is in agreement with the presence of brackish water marshes between 3300 and 2000 BP (Stefani and Vincenzi, 2005), the high organic matter content of the sediment, and the occurrence of peat layers in large part of the aquifer.

The comparison between the major ions (Br^- , Na^+ , SO_4^{2-} and Mg^{2+}) of groundwater samples, seawater (Adriatic Sea) and freshwater end-members (irrigation canals), displays a mismatch and deviations from the mixing line (purple line in Fig. 4.5). Br^- vs Cl^- plot suggests a salinization mechanism, which follows an evaporation trend rather than a mixing between freshwater and marine waters (Fig. 4.5a). Deviations from the mixing line are also observed for Na^+ in the most saline samples (Fig. 4.5b): the observed excess and deficit with respect to the non-reactive mixing may be due to cation-exchange processes occurring in the aquifer.

RESULTS AND DISCUSSION

SO_4^{2-} vs Cl^- concentrations show SO_4^{2-} depletion (Fig. 4.5c) indicating SO_4^{2-} reduction in all monitoring wells, except for samples of P3 and shallow groundwater samples of P34. SO_4^{2-} depletion is commonly observed in aquifers affected by seawater intrusion (Andersen et al., 2005). In many cases it can be attributed to SO_4^{2-} reduction processes. The supply of reactive organic C required for SO_4^{2-} reduction derives from the peat layers enriched with organic matter found in the aquifer. This result agrees with the strong and typical smell of H_2S noted in the field during groundwater sampling and with measured concentrations of up to 50 mg/l of dissolved H_2S in P34 (not shown). Mg^{2+} excess in Fig. 4.5d is likely explained by $\text{Ca}^{2+}/\text{Mg}^{2+}$ exchange due to elevated carbonate and dolomite minerals, which are abundant in this alluvial aquifer (Amorosi et al., 2002), as confirmed by CaCO_3 and $\text{MgCa}(\text{CO}_3)_2$ SI (Fig. 4.4).

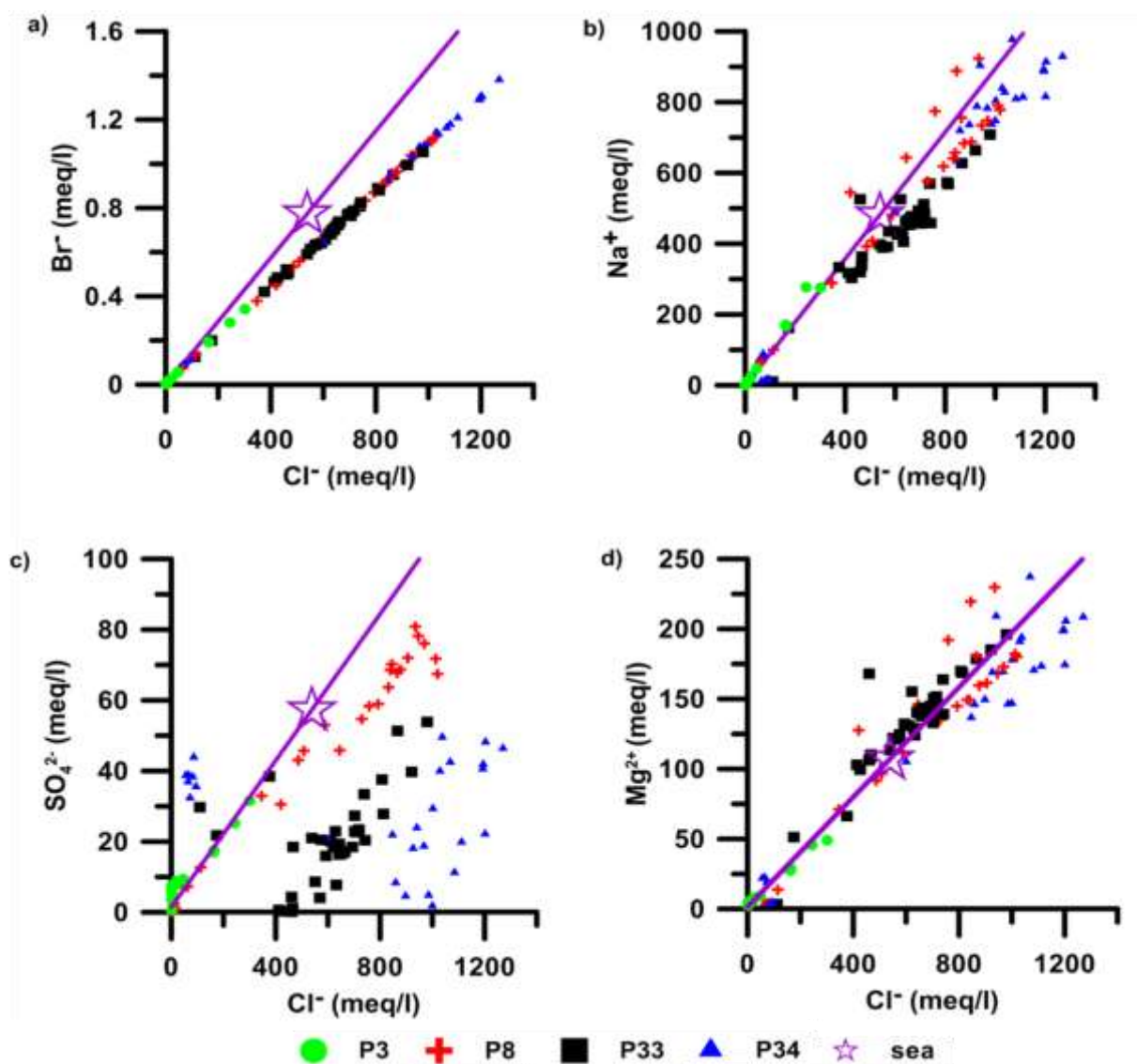


Figure 4.5 - Plots of the concentration of Br^- , Na^+ , SO_4^{2-} , and Mg^{2+} with respect to Cl^- . The purple lines indicate the non-reactive mixing line between freshwater and modern seawater; the star symbol indicates the concentration of the modern Adriatic Sea water.

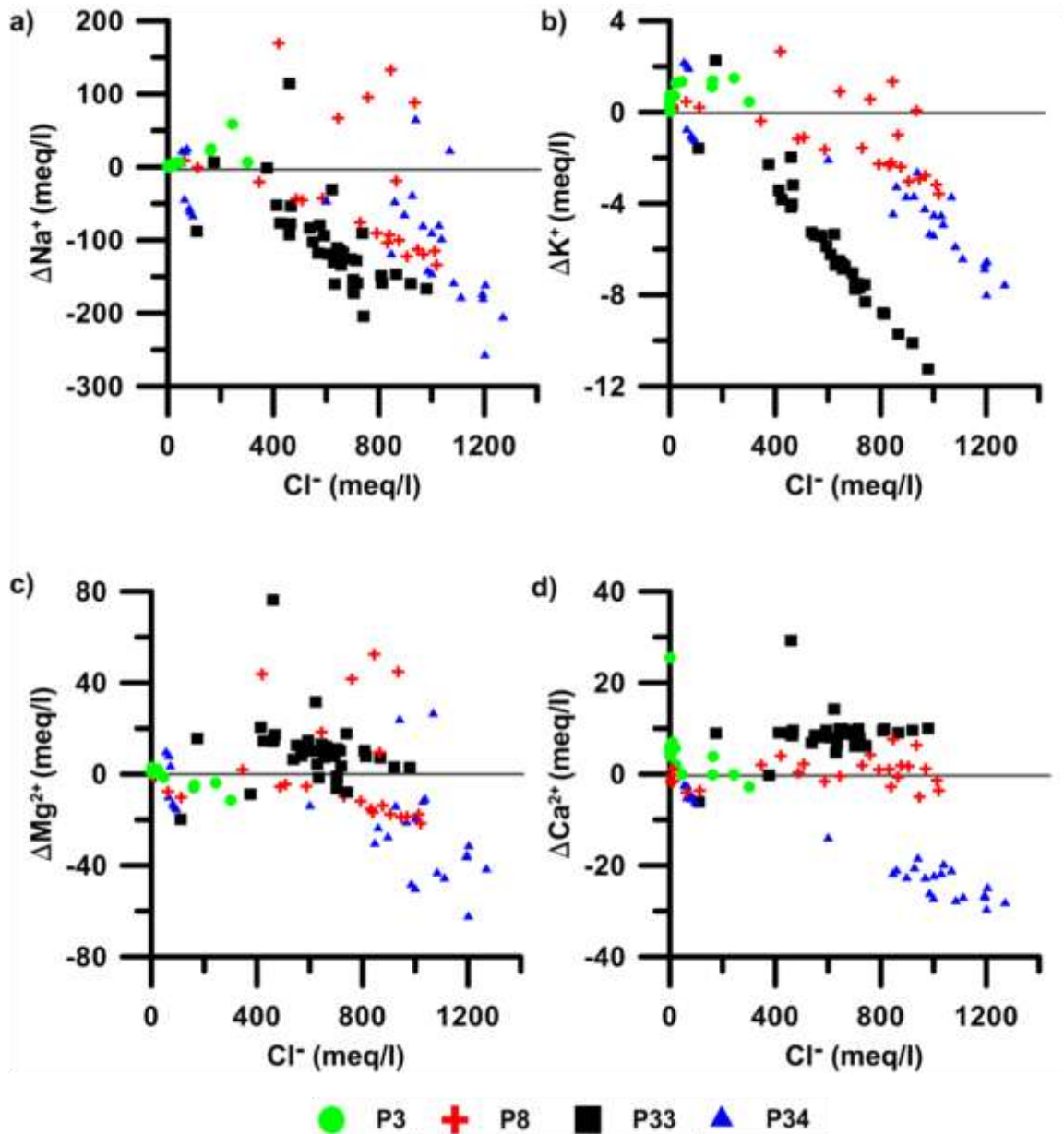


Figure 4.6 - Variation of sample concentration of Na^+ , K^+ , Mg^{2+} and Ca^{2+} with respect to the theoretical composition expected for a non-reactive mixing of Adriatic seawater and freshwater. Note: positive values indicate enrichment, while negative values indicate depletion.

The comparison between the major cation composition of groundwater samples and the theoretical composition expected for a non-reactive mixing between the two end-members (Adriatic Sea water and freshwater of irrigation canals) (Andersen et al., 2005; Appelo and Postma, 2005; Capaccioni et al., 2005; Ghiglieri et al., 2009), allows highlighting exchange processes within the aquifer. Most of the samples show Na^+ deficit (ΔNa^+) compared to the non-reactive model (Fig. 4.6a). The depletion is high and comes up to -260 meq/l for the most saline samples (P34); only occasional Na^+ enrichment can be observed. K^+ and Mg^{2+} depletion (ΔK^+ and ΔMg^{2+}) is observed together with Na^+ depletion (up to -11 meq/l for K^+ and -62

meq/l for Mg^{2+}). On the other hand, Ca^{2+} values show a general enrichment (ΔCa^{2+}), except for P34 that shows Ca^{2+} depletion. The cation exchange process, which is a common process during saltwater intrusion in coastal aquifers in presence of exchangers (Andersen et al., 2005; Appelo and Postma, 2005), most likely explains the relative Ca^{2+} excess, the Na^+ and K^+ depletions. The sandy-clayey and sandy-silty matrix could be the cation exchanger, but the organic matter layers also have a higher cation exchange capacity (Appelo and Postma, 2005) and appear as the most likely exchanger in the transect.

The Ca^{2+} contribution from the cation exchange (Fig. 4.6d), the variation of Mg^{2+} concentration (Fig. 4.6d, and 4.6c) as well as the HCO_3^- increase (Fig. 4.3) from SO_4^{2-} reduction should affect the carbonate equilibrium, causing oversaturation with regard to calcite and dolomite, as confirmed by SI in Fig. 4.4 (de Montety et al., 2008).

These results highlight that each single cation concentration is determined by the whole equilibrium of many concurrent water-rock reactions. The ionic exchange intervenes as a buffer by tending to adjust for variations of chemical composition induced by the increase in salt content: such occurrence leads to feedback loops, producing strong changes of hydrochemical facies with respect to those indicated by non-reactive mixing. Precipitation phenomena, in this context, occur more particularly where salinity is high.

4.1.3 The origin of the salinization processes

The Ferrara coastal aquifer shows TDS values variable from a minimum of 0.47 g/l to a maximum of 74 g/l. The TDS versus depth scatter plot (Fig. 4.7) does not show a preferential trend and the data are scattered all over the graph.

The freshwater samples grouped on the left side of the graph belong to the monitoring well P4, whose TDS is between 0.47 and 0.55 g/l: these values testify the freshening of the local groundwater due to inflow from the Po River, located just 200 m away from the sampling point (see Fig. 2.2 for location). Low TDS are registered also in the monitoring well P9, located within a recent dune system, and in the monitoring well P7 due to the great amount of fresh water historically discharged into this area for rice cultivation. Shallow freshwater lenses, 2-4 m thick, are also found close to irrigation canals in P8 and in correspondence of topographic highs such as modern coastal dunes along the shoreline and palaeo-dunes, like in P3 and P5 (see Fig. 2.2 for location). The deepest portions of P3, P5 and P7 display brackish groundwater, which is also present in the top portions of the monitoring wells P2 and P34. Saline waters were found over the whole profile in P1 that is just 300 m away from the shoreline, and in the bottom portions of P2 and P3. Hypersaline groundwater was found at the bottom of P10, P8 and P33, with TDS ranging between 38 and 62 g/l. The highest TDS was found in P34 with values up to 74 g/l. In general TDS values increase with depth, because of the interaction between groundwater and the fine sediments of the deepest part of the coastal unconfined aquifer that were deposited in a back-barrier environment.

RESULTS AND DISCUSSION

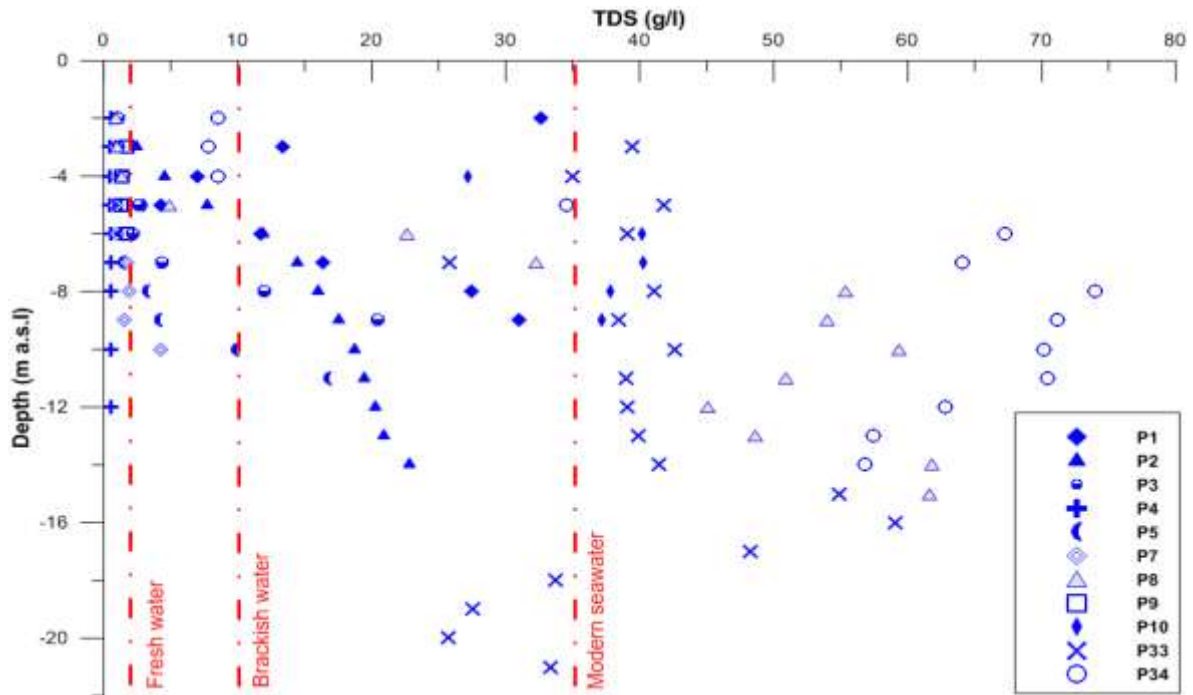


Figure 4.7 - TDS versus Depth, for 11 monitoring wells sampled via MLS technique. Water quality classes are drawn according to Davis and De Wiest (1996).

As an example the distributions of TDS with depth along the A-A' transect (Fig. 2.2) is shown in figure 4.8. There are no significant differences between the two monitoring campaigns carried out in June and November 2011; only the thickness of freshwater lenses varies of 0.5-1 m, while the high TDS values continue characterizing the entire coastal aquifer.

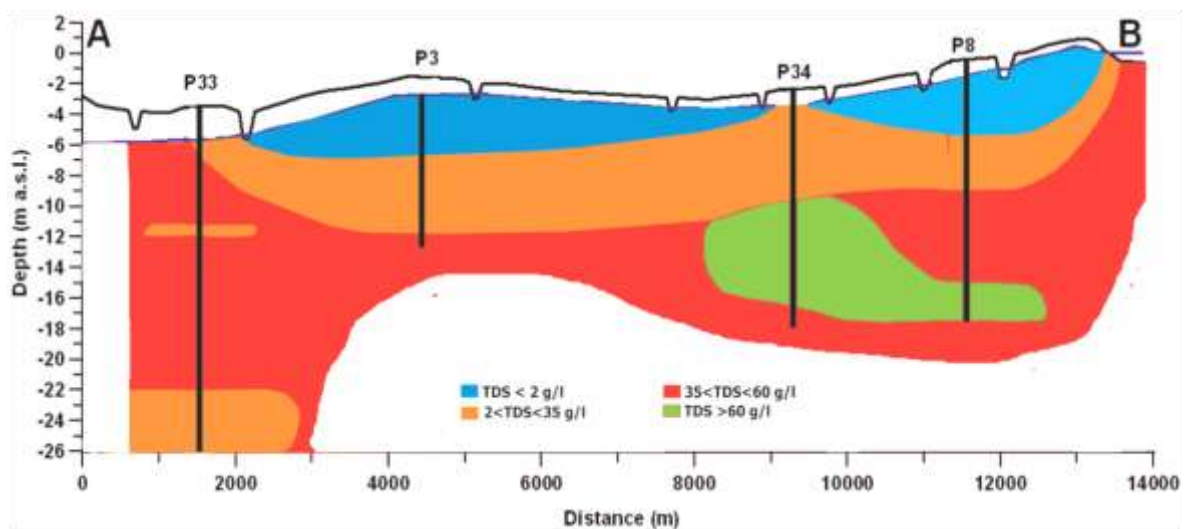


Figure 4.8 - TDS distribution along the A-A' transect of the coastal aquifer.

To investigate the origin of the high salinity of groundwater, Cl^- and Br^- have been used as natural tracers. In particular, their molar ratios plotted versus Cl^- concentrations could be a good indicator of groundwater origin as recently proposed by Hoque et al. (2014). Cl^- and Br^- in groundwater are tracers close to ideal conservative behaviour due to their hydrophilic character and small ionic size. Moreover, they do not take part in significant ion exchange reactions at low temperatures, nor are adsorbed onto mineral surfaces (Davis et al., 1998). The major reservoir of water (the ocean) has relatively uniform Cl^- and Br^- concentrations and their molar ratio is around 655 ± 4 (Alcalà and Custodio, 2008); however, for the study area the observed Cl^-/Br^- Adriatic Sea molar ratio is 696 ± 47 . This value is slightly higher than the ones reported by other authors, but it can be explained by seawater dilution near the delta due to freshwater input from the Po River branches (Artegiani et al., 1997).

Bromide and chloride data have been compared with those defined by the mixing line of seawater (Adriatic Sea) and freshwater end-members (irrigation canals). Given the inherent variability of TDS in both the end-members, a mixing area rather than a simple mixing line was constructed using the variance of 21 samples collected from 2010 to 2014 (Fig. 4.9, right panel).

The Cl^-/Br^- versus Cl^- plot (Fig. 4.9, left panel) shows that most of the samples are above the Adriatic Sea water (local) value: freshwater samples show Cl^-/Br^- molar ratios highly variable from 192 to 1440, while brackish, saline and hypersaline samples show almost constant Cl^-/Br^- molar ratios of 870 ± 70 , higher than in local seawater. The highest values of Cl^-/Br^- in the freshwater samples belong to the monitoring well P9, which is located within the residential area of Lido di Spina: this suggests that Cl^-/Br^- values are imputable to the presence of urban wastewater. The lowest values of Cl^-/Br^- in the freshwater samples belong to P7: considering P7 location, such values are ascribable to agricultural pollution due to rice cultivation. P4 values are typical of recharge waters from inland areas and show a perfect correspondence with the freshwater end-member, thus confirming the inflow from the Po River; the freshwater samples from the top portion of P3, P5 and P8 have Cl^-/Br^- molar ratios that seem to point to an ideal mixing between freshwater and an end-member that could be reasonably identified in the local bulk deposition (wet and dry) with Cl^-/Br^- molar ratios of 930 ± 66 , owing to the chemical fractionation during evaporation of sea droplets generated by winds. Cl^-/Br^- molar ratio in bulk deposition controls the Cl^-/Br^- ratios in groundwater since the water table in this coastal area is shallow and consequently the recharge water has a short residence time in the unsaturated zone: physical processes taking place in soil (dilution, evapotranspiration and mixing) do not significantly modify the Cl^-/Br^- ratio, but can change the absolute concentrations of Cl^- and Br^- (Alcalà and Custodio, 2008; Edmunds, 2001). This behaviour characterizes both shallow and deep groundwater; on one hand, in fact, P1 samples show molar ratios up to 888, but with absolute concentrations of Cl^- up to 18.700 mg/l and Br^- up to 47 mg/l, and, on the other hand, the samples from the deep portions of P33 and P34 show molar ratios up to 925, but with absolute concentrations of Cl^- up to 45.000 mg/l and Br^- up to 110 mg/l. From the general trend of all the collected MLS samples, it is evident that salinization is not due to mixing with present seawater, even in monitoring wells located close to the coastline, like P1.

In fact, the line representing the Adriatic Sea water Cl⁻/Br⁻ molar ratio is located above and below the trend individuated by groundwater samples (Fig. 4.9, left panel). Moreover, the Br⁻ versus Cl⁻ plot (Fig. 4.9, right panel) has a good correlation, indicating a similar origin for the two ions.

The Cl⁻/Br⁻ ratio is constant during seawater evaporation. At the onset of halite or other chloride mineral precipitation, bromides preferentially are left in residual seawater: under continuous evaporation, while the Cl/Br ratio of the residual brine progressively decreases, precipitated minerals develop elevated Cl/Br ratios (Stueber and Walter, 1991). Consequently, leaching of evaporite would produce groundwater with Cl⁻/Br⁻ ratio higher than the seawater; on the contrary, mixing with brines will lead to Cl⁻/Br⁻ ratios in groundwater lower than seawater. The Cl⁻/Br⁻ ratio less than 1000 shown by waters of high salinity cannot be explained by only dissolution and leaching of salts: these values of the ratio probably derive from both dissolution of salts and mixing with residual brines found in the deepest part of the aquifer. They were most probably formed in back barrier inter-basins during the Holocene transgression. The residual brines and evaporite salts have been probably preserved from flushing being trapped into fine-grained sediments, thus forming saline inter-layers, which in turn led to the formation of saline and hypersaline groundwater (Lorenzen et al., 2012).

The inverted head gradient created by the constant pumping of the drainage network has mobilized and slowly transported upward these saline waters preserved in the deepest portion of the aquifer within low permeability sediments (Giambastiani et al., 2013).

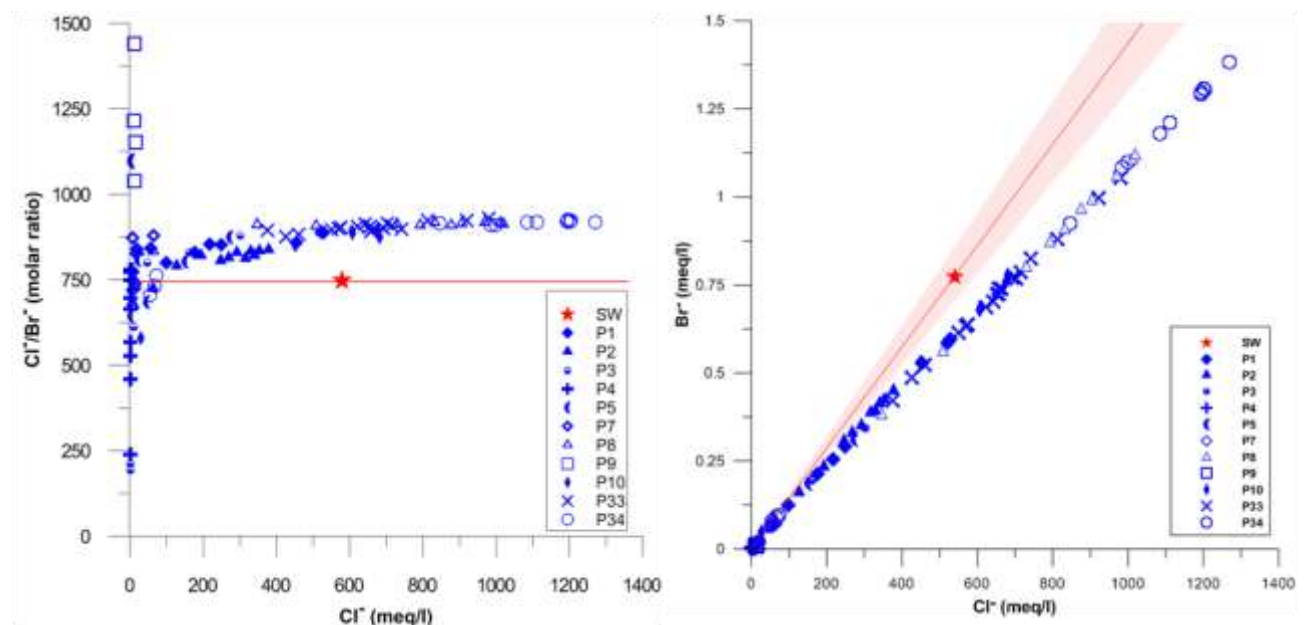


Figure 4.9 - Plot of Cl⁻/Br⁻ molar ratio versus Cl⁻ (meq/l) for the groundwater samples (left panel). Plot of Br⁻ versus Cl⁻ (meq/l) for the groundwater samples (right panel). Red lines indicate the ideal mixing line between freshwater and present Adriatic seawater, while the red shaded areas represent the mixing area.

To confirm what discussed so far, figure 4.10 shows that evaporation plays an important role in the evolution of the majority of groundwater samples collected both via MLS and IDS techniques. In particular, samples collected in P33 and P34 are grouped in the top right area of the Gibbs diagrams: this testifies a considerable role of evaporation in the geochemical evolution of saline water that lead to TDS concentration up to 74 g/l. Samples from P1, P2, P8 and P10 also have a clear evaporative trend, especially evident in the deepest samples. On the other hand, P4 and the top part of P5 and P7 samples fall in the water-sediment interaction area of the Gibbs diagrams. These samples, affected by freshwater both from the Po River and irrigation, have a weight ratio of $\text{Na}^++\text{K}^+/(\text{Na}^++\text{K}^++\text{Ca}^{2+})$ up to 0.6 mg/l and a low weight ratio of $\text{Cl}^-/(\text{Cl}^-+\text{HCO}_3^-)$, which indicate that cation exchange with the clay minerals present in the aquifer matrix played a role by increasing Na^+ and K^+ and decreasing Ca^{2+} under the background of water-sediment interaction dominance. The low values of $\text{Cl}^-/(\text{Cl}^-+\text{HCO}_3^-)$ weight ratio are imputable to an excess of bicarbonate more due to the organic matter mineralization processes, which cause an increase in alkalinity, rather than to the dissolution of carbonates present in the aquifer matrix.

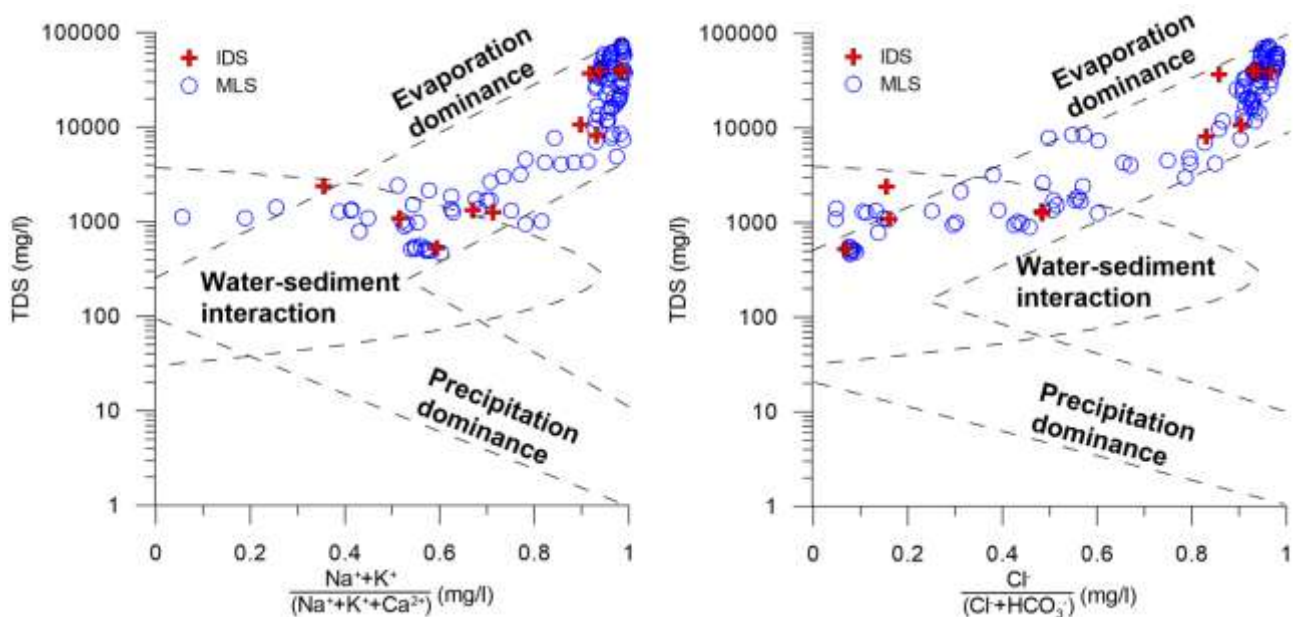


Figure 4.10 - Gibbs diagrams for cations (left panel) and anions (right panel).

4.2 The importance of data acquisition techniques in saltwater intrusion monitoring

The delineation of the results gained from the fulfilment of the first objective of this thesis, i.e a detailed vertical characterization of the Ferrara coastal aquifer to monitor salinity distribution. Different approaches exist to perform a depth-dependent characterization of an aquifer.

This paragraph illustrates the application of three different monitoring and sampling techniques to the coastal aquifer of Ferrara: the open-borehole logging (OBL), the integrated-depth sampling (IDS) and the multi-level sampling techniques (MLS) via straddle packers. The OBL led to a satisfactory reconstruction of the extent of the fresh-saltwater interface, but provided a misleading characterization of the distribution of redox environments within the aquifer. The IDS conceptual model individuates present seawater intrusion as the active phenomenon, given that measured Cl^- concentrations never exceed that of seawater and there is no indication of hypersaline groundwater all over the study area. On the contrary, good fit among sedimentological, stratigraphical and physical-chemical data were obtained using the MLS. In fact, in the MLS conceptual model the lower portion of the unconfined aquifer presents hypersaline groundwater: this finding constrains to consider salinization processes other than seawater intrusion, like the water/sediment interaction or the geochemical evolution of groundwater due to evapo-concentration.

This study demonstrates that, within coastal shallow aquifers evenly recharged by irrigation canals, the simple and economical OBL and IDS technique can lead to misleading results when used to characterize density dependent groundwater stratification. Thus, results entail the need of using MLS in reconstructing a reliable conceptual model, especially in areas where the density contrast between fresh and saline groundwater is large.

4.2.1 Open-Borehole Logging and Multi-Level Sampling

Figure 4.11 shows the salinity profiles for the four monitoring wells along transect A-A' (Fig. 2.2). Considering both OBL and MLS profiles, the aquifer displays fresh water (salinity <0.5 g/l) in the uppermost section of P3 and P8, from the top of the water table down to -9 and -6 m a.s.l. respectively, and a transition zone of brackish water (from 0.5 to 30 g/l) with a thickness ranging from 1 to 4 m. Finally, saline (from 30 to 50 g/l) to hypersaline (>50 g/l) water is present in the remaining thickness of the aquifer. Overall, the absolute salinity residual for all the monitoring wells is 4.31 g/l and the R^2 is 0.92, which is deemed as acceptable goodness of fit between the two techniques. Since the two different acquisition techniques, i.e. the OBL and MLS methods, give approximately the same classification and distribution of the water types in the aquifer, it follows that the OBL method can be successfully used for a preliminary determination of the position of the freshwater/saltwater interface in aquifers with normal density stratification (freshwater near the water table and saline groundwater towards the bottom). Nevertheless, analysing in more detail the OBL salinity profiles against the MLS profiles, some considerable differences are apparent. In P8 and P34 the OBL technique displays a somewhat constant concentration profile in the lower part of the aquifer where hypersaline water is present. The MLS technique on the other hand, is able to distinguish in both monitoring wells a considerable variability in the concentration profiles. In particular, the salinity distribution in P8 slowly increases from saline (-8 m a.s.l.) to hypersaline water (-17 m a.s.l.), showing salinities always lower than the ones recorded at the same depths by OBL.

RESULTS AND DISCUSSION

In the hypersaline bottom part of the aquifer the deviation of the MLS profile from the OBL profile is even more evident; in P34 the MLS profile shows a correlation between the salinity distribution and the stratigraphy, witnessing water-sediment interactions. Accordingly, in P33, the MLS profile demonstrates that the change in sediments reflects a change in salinity: at -20 m a.s.l. salinity increases up to 53 g/l in correspondence with a peaty layer.

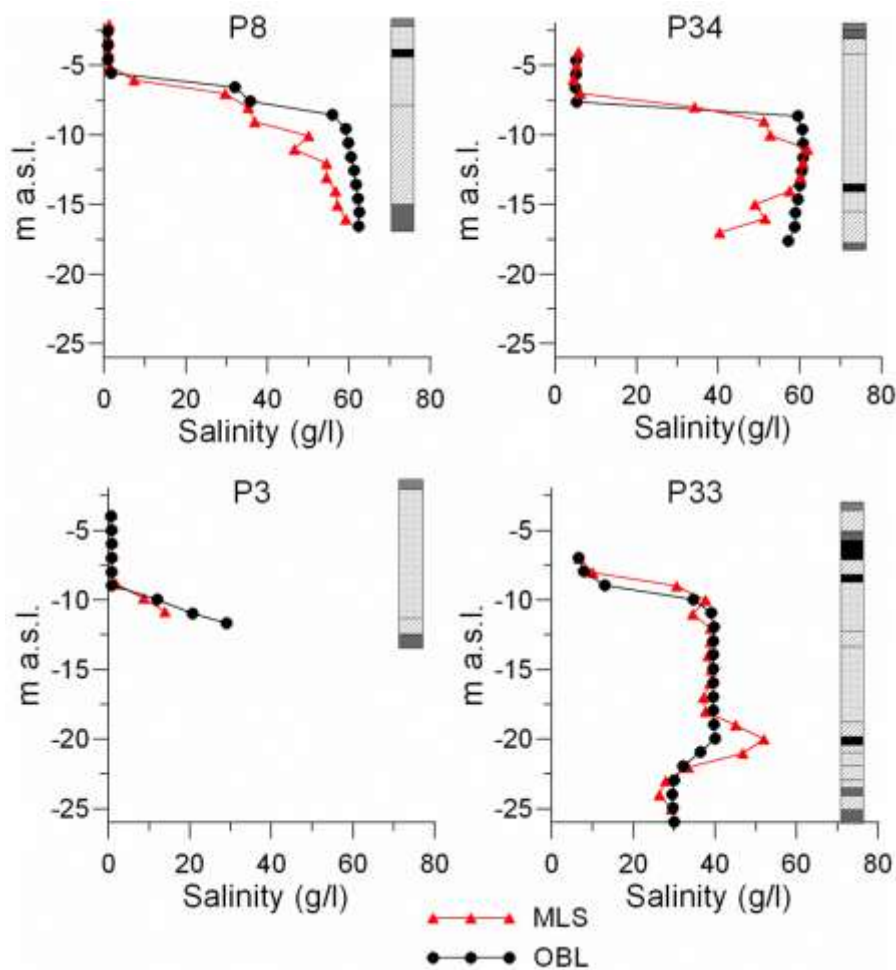


Figure 4.11 - Plots of salinity with MLS versus OBL data for each monitoring well along A-A' transect (see Fig. 2.2 for location); stratigraphy (core logs data) is displayed on each plot to assist the interpretation.

The misleading distribution of salinity values above seawater concentration recorded via the OBL technique is thought to be due to both the mixing of water into the monitoring wells induced by the density dependent flow and to the downward and upward movement of the probe within the borehole casing during the monitoring procedure. These biases are obviously avoided using the MLS techniques. As for the salinity values above seawater concentration, the OBL and MLS techniques present a discordant picture of the physico-chemical parameter profiles of the coastal shallow aquifer.

RESULTS AND DISCUSSION

Fig. 4.12 describes pH profiles collected via OBL and MLS techniques. The profiles are not in good agreement, with an absolute residual for all monitoring wells of 0.37 and a R^2 value of 0.72. The pH measured by MLS is regularly higher than the one measured by the OBL technique, even if in both cases the ambient groundwater is characteristic of the basic environment. A sharp pH change is recorded with the OBL technique at the fresh-saltwater interface. On the contrary the MLS profiles display smoother and more regular changes, which can be directly related to recharge from the canals (having a typical pH around 8.4) and to the stratigraphy (i.e. in P8 where the sudden increase in pH is imputable to the presence of a peat layer). From Fig. 4.12 it is clear that the pH observed with the OBL technique reflects the pH of the stratified water column accumulated in the monitoring well, but it is not strictly representative of the aquifer pH.

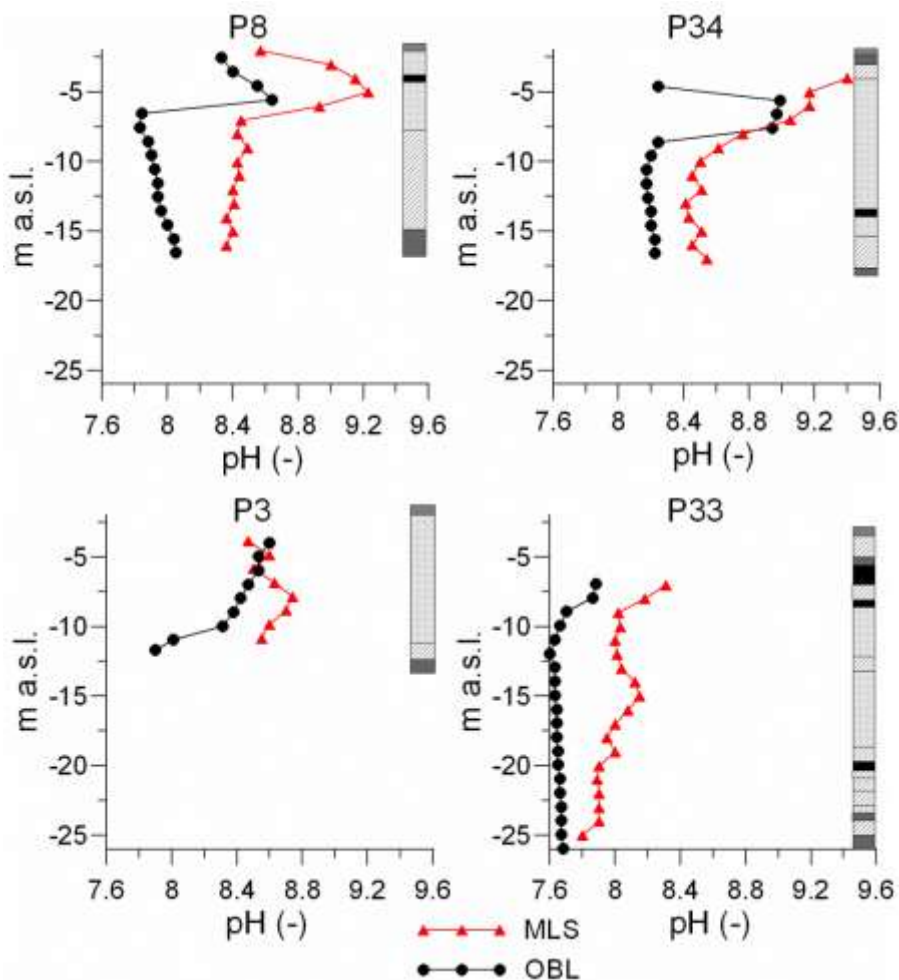


Figure 4.12 - Plots of pH with MLS versus OBL data for each monitoring well along the A-A' transect (see Fig. 2.2 for location); stratigraphy (core logs data) is displayed on each plot to assist the interpretation.

Fig. 4.13 shows the Eh profiles for the selected monitoring wells. Here the discrepancy between the OBL and MLS technique is even more pronounced, with an absolute residual for all the monitoring wells of 0.76 mV and a R^2 value of 0.22.

The profiles are not only different with respect to the registered absolute values, but the trends recorded by the two different techniques do not coincide as well. In P33 the most negative Eh values coincide with sampling depths at which a strong smell of H_2S was detected during the sampling procedure: thus it means that sulphate reduction probably takes place at levels where labile organic matter is present. As for the previously discussed Eh values, the agreement between OBL and MLS techniques in O_2 measurement is very low, with an absolute residual for all the monitoring wells of 0.25 mg/l and a R^2 value of 0.47.

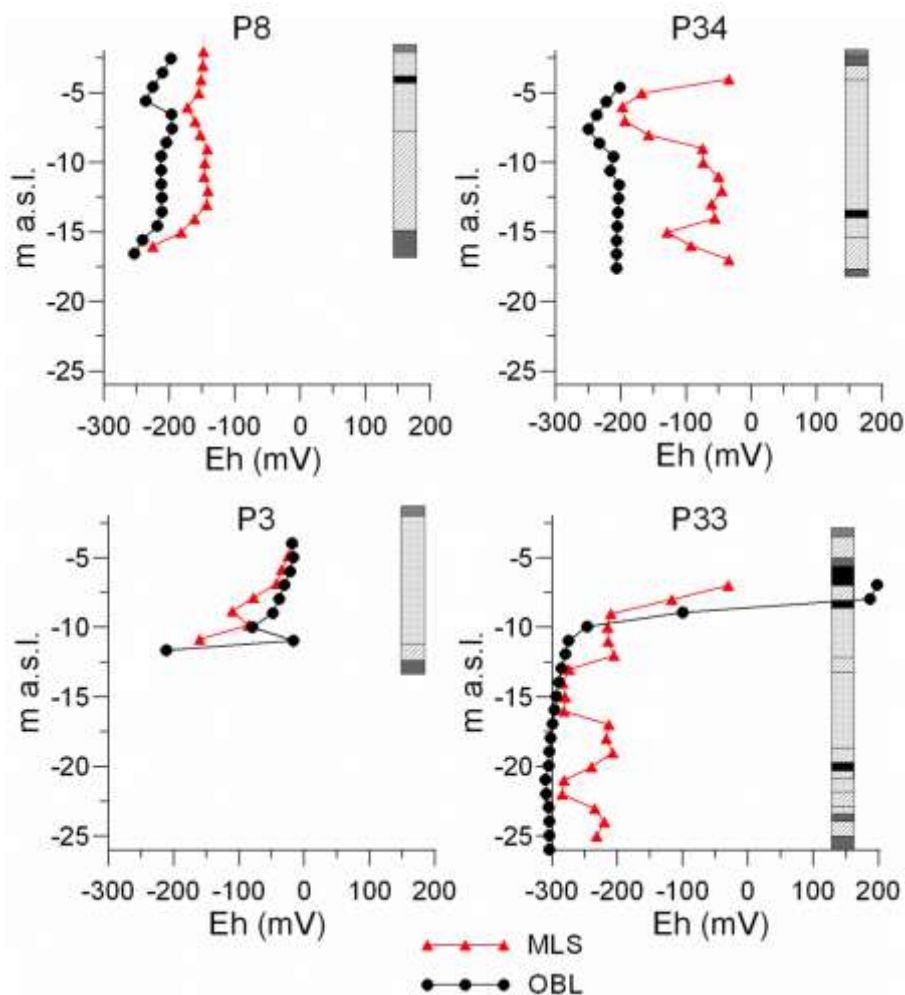


Figure 4.13 - Plots of Eh with MLS versus OBL data for each monitoring well along the A-A' transect (see Fig. 2.2 for location); stratigraphy (core logs data) is displayed on each plot to assist the interpretation.

RESULTS AND DISCUSSION

In agreement with the measured negative Eh, the O₂ concentration is always very low in all monitoring wells (Fig. 4.14). Generally, the O₂ concentration recorded via MLS is always higher at the top of the aquifer compared to concentration measured by the OBL technique. Oxidic conditions in the upper part of the aquifer are due to direct recharge from the canals network, usually showing O₂ concentration around 5 mg/l. O₂ concentration recorded via MLS decreases more rapidly with depth with respect to OBL, reaching anoxic condition in a range from 1 to 3 m below the water table. In the same time anoxic values are recorded between 4 to 7 m below the water table with the OBL technique.

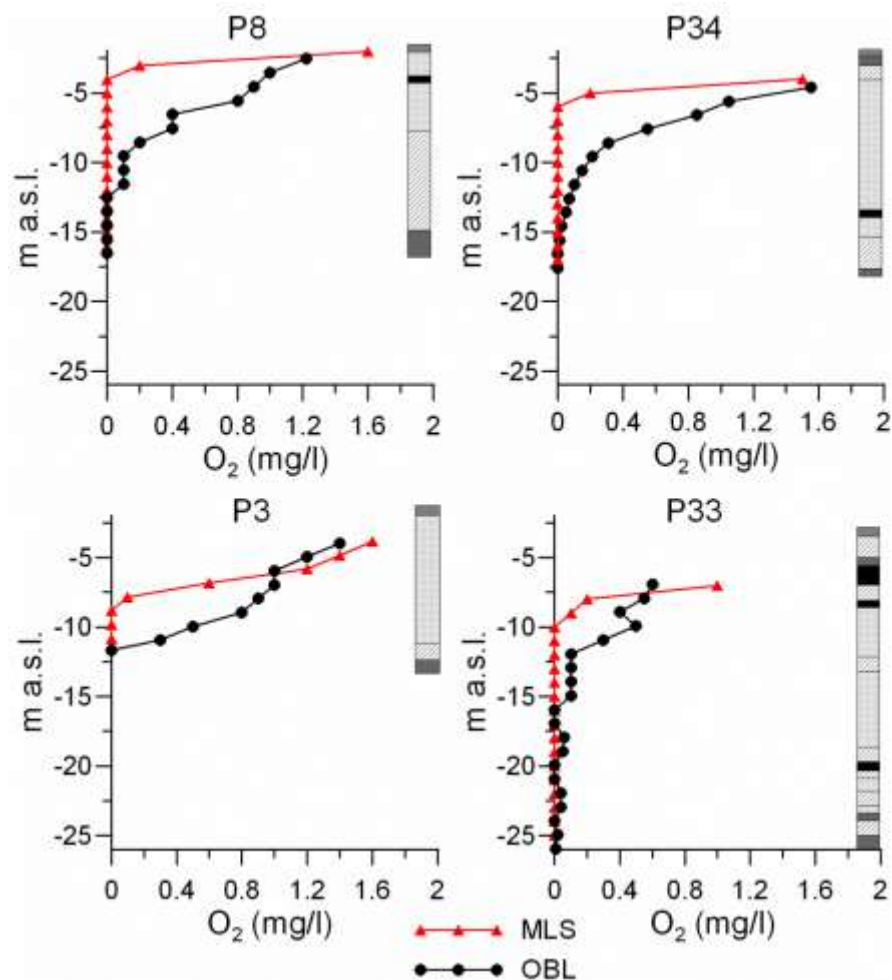


Figure 4.14 - Plots of O₂ with MLS versus OBL data, for each monitoring well along the transect A-A' (see Fig. 2.2 for location); stratigraphy (core logs data) is displayed on each plot to assist the interpretation.

The profiles of above reactive sensitive physico-chemical parameters (Figs. 4.12, 4.13 and 4.14) recorded via OBL and MLS techniques give a conflicting picture of the coastal shallow aquifer, as for the salinity values above seawater concentration (Fig. 4.11). This means that along the A-A' transect, even if the two different acquisition techniques give approximately

the same classification and distribution of the water types in the aquifer, the OBL method cannot be employed to characterize in detail the effects due to interactions between surface and ground waters. The OBL method demonstrates inappropriate in defining the trend in redox processes occurring within the aquifer, especially in correspondence with sediments bearing a high content of labile organic matter.

4.2.2 Integrated-Depth Sampling and Multi-Level Sampling

With respect to the comparison of IDS and MLS techniques, it is worth to note that the TDS concentration in IDS samples never exceeds 40 g/l within the saline groundwater zone, thus failing in the highlight of the presence of hypersaline water types at the bottom of the unconfined aquifer (Fig. 4.15).

Accordingly, the IDS technique is not capable to address the high variability of Eh with depth, thus preventing from recognizing the different terminal electron acceptor processes (TEAP) taking place within the aquifer (Fig. 4.16). IDS technique displays Eh values usually higher than MLS ones; an exception is given by the monitoring well P34, where silt and peat layers constitute the first meters of the unconfined aquifer. MLS plots of Eh versus depth show a general reducing condition into the aquifer with increasing Eh at increasing depth (Colombani et al., 2015c).

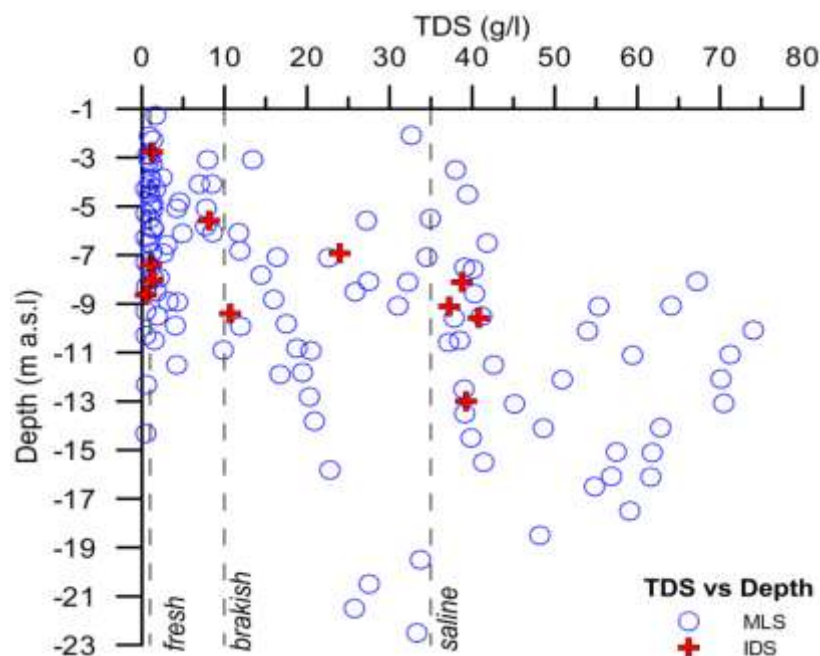


Figure 4.15 - TDS versus Depth, blue circles indicate the MLS samples and red crosses indicate the IDS samples. Water quality classes are drawn according to Davis and De Wiest (1996).

RESULTS AND DISCUSSION

The more superficial levels tend to be more oxygenated, becoming anoxic moving downward; in particular this is evident in the monitoring well P5 that passes from the initial oxidizing conditions to reducing conditions. This behaviour is caused by the presence in the sediments of the coastal Ferrara plain of large quantities of organic matter due to the geomorphological history of this deltaic environment (Stefani and Vincenzi, 2005).

In fact, it is generally observed in natural environments that the oxygenated water that enter an aquifer rich in organic matter will first be depleted in oxygen content and nitrate, subsequently iron is reduced and finally sulphate reducing condition and methane may appear in the water (Appelo and Postma, 2005).

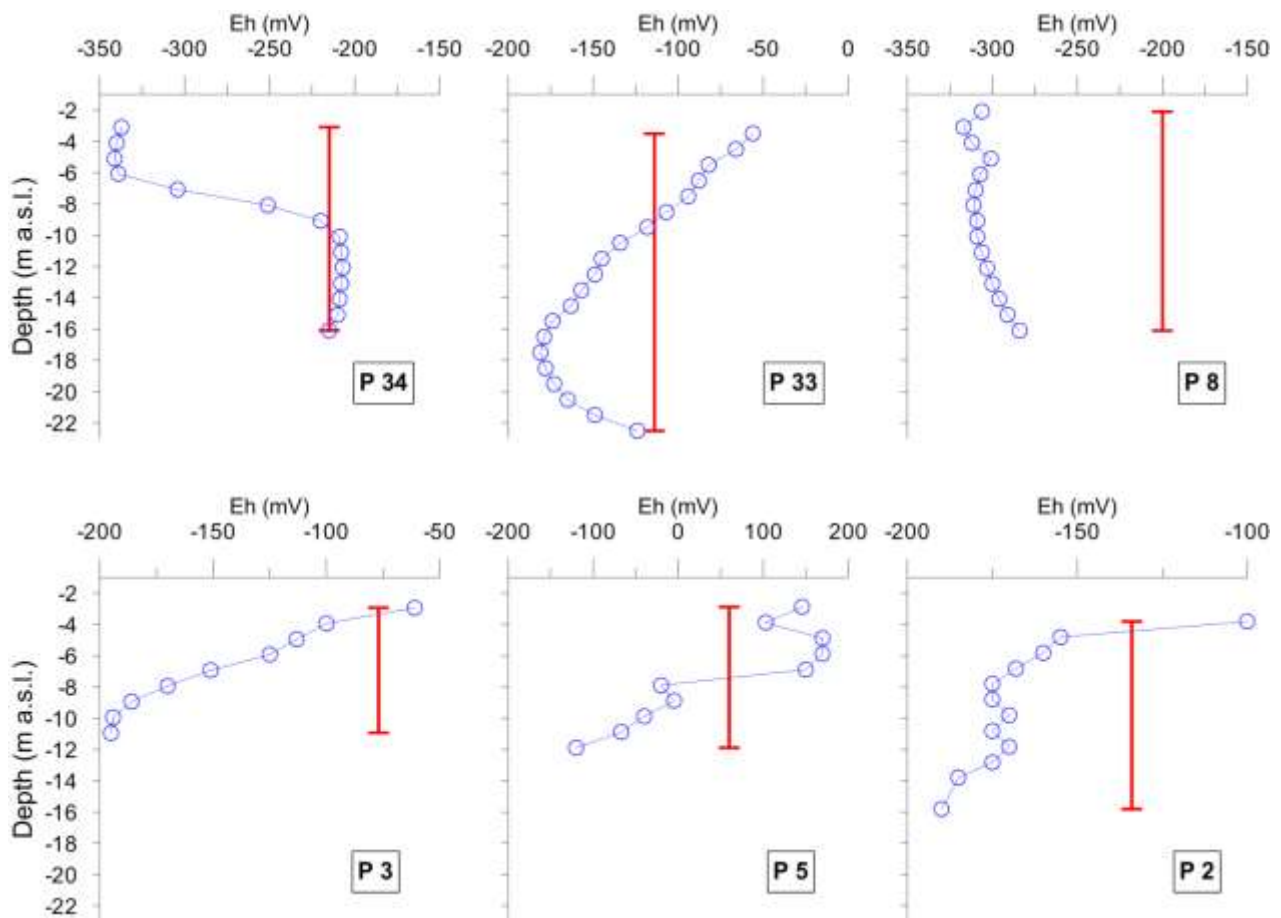


Figure 4.16 - Eh versus depth for selected monitoring wells. Blue circles indicate the MLS values and red lines indicate the IDS values.

The Eh versus pH diagram (Fig. 4.17) can be a helpful tool to distinguish between different TEAP. The main TEAP derived using MLS data are iron, sulphate reducing and methanogenic conditions, which are commonly observed in aquifers affected by seawater intrusion (Andersen et al., 2005). On the other hand, the IDS samples depict nitrate, manganese and iron reduction as the main TEAP, disregarding sulphate reduction and methane production.

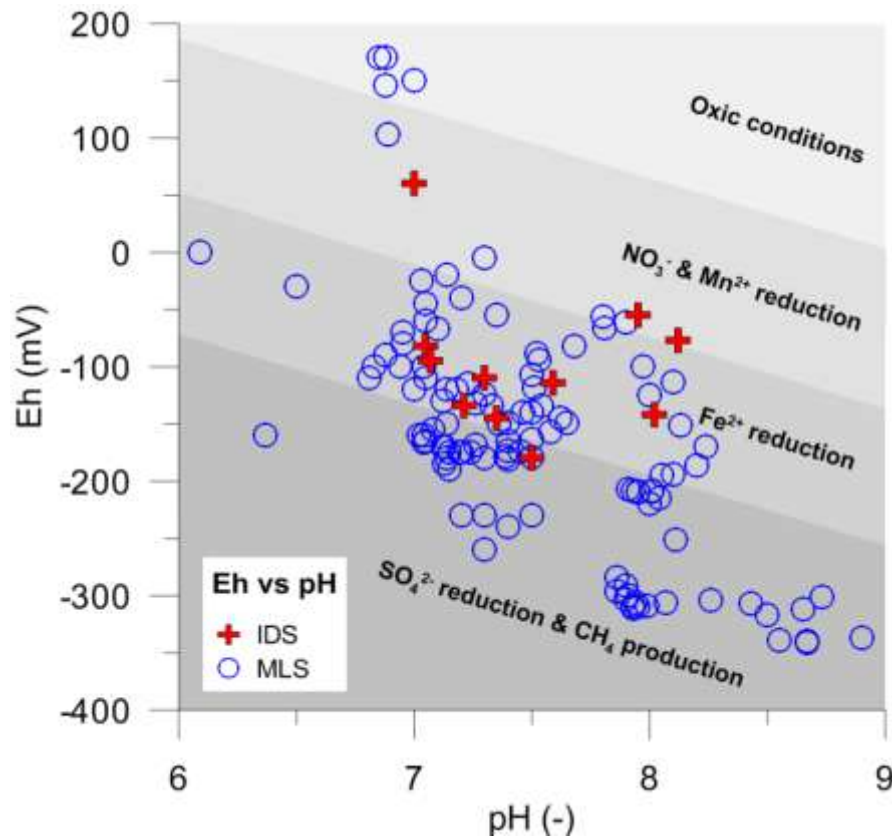


Figure 4.17 - Eh versus pH plot. Grey shaded areas identify the main TEAP environments.

4.2.3 Discrepancy between an integral-depth and a depth-dependent monitoring

From the foregoing reasoning it is clear that IDS and MLS techniques often give conflicting information. In order to quantify the differences, Table 4.3 and Table 4.4 report the discrepancies between MLS and IDS values concerning the major ions concentrations in groundwater and the aquifer physical-chemical parameters.

In Table 4.3, nitrate discrepancy has an average value of 141%, with a maximum of 187%; the phosphate discrepancy has an average of 95%, with a maximum of 188%. For these reactive species, the artificial mixing induced by the IDS technique within the long screen wells is therefore detrimental. On the other hand, calcium discrepancy is lower than previous ones, with an average value of 44% and a maximum of 92%. This behaviour is due to pH buffering, which involves precipitation/dissolution processes of calcite and dolomite, abundant in the Ferrara aquifer matrix. Chloride discrepancy shows a high value in P8 (150%) since the TDS distribution registered by the MLS technique is extremely variable and increases progressively with depth, from 0.9 mg/l at the aquifer to 61.8 mg/l at the aquifer bottom, while the IDS technique just gives a TDS value of 37.2 mg/l throughout the whole depth of the monitoring well.

RESULTS AND DISCUSSION

Table 4.3 - Discrepancy between MLS and IDS values concerning the major ions, the symbol – is used when concentrations are below detection limit.

	Chloride (%)	Sulphate (%)	Nitrate (%)	Phosphate (%)	Sodium (%)	Ammonium (%)	Calcium (%)
P1	81±70	46±56	187±36	-	72±72	94±65	33±45
P2	63±72	167±110	154±30	-	65±78	125±124	63±37
P3	134±132	71±92	-	152±175	132±141	55±76	48±44
P4	14±8	46±61	-	36±38	9±10	25±22	9±6
P5	87±99	39±43	175±76	92±107	81±91	171±19	41±33
P7	50±64	42±48	109±120	89±107	57±70	86±101	27±31
P8	150±142	161±145	-	155±92	146±134	76±73	92±86
P9	19±17	80±25	94±76	188±176	19±23	46±59	32±5
P10	39±75	31±43	96±58	51±59	47±69	48±82	39±24
P33	19±24	56±75	-	16±24	15±22	24±32	15±22
P34	75±94	54±71	171±79	74±94	88±100	89±97	68±82

Table 4.4 - Discrepancy between MLS and IDS values concerning the physical-chemical parameters

	Eh (%)	pH (%)	Alk. (%)	EC (%)	DO (%)
P1	56±14	2±4	23±28	72±66	12±5
P2	25±17	1±1	31±22	56±64	7±4
P3	59±36	1±1	28±46	142±60	14±6
P4	37±28	3±2	7±8	5±5	9±15
P5	101±110	2±2	36±34	65±72	14±9
P7	54±69	8±5	16±17	38±49	13±6
P8	139±2	2±4	14±18	85±104	21±27
P9	62±55	0±0	15±33	17±15	13±8
P10	44±12	1±1	46±69	37±69	4±9
P33	32±34	2±2	13±18	14±21	6±4
P34	18±22	3±4	12±6	69±83	2±7

RESULTS AND DISCUSSION

In Table 4.4, the most affected parameter is Eh with an average discrepancy of 57% and a maximum of 139%. pH, dissolved oxygen and alkalinity show discrepancies from low to moderate, mostly because they have a limited range of variability or are often below the detection limit. The EC follows the trend of Cl⁻ (Table 4.3) and its discrepancy is in general high or moderate, except for P4 where freshwater is present throughout the aquifer vertical profile.

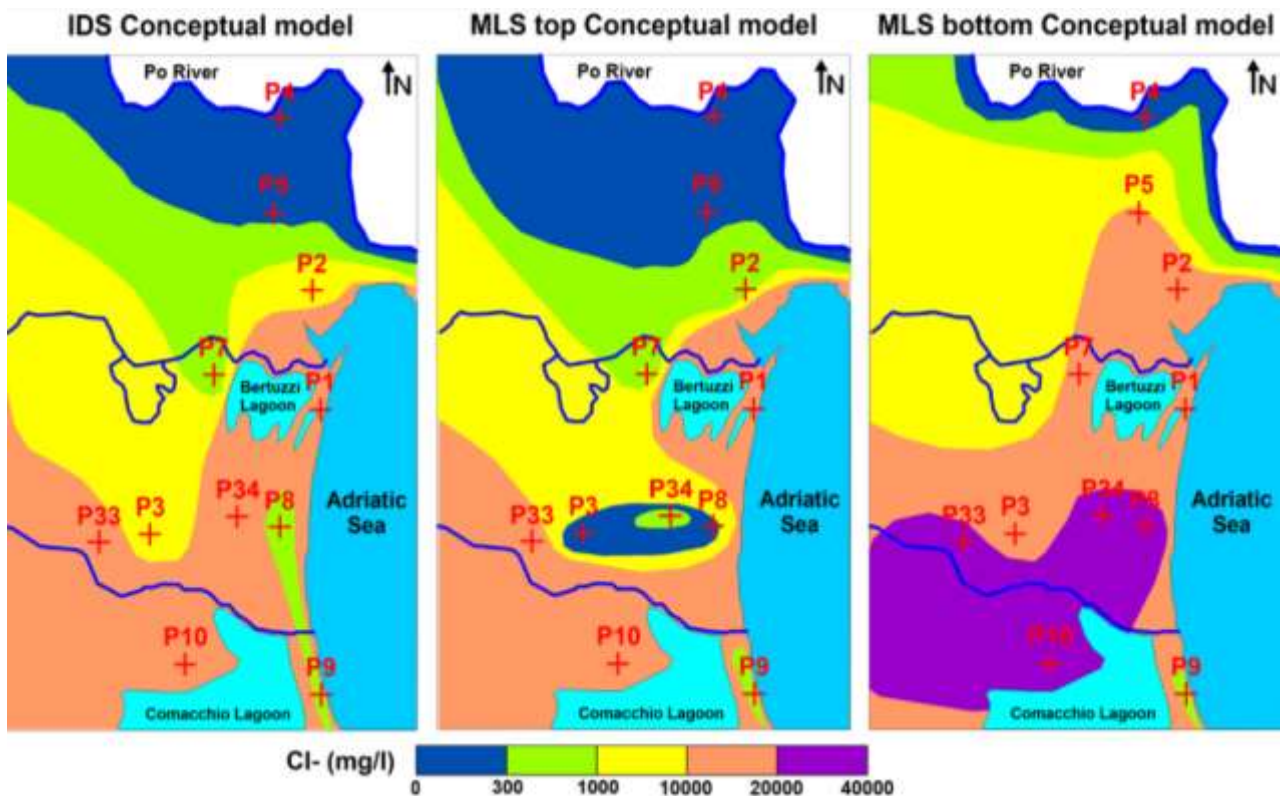


Figure 4.18 - Cl⁻ distribution maps, according to Stuyfzand classification (1989), derived using IDS data (left panel) and MLS data from the upper aquifer portion (mid panel) and from the lower aquifer portion (right panel).

Figure 4.18 shows the conceptual models of the Cl⁻ distribution derived using the IDS data (left panel) and the MLS data (mid and right panels). The IDS technique returns a conceptual model that recognizes present seawater as the main salt source. This indication comes from the following findings: maximum Cl⁻ concentration never exceeding that of sea water; presence of saline groundwater (10.000-20.000 mg/l) up to 5 km from the shoreline, in correspondence with the more recent sandy beach and dune deposits; brackish/saline groundwater (1.000-10.000 mg/l) in the area characterized by fine interbay deposits; brackish (300-1.000 mg/l) and fresh/brackish (<300 mg/l) groundwater moving towards the Po River in the northern part of the study area. A lens of brackish water is also hosted by the dunes system extending from P8 to P9 in proximity of the Comacchio Lagoon.

Hypersaline groundwater (>20.000 mg/l) is not present in the IDS conceptual model and therefore there is no need to evoke processes other than seawater intrusion. The remarkable extension of the saline groundwater might be explained by the disturbance of the drainage network that keeps the water table always below the Adriatic Sea level.

On the contrary, the MLS technique gives conceptual models of the top and bottom parts of the aquifer both different from the IDS conceptual model and quite different each other. In particular, the fresh/brackish groundwater area is much broader in the upper portion of the aquifer than in IDS model, while the same area it is only confined in proximity to the Po River, mainly within the sandy crevasse splay deposits in the lower portion of the aquifer. A wide lens of fresh/brackish groundwater is also present in the central part of the study area in correspondence to the maximum lateral extent of the dune system, testifying the effect of recharge on the groundwater salinity. In the lower portions of the aquifer, the whole southern part of the study area shows hypersaline groundwater that cannot be explained by present seawater intrusion. This leads to consider other sources of salinization like water/sediment interaction with the fine sediments that were deposited in a back-barrier environment during the Holocene transgression, or geochemical evolution of groundwater due to a considerable role of evaporation. Moreover, the Cl/Br molar ratio (Fig. 4.9, left panel), the Gibbs diagrams (Fig. 4.10) and the Eh versus pH (Fig. 4.17) analysed so far, also support the hypothesis that other sources of salinization play a role in the unconfined coastal aquifer of Ferrara.

On the light of above findings, it is clear that the IDS technique defines a simple but improper distribution of the salinity, considering that the actual vertical stratification of salinity is masked by the artificial mixing within the long screened wells. The conceptual model drawn on the base of results of the MLS technique allows inferring a more detailed and reliable distribution of salinity and identifying additional processes involved in the evolution of the local groundwater.

4.3 Numerical modelling to predict salinization trends in a lowland coastal aquifer

To quantify the impact of groundwater salinization on the whole coastal groundwater system in the Ferrara Province, a conceptual model was developed based on detailed topography and bathymetry, stratigraphic information from analysis of well logs, hydrodynamic information from heads monitoring and pumping tests, and hydrogeochemical information from Multi-Level Sampling. On the basis of such a conceptual model, a three-dimensional variable-density groundwater flow model coupled with solute transport was developed and calibrated with MODFLOW-2000 using highly parameterized inversion techniques, to help ensure that the model was a reasonable representation of the system. The calibrated model was employed to investigate the extent of autonomous salinization via seepage of saline groundwater in the Ferrara coastal aquifer.

To better study the interactions between the coastal unconfined aquifer and the canals network, and to quantify the possible future effects of climate change on groundwater salinization, a calibrated two-dimensional model was implemented using SEAWAT with a

multiple scenario approach: (i) increase in evapotranspiration induced by temperature increase; (ii) increase in the frequency of severe high rainfall events; (iii) extreme drought conditions; (iv) and canal dewatering due to salinization of the water courses. The first three scenarios had only a minor influence on the aquifer salinization rate, while the fourth one predicted serious upward flux of the high salinity groundwater actually residing at the bottom of the unconfined aquifer. The scenarios quantified the possible future effects on groundwater salinization: they could be useful to find adaptation strategies to manage the water resources of this and similar areas.

4.3.1 Three-dimensional model calibration and sensitivity analysis

The first step in the calibration process was to compare the outflow from the drainage network calculated in the numerical simulation with the average discharge data from 2010 to 2013 supplied by the Consorzio di Bonifica Pianura di Ferrara (Tab. 4.5). In order to have a direct comparison with the discharge data, different sub-drainage basins have been isolated, according to the Consorzio zonation map (Fig. 4.19).

Table 4.5 - Comparison between the observed and calculated volumes of water (m³/s) discharged to the sea by the 5 main dewatering stations.

	BONELLO	ROMANINA	GIRALDA	ACQUE ALTE	ACQUE BASSE	Total
Observed	5.88E-01	5.16E-01	1.19E+00	3.54E+00	8.03E+00	1.39E+01
Calculated	4.41E-01	4.77E-01	1.29E+00	5.71E+00	4.64E+00	1.26E+01

To achieve a good fit between simulated fluxes and observed ones, at first the drain parameters were adjusted changing the conductance (m²/s) and the elevation of the drains' bottom (m) that went dry. In addition, to get a closer fit with the observed fluxes, it was necessary to increase the recharge (from 80 mm/y to 95 mm/y), because the calculated groundwater outflowing toward the drainage network continued to be insufficient. To assure a good match between measured and observed hydraulic heads and to reach an acceptable variance (Fig. 4.20), the location of drains was carefully checked, since they are the main drivers of fluxes within the model domain.

Regarding salt concentrations, calibration and adjustment of transport parameters like dispersivities were not necessary. In fact, after the rigorous calibration of flow parameters, the scatter diagram between observed and calculated concentrations resulted satisfactory (Fig. 4.20b). The model efficiency (Nash-Sutcliffe, 1970) for concentrations was 0.87, while for hydraulic heads was 0.72. Given the regional scale of the model, the results were considered acceptable (Colombani et al., 2015b).

Composite scaled sensitivities (CSS) were used to perform a sensitivity analysis on the model parameters. CSS are calculated for each parameter using the dimensionless scaled sensitivities for all observations (Hill, 1998). Because CSS are dimensionless, they can be used to compare the amount of information provided by different types of parameters. Model simulation results will be more sensitive to parameters with large CSS.

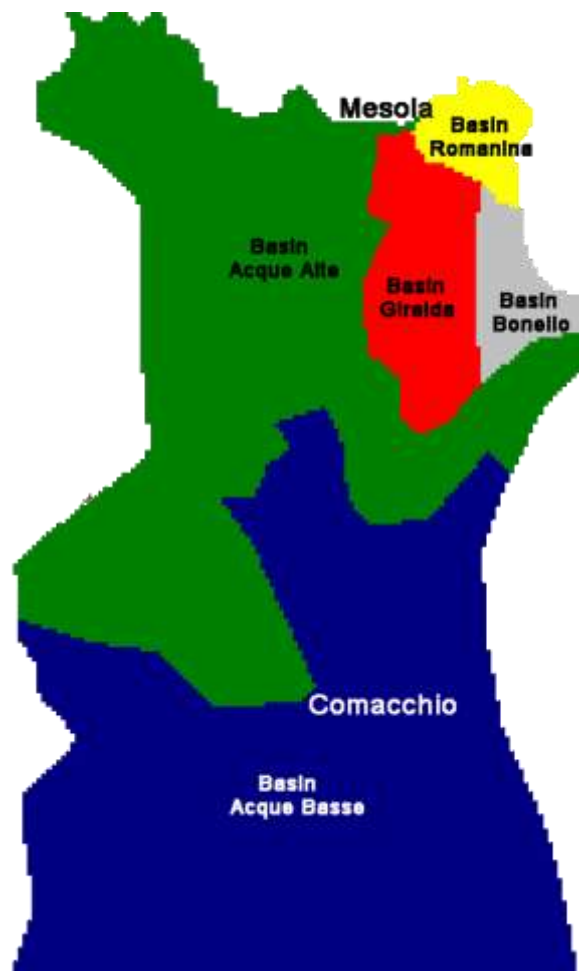


Figure 4.19 - Subdivision of the three-dimensional model domain in drainage basins.

The CSS values indicate which parameter has large influence on the model results. If the CSS value of a given parameter P_i is high, this parameter P_i is more sensitive to percentage changes in its value, and the resulting modelled hydraulic heads depending on P_i are more variable. It can be noticed that the hydraulic conductivity set for the top layers 2 has the highest CSS; therefore the k value assigned to the model is the most uncertain, since a single value was used for the entire aquifer (Tab. 4.6). Moreover, this parameter is highly correlated with the drains conductance, since the drains are all located in the top layers. Secondly, model results are also sensitive to recharge. Thus, to improve the model efficiency, an accurate reproduction of the recharge should be introduced, for instance including seasonal variations

RESULTS AND DISCUSSION

instead of the single steady state value actually employed. In any case, all the CSS values for the three-dimensional model have values somewhat low: therefore, any change in the parameter set will have little effects on the result. The sensitivity analysis also shows that the drain conductance, the evapotranspiration and the hydraulic conductivities of the lower layers are relatively insensitive to the change of parameters.

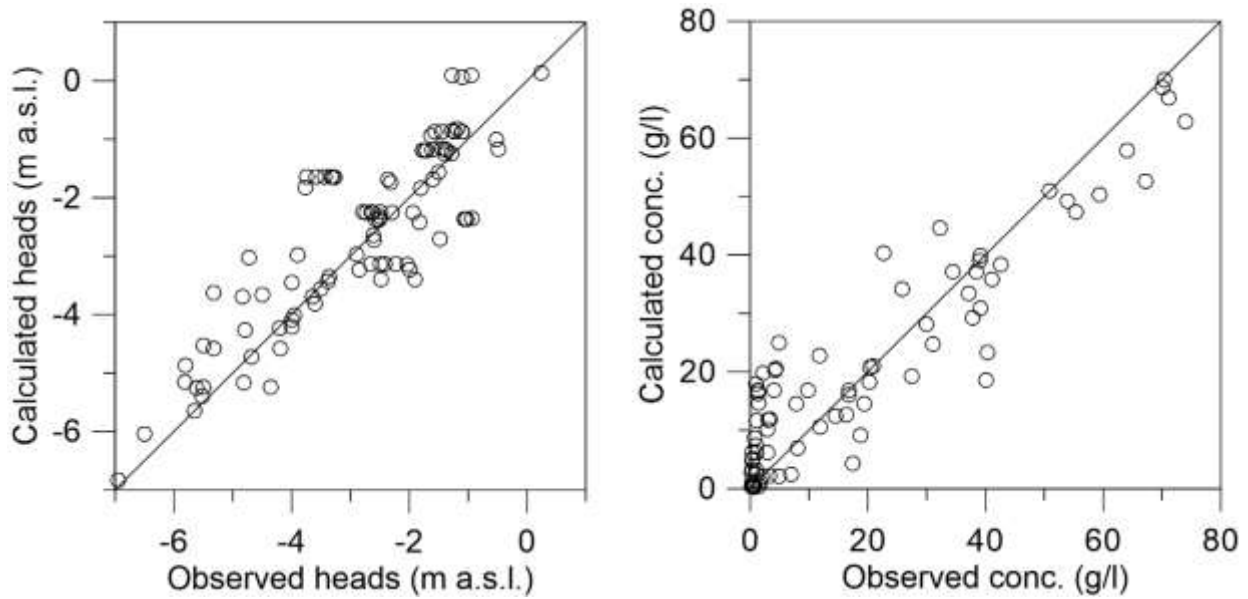


Figure 4.20 - Scatter diagrams of calculated and measured hydraulic head (left plot) and of salt concentrations (right plot).

Table 4.6 - Hydraulic heads composite scale sensitivity values calculated by PEST.

PARAMETERS	COMPOSITE SCALE SENSITIVITY
Hydraulic conductivity_1 (layer 2-3)	0.1117
Hydraulic conductivity_2 (layer 4-5)	0.0758
Recharge	0.0671
Hydraulic conductivity_3 (layer 6)	0.0467
Drain	0.0343
Evapotranspiration	0.0199
Hydraulic conductivity_4 (layer 7-8)	0.0045
Hydraulic conductivity_5 (layer 9-10)	0.0003

4.3.2 Three-dimensional model results

The piezometric map shown in figure 4.21 highlights that most of the aquifer displays head values below mean sea level, except for the palaeo-dune system and the present dune system. The most depressed hydraulic heads are found in the recently reclaimed lands located in the South-western corner of the model domain (Mezzano).

A Three-dimensional isoconcentration map has been drawn to represent the computed salt concentrations (Fig. 4.22). In the A-A' transect the groundwater upward flux with high salts concentration (up to 70 g/l) is fairly appreciable. This upward flux is responsible for the salinization of the upper portion of the unconfined aquifer and for the discharge of saline waters in the drainage network as well.

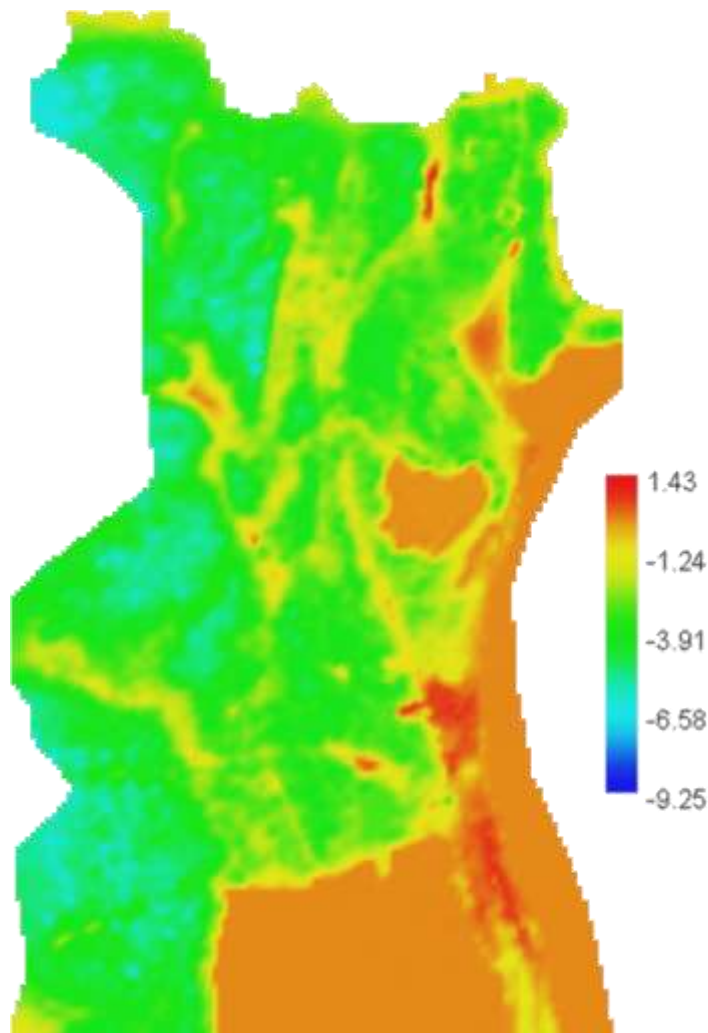


Figure 4.21 - Piezometric map of the calculated heads (m a.s.l.).

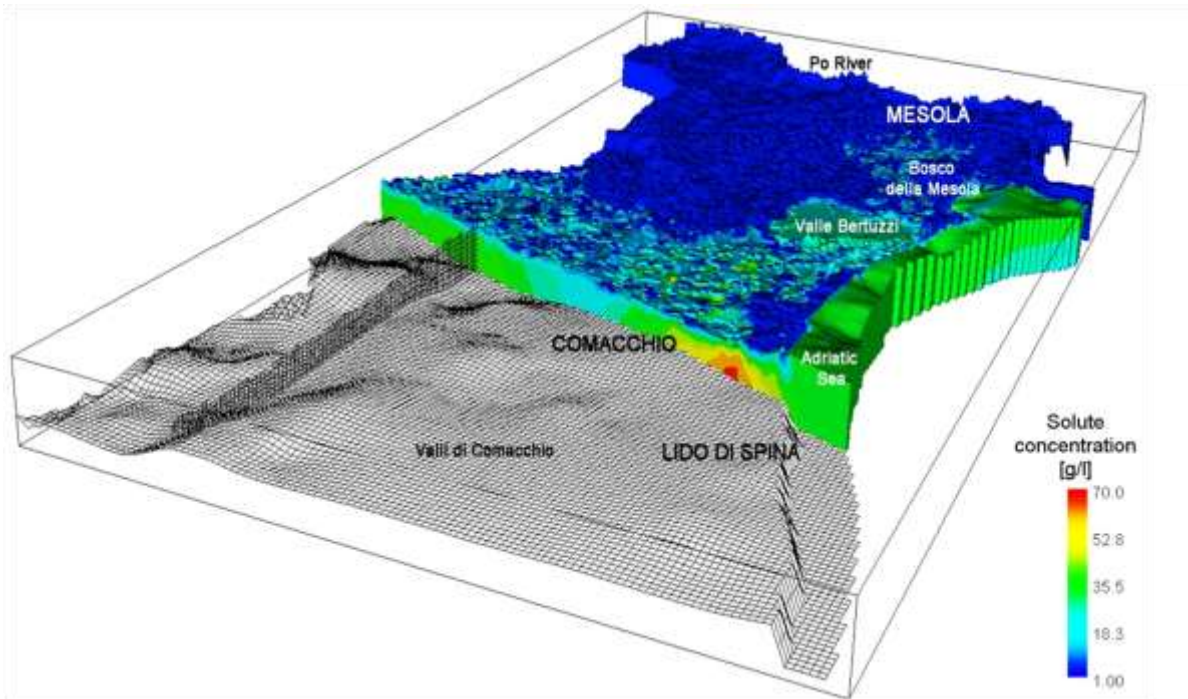


Figure 4.22 – Three-dimensional isoconcentration map of the calculated salt concentrations, along the transect A-A’.

A significant model output consists in the calculation of the salt masses entering and leaving the model domain. Currently, the salt mass discharging from groundwater into the drainage network equals 1714 t/y. The Po River recharges the unconfined aquifer with 0.3 t/y of salt, effective rainfall (recharge) contributes with 48 t/y of salt, while evapotranspiration exports from the model domain 26 t/y of salt. Converting the salt discharge in the drainage network into a surface load, this mass flux is equal to 22.7 kg/ha/y, which is consistent with the salt load found in the Netherland by a similar large scale modeling study (Oude Essink et al., 2010).

4.3.3 Tidal forcing effects on groundwater fluctuation

To confirm that the main driver of groundwater salinization is the upward flux induced by dewatering activities necessary to keep the coastal area dry, the effect of tidal fluctuation on groundwater dynamics and consequently on seawater intrusion were investigated in P8, which is the monitoring well nearest to the coastline (Fig. 2.2).

Fig. 4.23 shows the relationship between tidal fluctuation and groundwater level in the monitoring well P8 from August 2009 to May 2010. It is clear from this plot that the tidal amplitude is approximately 0.4 m, the tidal range is 0.8 m and the average tidal level is 0.18 m a.s.l., with the highest sea levels occurring during winter time due to storm events (Martinelli et al., 2010).

RESULTS AND DISCUSSION

The piezometric heads recorded in the monitoring well P8 meanwhile are quite stable in summer and early autumn, with a sudden 0.5 m decline in November 2009 and a steep rise in April 2010 following the irrigation/drainage canals regime. Overall, the maximum piezometric head variation during the monitoring period was 0.83 m with a mean value of -1.80 m a.s.l.

The low piezometric head variation during the hydrologic year shows that the unconfined aquifer is affected by the channel network, and the fact that values are always below mean sea level confirms that the groundwater flow is always directed inland, favouring seawater intrusion. The right panel in Fig. 4.23 indicates the results of the analysis during a period of only one week, when the hydrometric level of the nearby canal was stable and precipitation absent. In this period of time the correlation with the tidal fluctuation is more evident, with a lag phase between peaks of 18-19 hours, although the average groundwater fluctuation due to tidal forcing is only 0.02 m in P8.

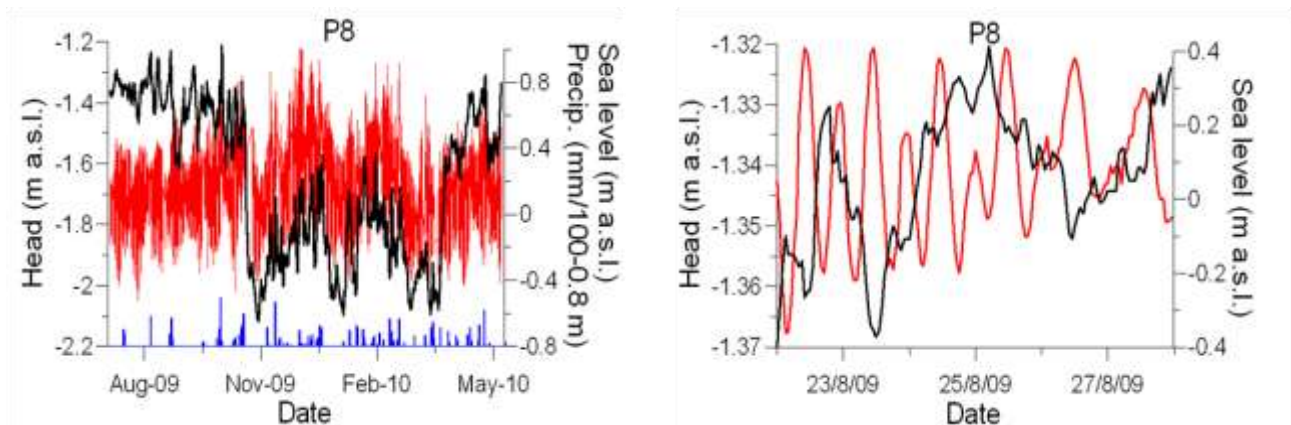


Figure 4.23 - Plots of continuous piezometric head monitoring of monitoring well P8 (black line) and sea level (red line). The left plot shows the entire monitoring period, while the right plot shows a zoomed timeframe of one week when the tidal oscillation is more evident. Note that the y scales have different ranges.

It can therefore be inferred that P8 and the nearby surface water level are not affected by tidal fluctuations. For this reason, a two-dimensional flow and transport model was implemented across P8 and Canale della Gronda (Fig. 4.24) to study the interactions between the coastal unconfined aquifer and the canals network, and to quantify the possible future effects of climate change on groundwater salinization.

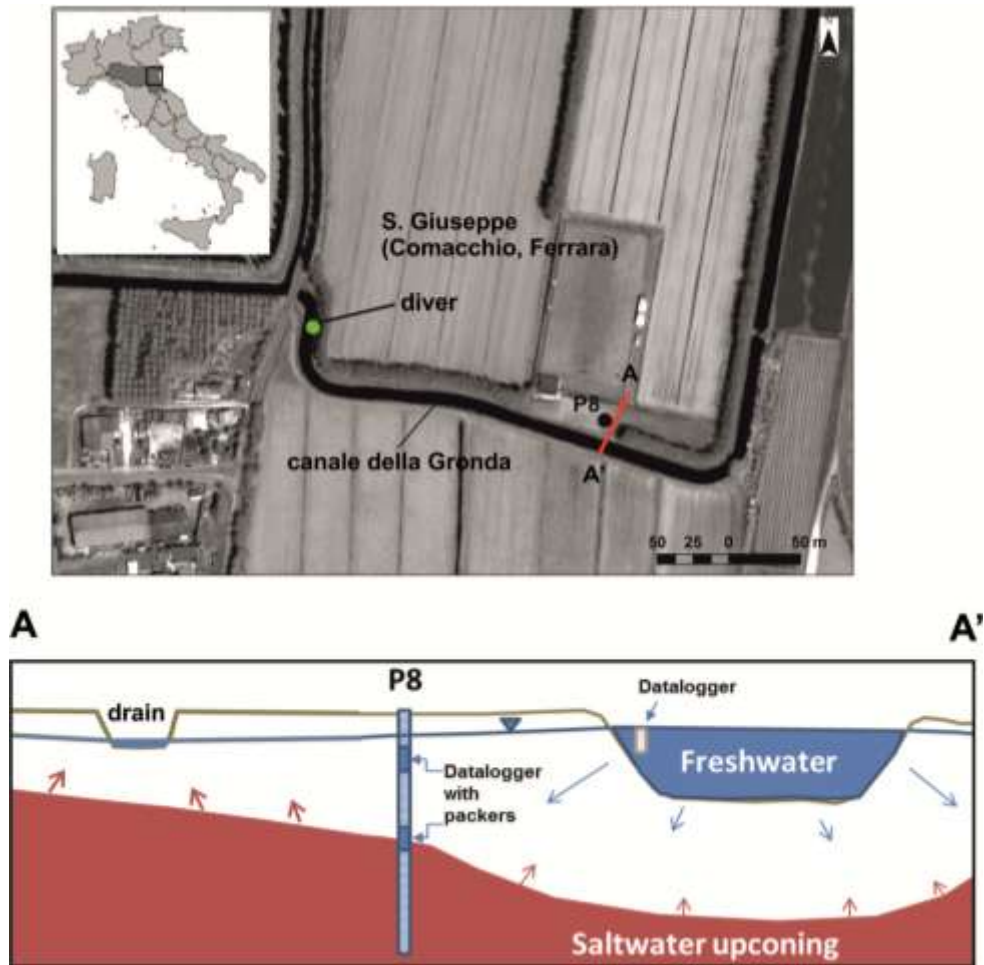


Figure 4.24 - Location of the study area and conceptual model of the A-A' transect across monitoring well P8 and Canale della Gronda, selected for the two-dimensional numerical model.

4.3.4 Two-dimensional model calibration and validation

Figure 4.25 shows the calibration results of measured versus computed TDS and hydraulic heads in monitoring well P8 (at -4 and -8 m a.s.l.) and in the nearby drain ditch (Fig. 4.24). Good calibration has been achieved for both heads and TDS throughout the simulated period, showing the presence of high TDS value in the deep portion of the aquifer and the presence of a shallow freshwater lens with evident freshening induced by the leaking canal. The inverse parameters estimation procedure performed with PEST resulted in the absolute mean errors between simulated and observed heads and TDS of 2.3 cm and 1.64 g/L, respectively (Table 4.7). These errors correspond to 4.0% of the observed piezometric range and to 3.7% of the observed TDS range during the monitored period. The daily variability of recorded heads and TDS is very high: as a consequence, a detailed temporal discretization would be required to accurately reproduce all the variations induced by small changes in canal water level. In any case, the model conveniently reproduced the piezometric head trend induced by recharge events and canal water level changes.

RESULTS AND DISCUSSION

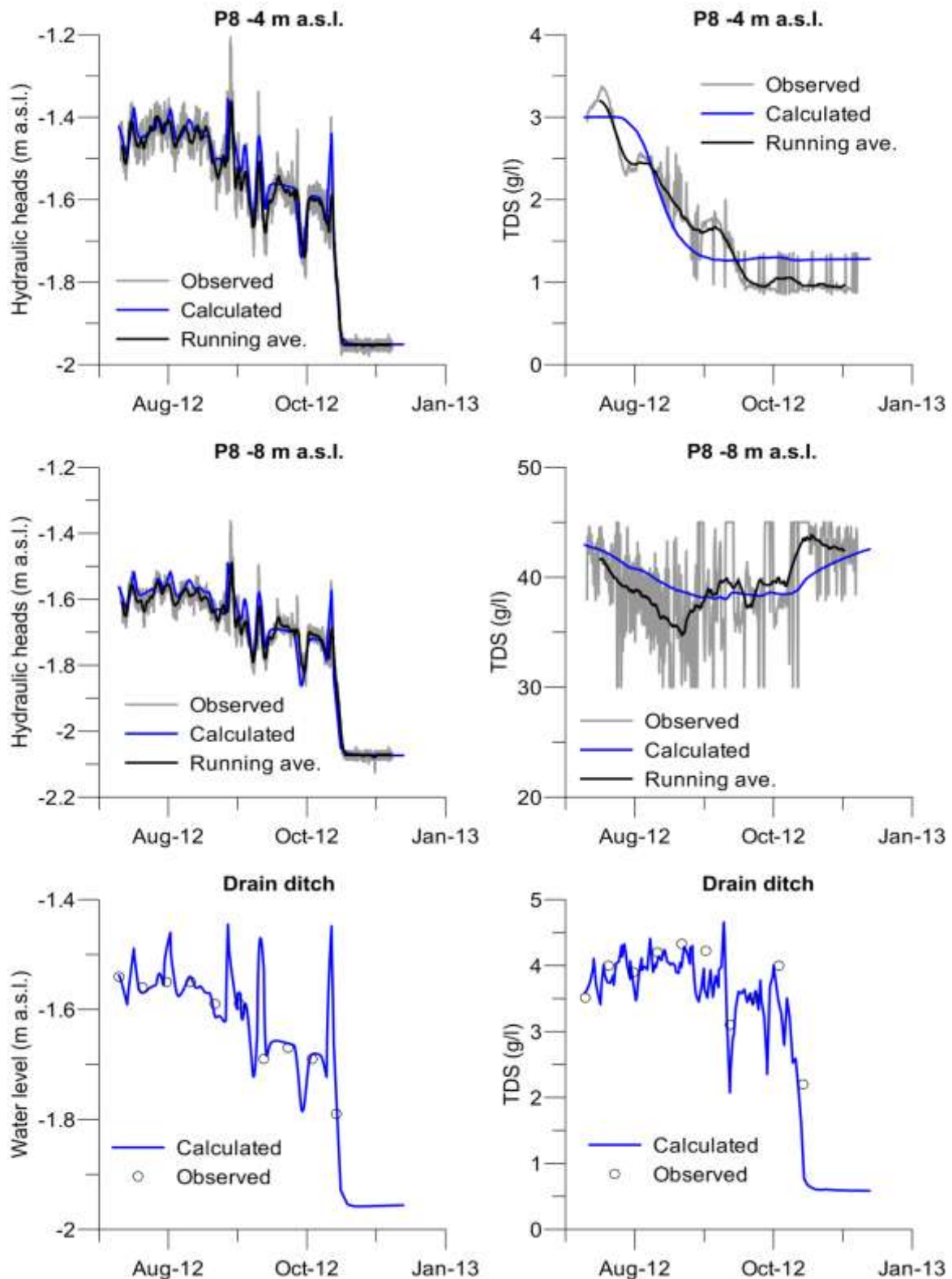


Figure 4.25 - In the left hand side plots: comparison of modelled hydraulic heads (blue lines) versus observed hydraulic heads (grey lines) and their running average with daily period (black lines), In the right hand side plots: comparison of modelled TDS (blue lines) versus observed TDS (grey lines) and their running average with daily period (black lines). The observed water levels and TDS in the drain ditch are plotted with black open circles.

Table 4.7 - Absolute mean error between observed and calculated values of the calibrated and validated models.

Simulation	Hydraulic heads	Concentration
	absolute mean error (cm)	absolute mean error (g/L)
Calibrated model	2.3	1.64
Validated model	2.3	2.01

In particular, figure 4.25 evidences the piezometric heads drop induced by the canal's dewatering after the growing season, which also induces the drain ditch dewatering.

The simulated TDS in P8 at -4 m a.s.l. followed the recorded decreasing trend, but it did not reproduce the various observed sub-peaks: these were probably due to lateral TDS heterogeneities or geochemical reactions that were not included in the simulation. Also the TDS in P8 at -4 m a.s.l. followed the observed trend, with an initial decreasing trend due to downward movement of the more saline groundwater displaced by freshwater coming from the leaking canal; then, when the canal was dewatered saltwater raised again upward diminishing the freshwater lens thickness. The hand collected data of both heads and TDS in the drain ditch matched quite closely the simulated values.

Figure 4.26 shows the TDS spatial maps and TDS profiles along the monitoring well P8 used to validate the numerical model. The model well reproduced the TDS profiles in both the sampling rounds, with an absolute mean error between simulated and observed TDS values of 1.52 g/L for the sampling round of the 12th of December 2012, and 2.51 g/l for the sampling round of the 26th of February 2013 in P8 (Table 4.7). These errors correspond to 2.4% and to 4.0% of the observed TDS range in the first and second sampling round, respectively. Looking at the freshwater lens shapes of figure 4.26, it could be noted that the mixing zone between saline and freshwater is quite sharp, approximately 2 m thick, and it moved upward of 1 m when the canal was dewatered. The sharp gradient between saline and freshwater could be justified by the relatively low value of vertical dispersivity found via inverse modelling (Table 3.1).

During the irrigation season (spring and summer) the canal stage is kept constant thanks to the complex agricultural drainage system that controls the water level and guarantees freshwater for crop irrigation.

After summer the brackish-freshwater interface is deeper and the freshwater lens maximum thickness is about 4 m due to canal recharge. During winter and autumn the canal is not used for irrigation purposes and left completely dry. During this period the freshwater lens tends to shrink, becoming only 3 m thick, and it is preserved only by recharge events (Fig. 4.26). The results of the validated model indicate the strong link between surface water bodies and coastal aquifer; the Gronda canal artificially recharges the aquifer during the cropping season, while during winter time the saltwater interface can migrate upward since the canal is kept dry for hydraulic protection purposes.

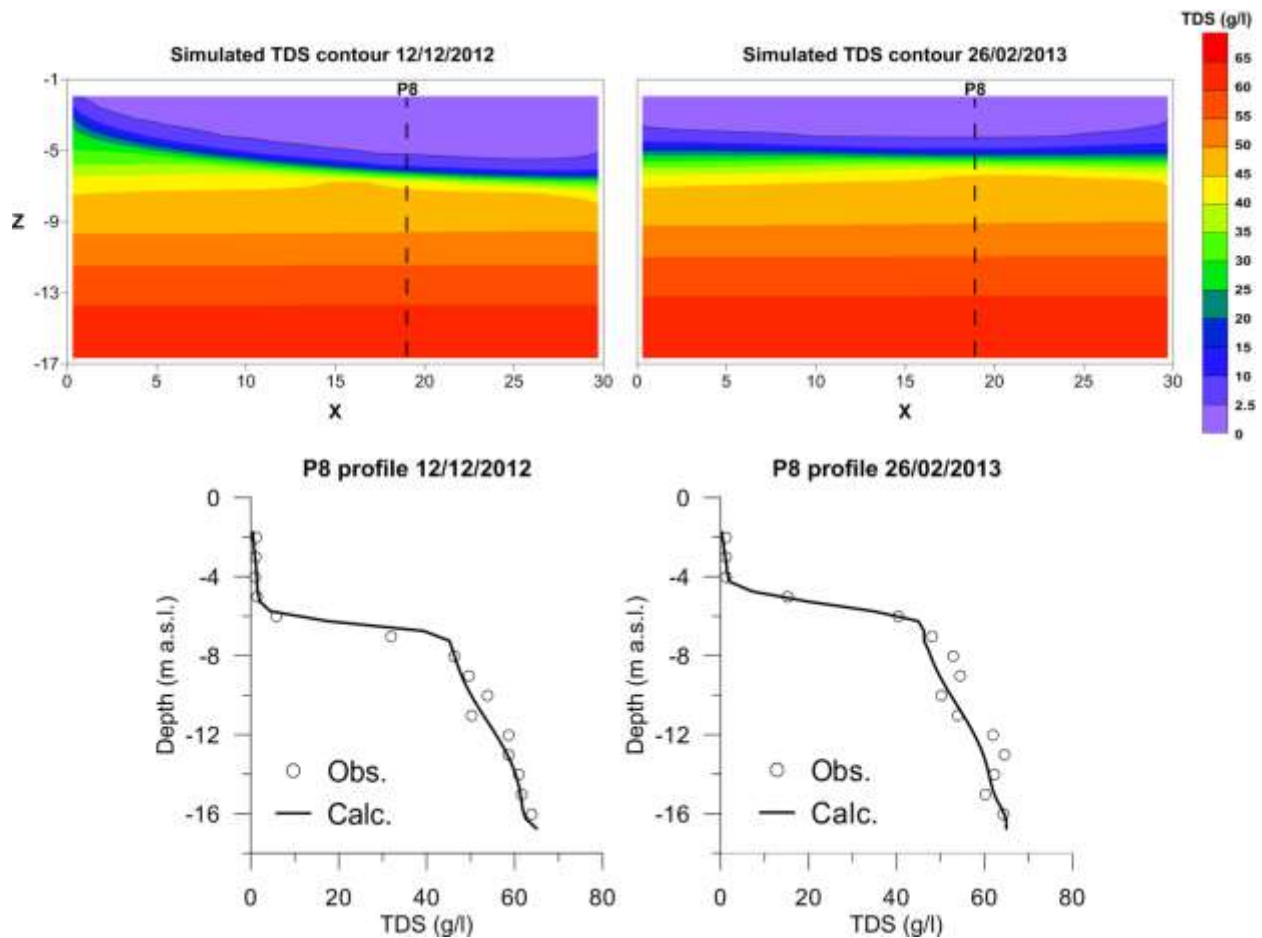


Figure 4.26 - In the upper panels the simulated TDS contours for 12/12/2012 (left panel) and for 26/02/2013 (right panel) are shown together with the location of P8. Profiles in P8 of modelled (black lines) versus observed (black open circles) TDS used to validate the numerical model are shown in the lower plots.

4.3.5 Future scenarios

The maximum thickness of the shallow freshwater lens in the current situation (TDS<2.5 g/L) was then compared with the results of the four scenarios in order to investigate the change in the brackish-freshwater interface depth and geometry. The comparison between different scenarios allowed quantifying the possible future effects of climate change on groundwater salinization in the coastal aquifer. In addition, the sub-scenarios exemplified the impact of the projected low sea level rise (LSLR) and high sea level rise (HSLR) on saltwater upward flow (Figure 4.27 and Table 4.8).

Figure 4.27 shows the actual average TDS contours at the end of the summer season and at the end of the winter seasons (upper panels). The future scenarios were all plotted for the end of the summer conditions, with projected LSLR in the left panels and projected HSLR in the right panels. To help the reader, the 2.5 g/L TDS isoline was also plotted. In the first scenario, the increase of precipitation and temperature based on the climate change projections for the

RESULTS AND DISCUSSION

Mediterranean region (CIRCE project) (Giorgi and Lionello, 2008; Gualdi et al., 2013) caused only minor effects on the brackish-freshwater interface. The interface fluctuated about 0.4 ± 0.15 m (Table 4.8) upward in winter with a small decrease in freshwater lens thickness, especially in the portion of the aquifer close to Gronda canal. No significant change is shown during the summer period (Fig. 4.27): this means that the increase in evapotranspiration is basically compensated by the small increase in precipitation. Some remarkable differences are visible between the LSLR and HSLR sub-scenarios (Fig. 4.27): there is an evident shrinking of the freshwater lens in the HSLR case respect to the LSLR case. The lens shrinking is accompanied by the consequent upward movement of high TDS groundwater.

Table 4.8 - Scenario modelling of the predicted variations of freshwater maximum thickness respect to the actual situation, with sub-scenarios of projected low sea level rise (LSLR) and high sea level rise (HSLR). Positive values indicate thinning of freshwater lens, while negative values indicate thickening.

Simulation	Change of freshwater maximum thickness (m) LSLR	Change of freshwater maximum thickness (m) HSLR
Scenario 1	-0.4±0.15	-0.62±0.33
Scenario 2	0.12±0.05	0.26±0.06
Scenario 3	0.13±0.06	0.26±0.06
Scenario 4	1.15±0.6	1.15±0.6

The second scenario (Scenario 2 in Figure 4.27 and Table 4.8) did not significantly affect the freshwater lens and aquifer salinization as well. The conditions remained basically those of the calibrated model, meaning that severe high rainfall events will not improve the natural recharge of the aquifer and will not prevent an upward movement of the saline groundwater interface from the bottom. Once again, an evident shrinking of the freshwater lens in the HSLR case respect to the LSLR is appreciable in figure 4.27. This is a quite important point to stress, since the impact of the projected sea level rise seems much more important than the projected climate changes for this zone. The same considerations apply also for the third scenario, where extreme drought conditions were simulated. This supports the results found in the first two scenarios, since even without recharge for a prolonged period the freshwater lens thickness was only slightly changed compared to the base case (Scenario 3 in Figure 4.27 and Table 4.8).

RESULTS AND DISCUSSION

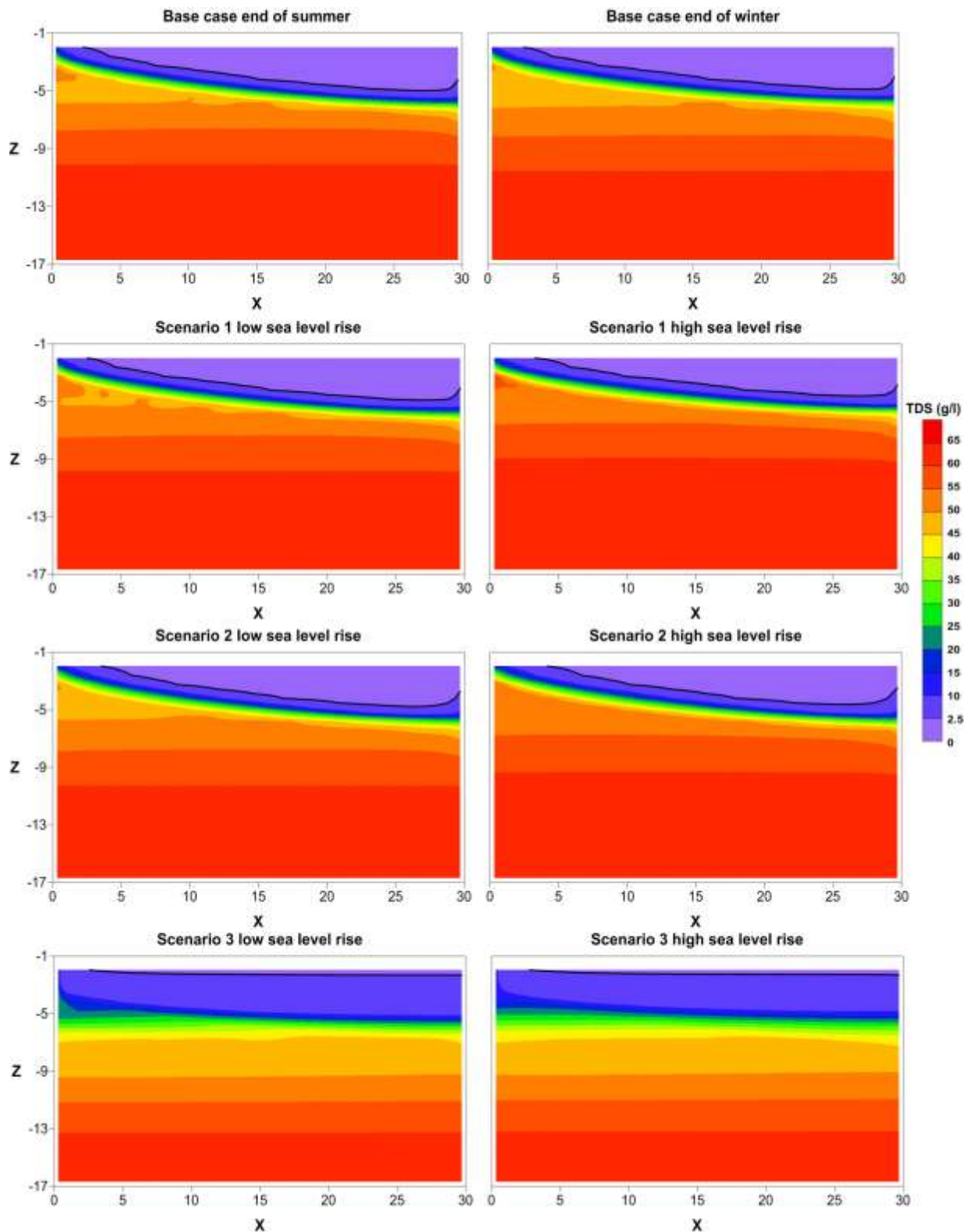


Figure 4.27 - In the upper panels the actual average TDS contours for the end of the summer (left panel) and for the end of the winter (right panel) are plotted, while the future scenarios are all plotted for the end of the summer conditions. The projected LSLR are shown in the left panels and HSLR are shown in the right panels. The black line represents the 2.5 g/L TDS isoline.

The major variations in freshwater lens maximum thickness are shown in the fourth scenario. The interruption of water flow within the canal during the irrigation season, due to hypothetical salinization of the nearby water courses, could create an upward movement of the high salinity groundwater, which actually resides in the aquifer bottom. In figure 4.27 the lower panels (representing the scenario with canal dewatering for 6 months) show very thin freshwater lenses, with an almost complete salinization of the aquifer. In contrast with the other scenarios, the sub-scenarios of LSLR and HSLR show very similar results, confirming that the canal is the main driver of aquifer freshening. In the worst case of Scenario 4 (Table 4.8), where the canal interruption lasted for 9 months, the freshwater maximum thickness decreases from 4.6 to 0.6 m in the summer, and from 4 to 0.9 m in the winter.

In general, the simulations indicate that an increase in temperature or an increase in the severe high rainfall events have only a minor influence on the aquifer salinization rate, while an interruption of the canal usage could create serious upward movement of the high salinity groundwater currently residing in the aquifer bottom. Besides, the impact of the projected sea level rise seems much more important than the projected climate changes; thus, future studies will need a better delineation of forthcoming sea level rise at local scale.

4.4 Ammonium occurrence in a salinized lowland coastal aquifer

Recent studies suggested that climate changes can alter the present chemical-physical and hydrogeological conditions in coastal aquifers, increasing the risk of transfer of contaminants to the water cycle. For instance, the increase of autonomous salinization due to sea level rise may even induce the remobilization of geogenic elements. To understand if the increased ionic strength within the aquifer caused by salinization of the Ferrara coastal aquifer could shift the chemical equilibrium in the water-soil-air continuum favouring desorption/dissolution reaction, the contribution of water-sediment interaction and the anthropogenic influence on groundwater quality have to be firstly distinguished. The attention was focused on (i) nitrogen species (paragraph 4.4), since ammonium and nitrate contamination is a well-known issue in the intensively cropped Po plain and on (ii) trace elements (paragraph 4.5) because in general alpine sediments, that constitute the Po plain, are known to be rich in some of these compounds.

To understand the spatial distribution and the possible sources of high ammonium concentration in the unconfined coastal aquifer of the Po River Delta lowland (Italy), a detailed characterization of inorganic nitrogen species was completed on 59 monitoring wells (Fig. 2.2). The ammonium resulted the prevalent nitrogen inorganic species in groundwater, and its concentration increases with depth and salinity. Very high ammonium concentrations are found in coincidence with peaty sediments in the salinized anoxic aquifer and in the low-lying aquitard. Results from this study show that the elevated ammonium concentration derives from the mineralization of organic matter present in fine sediments deposited in palaeo-marsh environments.

4.4.1 Water table elevation and ammonium mapping

The analysis of the water table elevation highlights that the hydraulic head is below the sea level at all locations, with values up to -7 m a.s.l. The central part of the study area is characterized by a stagnant zone drawing groundwater from both the western and eastern sides, with head gradients ranging from 0.03% to 0.06%. This area corresponds to a North-South drainage axis induced by dewatering pumping stations, which are used to reclaim swamps that previously occupied the area.

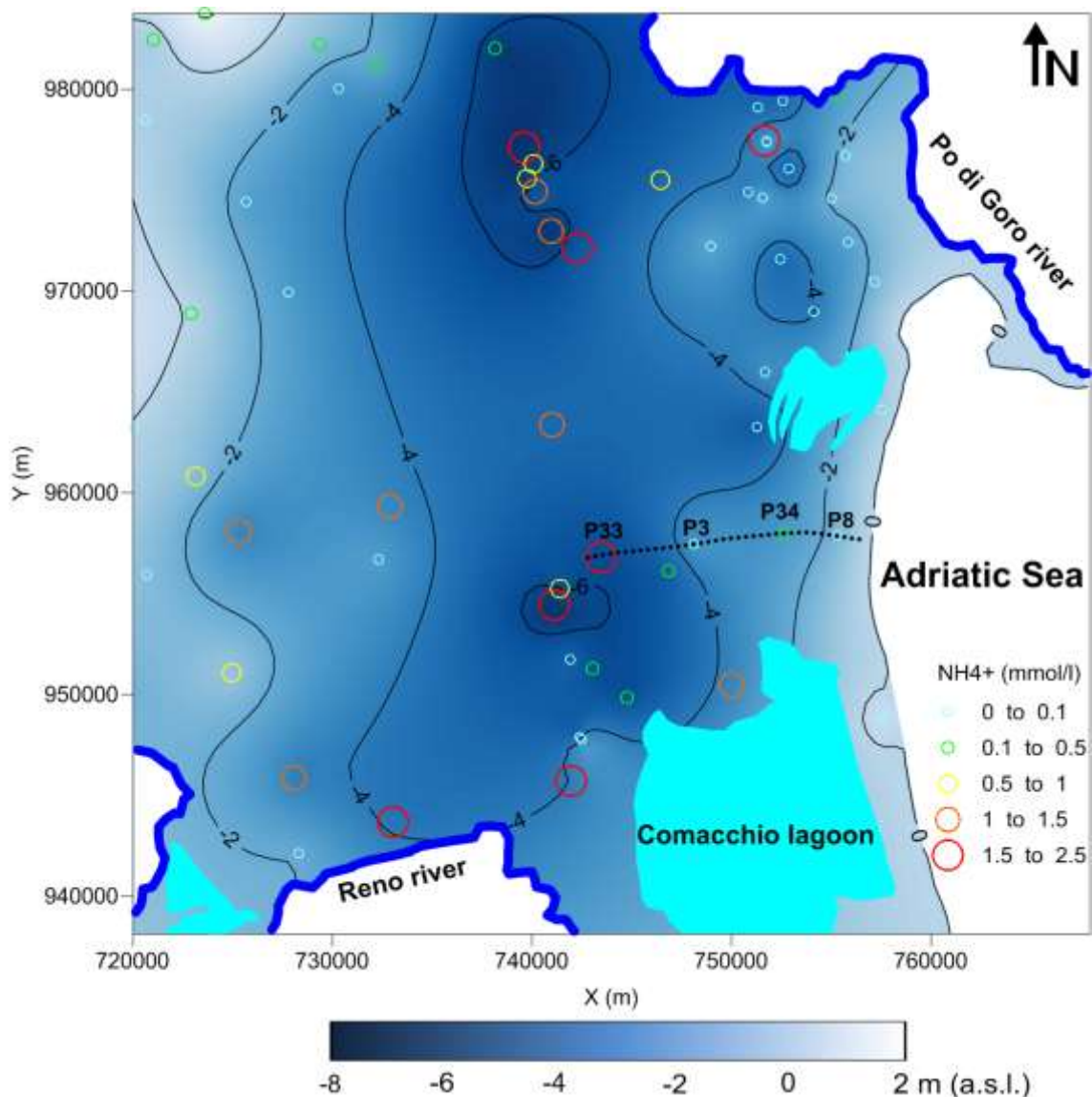


Figure 4.28 - Location of the study area with the piezometric contour map (black lines); circles represent the groundwater NH_4^+ concentration at 1 m below the water table in the 59 piezometer investigated; in black colour the four selected piezometers along a flow line (dashed line corresponding to A-A' transect in Fig. 2.2).

NH_4^+ classed concentration map of Fig. 4.28 shows values ranging from 0 to 2.5 mmol/l with a mean value of 0.46 mmol/l. The higher concentrations are found in the reclaimed peaty land in coincidence with lower piezometric heads, with a maximum NH_4^+ concentration higher than 2 mmol/l and a mean concentration of 1.4 mmol/l. The spatial distribution of NH_4^+ and groundwater elevation indicate a reducing environment in the lowland reclaimed area consisting of peaty soils (Mastrocicco et al., 2011b): this is due to elevated TOC and stagnant groundwater that often lead to hydrogen sulphide formation (not shown) even at shallow depths, as the ones investigated by this monitoring network. In the area surrounding the stagnant zone, N is still present, mainly in the form of NO_3^- at much lower concentration than NH_4^+ (Fig. 4.29). This behaviour can be explained taking into account the stability of the N species as a function of the redox potential values distribution (Landon et al., 2011). The eastern and western parts of the aquifer within the study area are characterized by an oxidizing aerobic environment, due to the presence of coarser sediments with lower content of TOC and higher O_2 mass flux compared to remaining parts; as a result, away from the stagnant zone, the dominant N species is the oxidized NO_3^- form. On the contrary, in the central part of the study area, where an anaerobic reducing environment is present, the prevailing form of N is NH_4^+ .

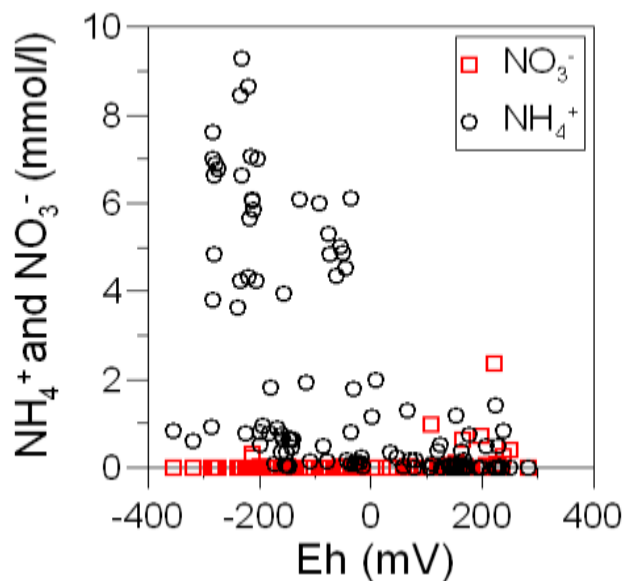


Figure 4.29 - Distribution of NO_3^- and NH_4^+ concentrations for the 59 monitoring wells with respect to redox values (Eh).

4.4.2 Core samples depth profiles

Core sample profiles of monitoring wells P33 and P34 show that sediment TOC and TLN are very high in recent peaty layers (up to 30 mol/kg and 35 mmol/kg respectively) (Fig. 4.30).

RESULTS AND DISCUSSION

The elevated sedimentary organic matter content, rich in organic N, is likely to give rise to the abundance of NH_4^+ in the aquifer-aquitard system via organic matter mineralization, as recently proposed by Jiao et al. (2010).

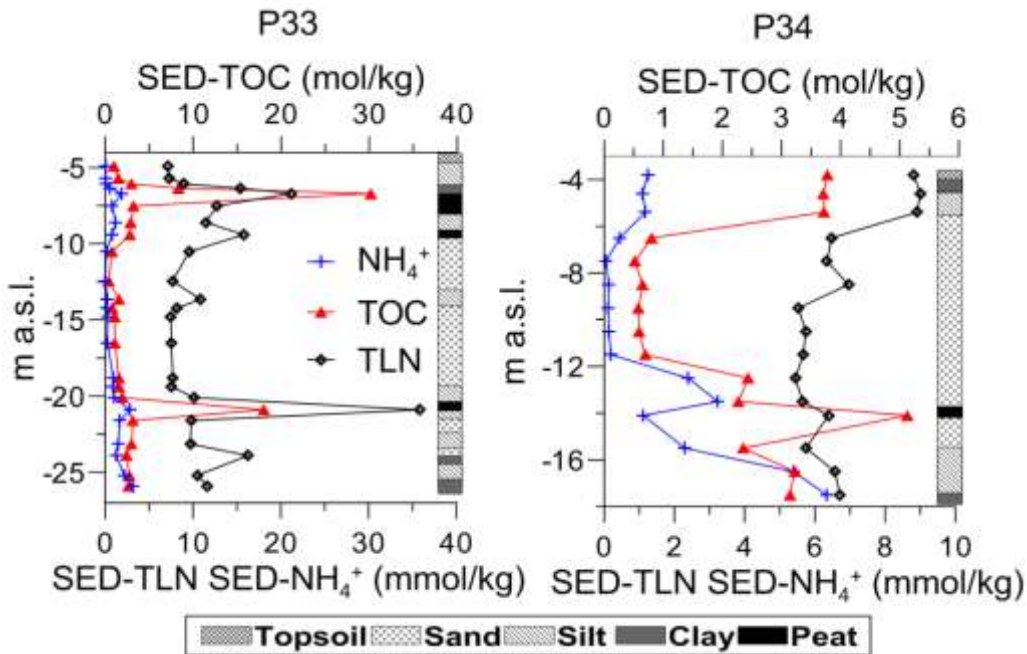


Figure 4.30 - Depth profiles of sediment TOC, TLN and NH_4^+ ; stratigraphy (core logs data) is plotted on each graph to facilitate the interpretation.

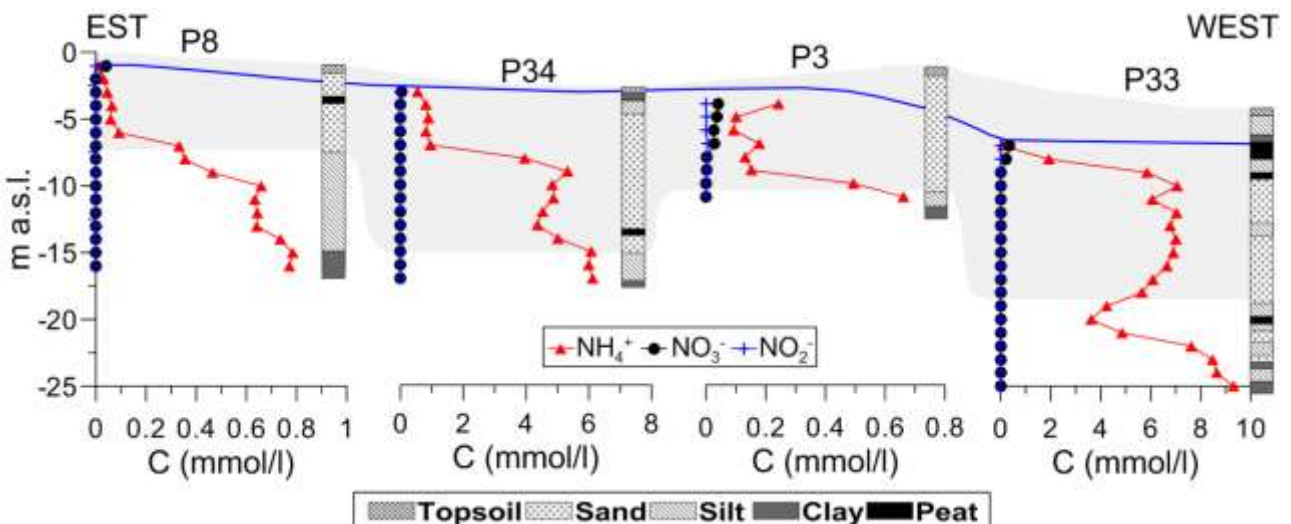


Figure 4.31 - Transect along the selected flow line (refer to Fig. 4.28 for the location) with concentration profiles of NH_4^+ , NO_3^- and NO_2^- ; unconfined aquifer thickness (shaded grey area), water table (blue line) and core logs stratigraphy are also shown. Note that curves are plotted at different horizontal scale to facilitate the graph interpretation.

NH₄⁺ in the sediments increases with depth, with spikes corresponding to the peaty layers, while the concentration is very low within the coarse sand layers because of the low cation exchange capacity (CEC) of sandy sediments. On the contrary, higher CEC values of clay and organic layers favour the adsorption of NH₄⁺, which is not easily displaced from the exchange sites. This is even confirmed by the groundwater concentration profiles reported in Fig. 4.31 showing high NH₄⁺ concentration within the sandy units and low values where the peaty layers trap NH₄⁺.

4.4.3 Groundwater quality depth profiles

Considering the water samples collected along the flow line (corresponding to the sequence of P3, P8, P33 and P34 in Fig. 4.28), the main result of inorganic N speciation is that in all cases NH₄⁺ is the prevalent species in all the four monitoring wells and NH₄⁺ concentration increases with depth (Fig. 4.31). The highest NH₄⁺ concentrations are found in the aquitard, located at the base of the unconfined aquifer. NO₃⁻ is below detection limits except in the upper part of the aquifer where NH₄⁺ is very low. Here NO₃⁻ is present at low concentration, especially in the zone where fresh recharge water infiltrates the aquifer causing nitrification processes. According to Equation (15), the classical nitrification stoichiometry states that all available NH₄⁺ is transformed into NO₃⁻ (Appelo and Postma, 2005) in presence of oxic conditions:



Mass balance for Equation (15) shows that NH₄⁺ consumption seems to be sufficient to explain NO₃⁻ increase at the top of the aquifer (Fig. 4.31), at least for monitoring wells P8, P34 and P33; P3 shows instead a not clear trend, with other possible N sources, such as dry deposition or fertilizer leaching. In addition, this reaction produces acidity that is largely buffered by the elevated carbonate presence in these sediments with more than 20% of carbonates (Amorosi et al., 2002). Accordingly, the measured average pH in the four monitoring wells is 8.4 (ranging between 7.4 and 9.4), thus witnessing basic condition within the aquifer-aquitard continuum. The elevated pH could also lead to NH₃ generation and volatilization, although this species was not measured. Since the study area is all subjected to intensive agriculture, the recorded NO₃⁻ and NH₄⁺ concentrations in the shallow part of the aquifer could be also due to fertilizer leaching. Although, recent studies have shown that NH₄⁺ is rapidly nitrified in the top soil and NO₃⁻ leaching is usually limited by denitrification, the latter is stimulated by the addition of fresh and reactive organic matter (chicken manure) in these recharge areas to improve the soil fertility (Mastrocicco et al., 2012a).

Fig. 4.32 shows TDS and NH₄⁺ profiles for the four monitoring wells along the selected transect (Fig. 4.28). The aquifer displays fresh water type (TDS <0.014 mol/l) only in the upper section of P3 and P8 (approximately 5 to 7 m thick), and a transition zone of brackish water type (from 0.014 to 0.86 mol/l) with a thickness ranging from 4 to 6 m in P3, P8 and

RESULTS AND DISCUSSION

P34, and for the whole depth in P33. Saline (from 0.86 to 1.43 mol/l) to hyper saline (>1.43 mol/l) water types are present in the remaining thickness of the aquifer in P8 and P34. Groundwater in the coastal unconfined aquifer of the Ferrara Province often displays very high salinity (>0.2 mol/l), which is likely due to the presence of palaeo-seawater rather than to modern seawater intrusion. The latter is also unlikely to happen both because groundwater salinity in this area is often more than twice higher than present seawater concentration (Fig. 4.32), and because over the past few decades groundwater has been only minimally exploited due to its elevated salinity.

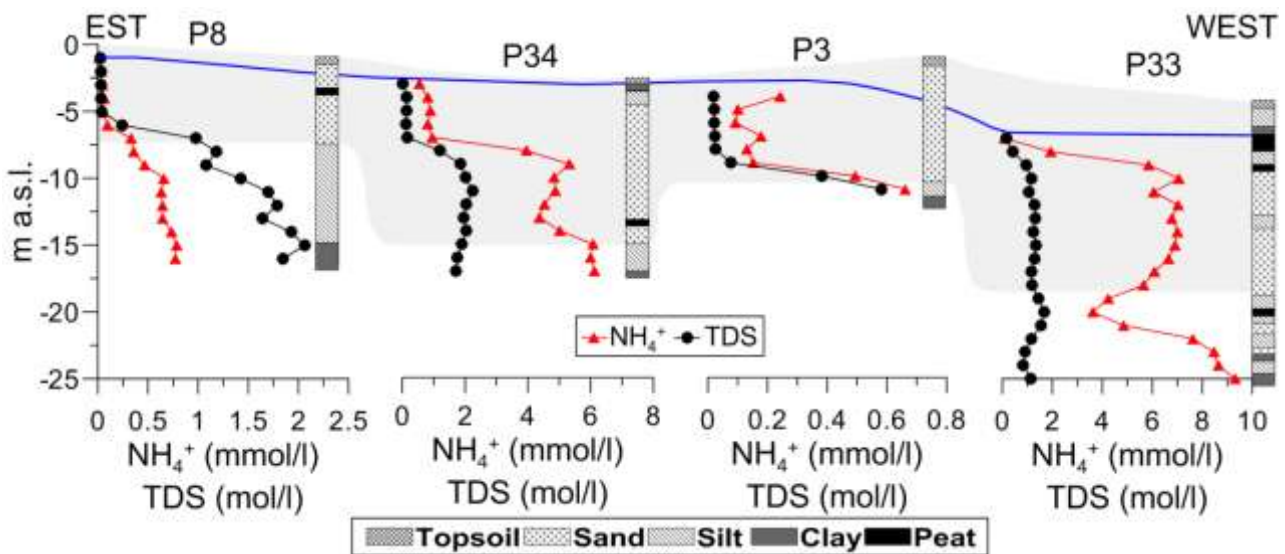


Figure 4.32 - Transect along the selected flow line (refer to Fig. 4.28 for location) with concentrations profiles of NH_4^+ and TDS; unconfined aquifer thickness (shaded grey area), water table (blue line) and core logs data are also shown. Note that curves are plotted at different horizontal scale to facilitate the graph interpretation.

The upper part of monitoring well P8 displays low TDS and NH_4^+ concentrations since is located 10 m from a canal, which contributes to dilute groundwater, and it has TDS and NH_4^+ concentrations of 0.019 mol/l and 0.013 mmol/l, respectively. Monitoring well P3 is located in a palaeo-dune topographically higher than the nearby sediments, thus being a recharge zone where infiltrating rain creates a freshwater lens floating over the saline groundwater. This explains the low TDS and NH_4^+ concentrations recorded at the top of the P3 profile.

Fig. 4.32 also shows a close relation between TDS and NH_4^+ increases in groundwater. In fact, although the correlation between TDS and NH_4^+ is low ($R^2= 0.28$), at elevated ionic strength (like in P34 and P3) a sharp increase of NH_4^+ is present. Elevated NH_4^+ concentrations are often associated with high groundwater salinity, and recently it has been suggested that saltwater environments are favourable to the release in groundwater of NH_4^+ adsorbed onto sediments (Bratton et al., 2009; Jiao et al., 2010).

4.4.4 Groundwater mineralization processes

A comparative analysis of salinity and strontium (Sr^{2+}) has been performed to further elucidate the processes that lead to such high NH_4^+ concentration in both sediments and groundwater. The left graph in Fig. 4.33 shows that almost all deep samples have a higher salinity and Sr^{2+} with respect to the composition of present Adriatic seawater: this suggests the presence of ancient salt fluids rather than modern saltwater intrusion or mixing processes.

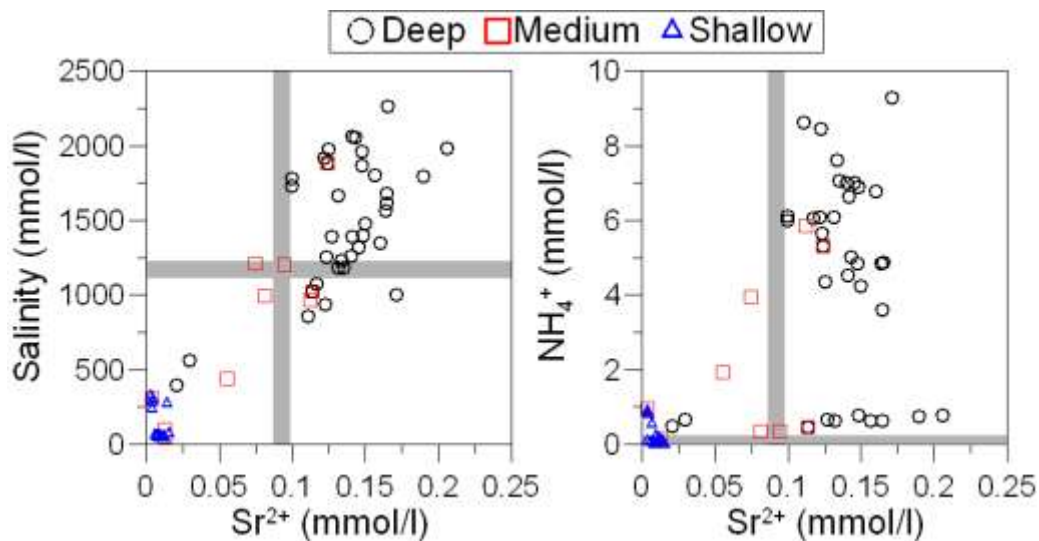


Figure 4.33 - Salinity versus Sr^{2+} concentration in deep (from -25 to -9 m a.s.l.), medium (from -9 to -7 m a.s.l.), and shallow (from -7 to +1 m a.s.l.) samples (left graph); grey bars represent salinity and Sr^{2+} concentration of the Adriatic seawater. NH_4^+ versus Sr^{2+} concentration in deep (from -25 to -9 m a.s.l.), medium (from -9 to -7 m a.s.l.), and shallow (from -7 to +1 m a.s.l.) samples (right graph); grey bars represent NH_4^+ and Sr^{2+} concentration of the Adriatic seawater.

This indicates an enrichment of major and minor elements in deep groundwater samples and consequently a longer transit time of these ground waters with respect to the shallower ones. Only two deep samples fall on the lower left corner of the graph within the area of low salinity and Sr^{2+} concentrations. These two samples belong to monitoring well P3 located within a recharge area, and their salinity and Sr^{2+} concentration values are probably due to mixing processes between fresh recharge water and old saline groundwater (Fig. 4.32). Additional age tracer studies, e.g. $^{87}\text{Sr}/^{86}\text{Sr}$, are needed to further refine the residence time of water.

The left graph in figure 4.33 shows the presence of some samples (belonging to monitoring wells P33 and P3) with elevated Sr^{2+} concentration and salinity slightly below than the actual seawater value: these are possibly due to water/sediment interactions. Medium samples lie between the shallow and deep samples, as expected. The shallow samples are all grouped in the lower left corner, clearly meaning fast travel time and young groundwater.

NH_4^+ is plotted versus Sr^{2+} concentration in the right graph of Fig. 4.33. Again the deep samples show elevated Sr^{2+} concentrations, this time combined with elevated NH_4^+ concentrations. The shallow samples are the less mineralized and the medium samples lie in between. In particular, two distinct groups can be recognized: (i) high NH_4^+ - high Sr^{2+} group mostly referring to deep samples, and (ii) low NH_4^+ - high Sr^{2+} group referring to deep samples as well. Each of these two groups could define a different end-member along two different mixing lines drawn to (iii) the low NH_4^+ - low Sr^{2+} group of shallow samples. The first group includes P33 and P34 deep samples, which belong to lagoon and back barrier sediments usually enriched in TOC. The second group includes P8 and P3 deep samples, which belongs to beach ridges and prodelta sediments usually depleted in TOC respect to lagoon and back barrier sediments (Amorosi et al., 2003).

These patterns are indicative of elevated NH_4^+ contents of natural origin: they are not ascribable to fertilizer loading, because the elevated NH_4^+ concentration are found in strict association with the more mineralized and presumably older groundwater, and because the known type and amount of fertilizers applied in the study area are not sufficient to explain NH_4^+ concentration measured in deep groundwater samples (Mastrocicco et al., 2011b).

4.5 Trace elements mobility in a saline coastal aquifer of the Po river lowland

The effect of elevated salinity on the mobility of trace elements (TE) was studied within the shallow coastal aquifer. The use of intensive depth profiles gave insights into groundwater and sediment matrix interactions. The total concentration of TE within the aquifer matrix was higher in the fine sediments, since usually TE concentrate in the clay fraction, while groundwater concentrations generally increased with the ionic strength of the solution.

The only exceptions were V and As that did not followed this trend, being most probably released by fertilizer leaching. The increase of salinity in conjunction with a high content in carbonates stimulated a release of Pb and Zn, suggesting Pb and Zn surface complexation on carbonate and dolomite minerals. In addition, the elevated organic carbon content of the sediments induced reducing conditions throughout the aquifer, which further promoted TE dissolution.

4.5.1 Sediment composition

The chemical composition of the cores P33 and P34 is reported in Table 4.9, whereas in Table 4.10 are reported the calculated parameters values along with the previously published SOM and clay content (Mastrocicco et al., 2012c).

The values that have been found are in agreement with previous studies of soils (Amorosi and Sammartino, 2006) and sediments (Amorosi et al., 2002; 2004; Curzi et al., 2006) in the area: in particular, these soils and sediments are characterized by high concentrations of Cr and Ni related to the provenance of the sediments (Po river contribution).

RESULTS AND DISCUSSION

Figure 4.34 shows the clear positive trends between the clay content of the sediment samples and the selected TE, that highlight a typical enrichment in the fine fraction often reported in literature (Loring, 1991; Dinelli et al., 2007; Dou et al., 2013): this is displayed not only by the trends of V and Rb, but also by those of Zn and Pb (Fig. 4.34) and other possible hazardous metals, like Co, Ni and Cu. On the contrary, the enrichment trend in peat and SOM is negligible, indicating that TE are not adsorbed or complexed onto SOM.

Table 4.9 - Chemical composition of samples from P33 and P34. Depth is expressed as relative to mean sea level.

Sample	Depth (m)	SiO ₂ (wt%)	TiO ₂	Al ₂ O ₃	Fe ₂ O ₃	MnO	MgO	CaO	Na ₂ O	K ₂ O	P ₂ O ₅	LOI	Sc (ppm)	V	Cr	Co	Ni	Cu	Zn	As	Rb	Sr	Zr	Ba	La	Ce	Pb	Th	S
P33-01	-4.9	51.91	0.56	12.72	4.27	0.11	4.04	11.77	1.3	1.9	0.09	11.33	13	87	200	18	121	29	89	16	90	308	174	391	21	52	10	5	200
P33-02	-5.7	51.59	0.61	12.97	5.48	0.13	4.42	9.74	1.35	2.13	0.12	11.45	14	99	194	17	131	20	80	6	110	246	187	407	23	80	7	14	200
P33-03	-6.1	47.25	0.66	14.94	5.48	0.11	4.43	9.12	0.94	2.39	0.11	14.56	20	120	230	20	161	36	143	12	147	284	116	419	32	82	17	13	225
P33-04	-6.4	47.12	0.64	17.08	5.88	0.1	4.64	3.54	1.07	2.66	0.1	17.17	19	155	253	24	186	35	158	11	192	168	116	406	37	73	22	12	4070
P33-05	-6.7	15.69	0.22	7.95	3.38	0.04	3.1	1.74	2.32	0.97	0.08	64.51	<3	64	59	7	62	3	23	25	56	136	11	97	18	43	2	<3	45900
P33-06	-7.5	50.19	0.59	13.76	4.99	0.1	5.97	6.57	1.92	2.12	0.11	13.68	14	99	181	16	102	13	110	11	132	146	215	337	27	62	8	10	13200
P33-07	-8.6	45.16	0.56	13.47	5	0.1	5.46	9.09	2.57	2.06	0.1	16.44	4	102	174	17	104	17	86	12	142	247	190	328	26	70	17	11	12250
P33-08	-9.4	65.68	0.44	11.81	3.51	0.08	3.57	1.57	3.18	1.87	0.12	8.18	21	64	179	5	70	<3	69	<3	77	128	92	270	22	64	4	<3	12900
P33-09	-10.5	63.32	0.5	11.52	3.64	0.11	4.08	7.74	2.44	1.88	0.12	4.64	15	63	203	10	92	10	66	<3	73	236	107	331	21	41	3	9	3770
P33-10	-12.5	70.43	0.36	11.22	2.56	0.08	3.66	3.57	2.62	2.03	0.09	3.38	8	48	148	7	84	<3	49	8	94	183	96	355	10	41	3	4	2180
P33-11	-13.7	56.22	0.65	12.82	4.51	0.12	4.47	9.2	2.33	2.03	0.13	7.52	14	84	252	12	124	8	59	<3	104	265	252	368	31	67	10	10	3260
P33-12	-14.2	58.08	0.46	11.2	3.62	0.11	4.46	9.88	2.07	1.97	0.12	8.04	<3	61	145	12	84	8	76	3	103	277	169	324	19	58	2	5	540
P33-13	-14.8	56.49	0.51	10.59	3.53	0.12	4.69	11.34	2.27	1.73	0.17	8.58	6	69	143	5	71	9	71	6	79	281	161	293	29	69	2	4	2010
P33-14	-16.5	54.24	0.46	12.95	3.94	0.11	4.93	10.2	2.31	2.19	0.09	8.58	10	73	149	12	105	17	78	10	101	253	97	387	18	39	7	5	1980
P33-15	-18.8	48.88	0.54	10.45	3.38	0.11	4.97	11.99	2.81	1.55	0.11	15.2	4	66	148	6	66	6	39	<3	71	254	337	246	29	77	9	5	3470
P33-16	-19.4	45.48	0.54	9.27	3.52	0.13	4.17	17.47	2.76	1.49	0.1	15.08	<3	66	149	8	70	14	72	<3	76	320	329	330	23	44	6	<3	4720
P33-17	-20.1	41.12	0.5	11.7	4.49	0.12	5.77	13.19	2.56	1.93	0.06	18.56	<3	74	128	13	90	20	90	<3	122	313	131	323	19	44	10	3	200
P33-18	-20.9	36.5	0.49	11.79	4.82	0.13	5.83	11.87	4.58	1.94	0.06	22	<3	89	129	16	97	27	106	14	130	252	89	241	25	47	17	6	8720
P33-19	-21.6	43.49	0.48	10.71	3.5	0.11	5.69	16.35	2.08	1.66	0.07	15.85	<3	59	132	11	69	14	78	<3	88	285	129	297	16	51	7	6	4530
P33-20	-23.2	39.83	0.51	11.87	4.11	0.12	5.95	13.91	2.72	1.83	0.07	19.09	<3	78	108	10	82	13	70	15	112	258	151	251	24	67	15	5	4810
P33-21	-23.9	40.87	0.42	10.31	3.21	0.1	6.29	17.51	1.93	1.63	0.02	17.71	<3	48	82	3	56	9	70	<3	88	265	101	292	15	22	10	5	2640
P33-22	-25.2	42.39	0.53	12.34	4.68	0.12	5.55	12.19	2.56	1.96	0.08	17.59	<3	85	136	16	92	27	102	3	132	284	155	289	26	54	13	<3	9180
P33-23	-25.9	52.62	0.68	17.33	7.73	0.09	4.53	0.65	1.57	2.7	0.16	11.95	18	138	209	32	158	30	152	28	185	119	132	368	35	70	22	10	16900
P34-01	-3.8	49.42	0.62	15.5	6.27	0.14	4.84	4.09	1.36	2.44	0.13	15.19	16	123	217	22	155	30	133	<3	160	136	111	301	28	71	16	10	13100
P34-02	-4.6	45.02	0.53	12.78	5.04	0.13	5.43	9.45	1.63	2.05	0.08	17.87	<3	87	158	19	115	22	110	<3	143	280	162	236	27	62	18	11	11400
P34-03	-6.5	59.93	0.36	10.29	3.18	0.11	3.81	9.17	2.1	1.83	0.07	9.14	<3	47	117	7	80	4	40	6	91	290	73	291	25	50	9	<3	5450
P34-04	-7.5	66.89	0.28	9.67	2.34	0.09	3.08	6.2	2.45	1.87	0.08	7.06	<3	37	104	4	72	21	44	<3	86	249	76	319	7	36	2	6	3560
P34-05	-8.5	65.75	0.31	10.31	2.48	0.09	3.26	6.56	2.53	1.82	0.06	6.84	3	35	104	5	68	15	49	<3	72	200	50	160	13	51	4	10	2320
P34-06	-9.5	65.65	0.31	10.41	2.55	0.1	3.61	6.61	2.54	1.86	0.06	6.3	4	38	107	6	73	14	50	<3	76	210	60	191	12	41	4	9	3215
P34-07	-10.5	44.24	0.44	10.25	3.52	0.1	6.2	14.45	3.08	1.67	0.03	16.02	<3	61	112	6	63	11	73	<3	86	245	116	288	11	38	2	7	2170
P34-08	-12.5	43.52	0.43	10.15	3.42	0.1	6.16	14.34	3.07	1.66	0.03	17.12	<3	60	110	6	67	12	70	<3	85	241	112	279	11	39	2	7	1110
P34-09	-14.1	40.86	0.54	12.22	5.52	0.12	5.74	12.04	3.11	2.07	0.05	17.74	6	81	123	22	130	14	93	23	131	293	83	352	19	48	14	<3	7250
P34-10	-15.5	46.22	0.45	11.1	3.59	0.1	5.87	13.26	2.97	1.8	0.07	14.57	<3	62	117	10	71	12	75	<3	102	285	178	281	12	59	6	7	1580
P34-11	-16.5	44.6	0.53	12.74	4.66	0.11	4.67	10.69	3.34	1.98	0.08	16.6	3	89	141	11	103	26	107	<3	126	286	156	262	21	62	16	15	970

RESULTS AND DISCUSSION

Table 4.10 – Derived parameter values in the sediment samples collected from P33 and P34 (in italics). SOM and clay content reported from Mastrocicco et al. (2012c). Depth are expressed as relative to mean sea level

Sample i.d.	Depth (m)	<i>FeS₂</i> (wt%)	<i>Fe_{py}</i> (wt%)	<i>Fe_{Tr}</i> (wt%)	<i>Fe_{React}</i> (wt%)	<i>PRC</i> (meq/kg)	<i>CBPO</i> (mmol/kg)	SOM* (wt%)	Clay* (wt%)
P33-01	-4.9	0.04	0.02	1.31	1.30	1462	2707	2.1	21.4
P33-02	-5.7	0.04	0.02	2.39	2.37	2085	2410	3.1	30.1
P33-03	-6.1	0.04	0.02	1.97	1.95	4155	2283	6.2	52.9
P33-04	-6.4	0.76	0.35	1.90	1.54	12397	1187	17.2	83.0
P33-05	-6.7	8.56	4.00	1.48	0.00	52403	100	62.5	5.0
P33-06	-7.5	2.46	1.15	1.77	0.62	7479	1709	6.6	28.2
P33-07	-8.6	2.28	1.07	1.84	0.77	6902	2099	6.1	40.8
P33-08	-9.4	2.41	1.12	0.80	0.00	6882	100	5.8	8.8
P33-09	-10.5	0.70	0.33	0.98	0.65	1940	1893	1.6	5.5
P33-10	-12.5	0.41	0.19	0.04	0.00	1041	1126	0.8	1.1
P33-11	-13.7	0.61	0.28	1.52	1.23	2904	2228	3.2	13.9
P33-12	-14.2	0.10	0.05	1.03	0.98	1193	2447	1.6	1.0
P33-13	-14.8	0.37	0.18	1.07	0.90	1921	2708	2.2	13.3
P33-14	-16.5	0.37	0.17	0.96	0.79	1996	2528	2.3	8.6
P33-15	-18.8	0.65	0.30	0.96	0.66	2920	2829	3.2	6.2
P33-16	-19.4	0.88	0.41	1.34	0.93	3250	3636	3.2	5.5
P33-17	-20.1	0.04	0.02	1.73	1.71	2757	3278	4.1	25.8
P33-18	-20.9	1.63	0.76	2.02	1.26	26888	2786	37.3	44.6
P33-19	-21.6	0.84	0.39	1.02	0.63	5377	3701	6.5	15.0
P33-20	-23.2	0.90	0.42	1.34	0.92	5273	3293	6.2	28.2
P33-21	-23.9	0.49	0.23	0.83	0.60	3910	4077	4.9	5.3
P33-22	-25.2	1.71	0.80	1.77	0.97	5957	2774	5.7	28.6
P33-23	-25.9	3.15	1.47	3.56	2.09	7584	100	5.4	69.9
P34-01	-3.8	2.44	1.14	2.59	1.45	8269	1052	7.8	55.7
P34-02	-4.6	2.13	0.99	2.02	1.02	7784	2191	7.7	42.1
P34-03	-6.5	1.02	0.47	0.81	0.34	2375	2059	1.7	1.5
P34-04	-7.5	0.66	0.31	0.16	0.00	1557	1462	1.1	0.6
P34-05	-8.5	0.43	0.20	0.16	0.00	1435	1592	1.3	1.4
P34-06	-9.5	0.60	0.28	0.20	1.00	1705	1635	1.4	2.4
P34-07	-10.5	0.40	0.19	1.13	0.95	1448	3530	1.4	5.6
P34-08	-12.5	0.21	0.10	1.06	0.97	3617	3537	5.0	5.7
P34-09	-14.1	1.35	0.63	2.58	1.95	8767	2843	10.6	10.3
P34-10	-15.5	0.29	0.14	1.02	0.88	3617	3270	4.9	4.9
P34-11	-16.5	0.18	0.08	1.67	1.59	4671	2602	6.7	37.4

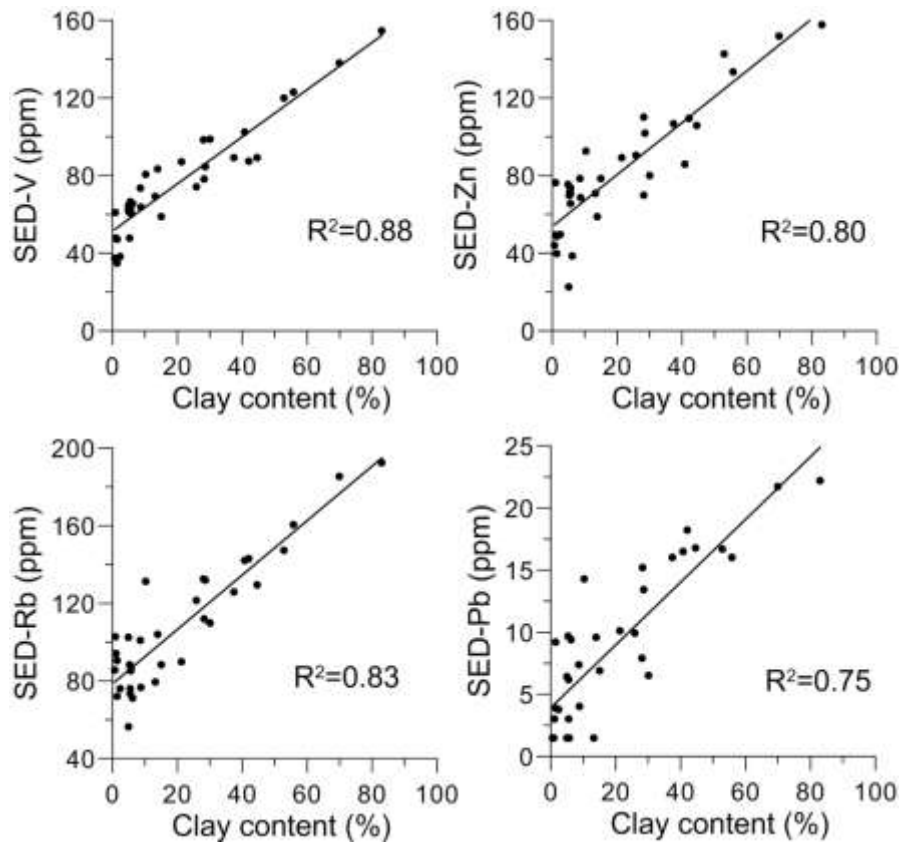


Figure 4.34 - Scatter plots of selected TE in sediments versus clay content and their relative regression coefficients (R^2) for linear fitting.

4.5.2 Hydrochemical conditions of the shallow aquifer

The studied groundwater is characterized in P34 and P35 boreholes by extremely elevated salinity (Fig. 4.35), which is well above the present Adriatic Sea salinity. Reducing conditions are observed throughout the aquifer thickness, as testified by the low Eh (Fig. 4.35) typical of Fe and SO_4^{2-} reduction in carbonate buffered systems (McMahon and Chapelle, 2008). The pH values are comprised between 8.4 to 9.4 in P34 and 8.2 to 8.9 in P33. The principal electron acceptors like O_2 and NO_3^- are not present except for the first 1-2 meters of aquifer (Mastrocicco et al., 2013b).

4.5.3 TE distribution in the shallow aquifer

Table 4.11 reports the TEs concentrations throughout the aquifer profile in P33 and P34. In general, the TE linked with saltwater intrusion (B, Sr and Ba) increase coherently with the salinity (Colombani et al., 2014). The maximum values of these saltwater intrusion markers are well above the actual mean ocean composition, with B up to 8.8 mg/l, Sr up to 16.5 mg/l and Ba up to 308 $\mu\text{g/l}$.

RESULTS AND DISCUSSION

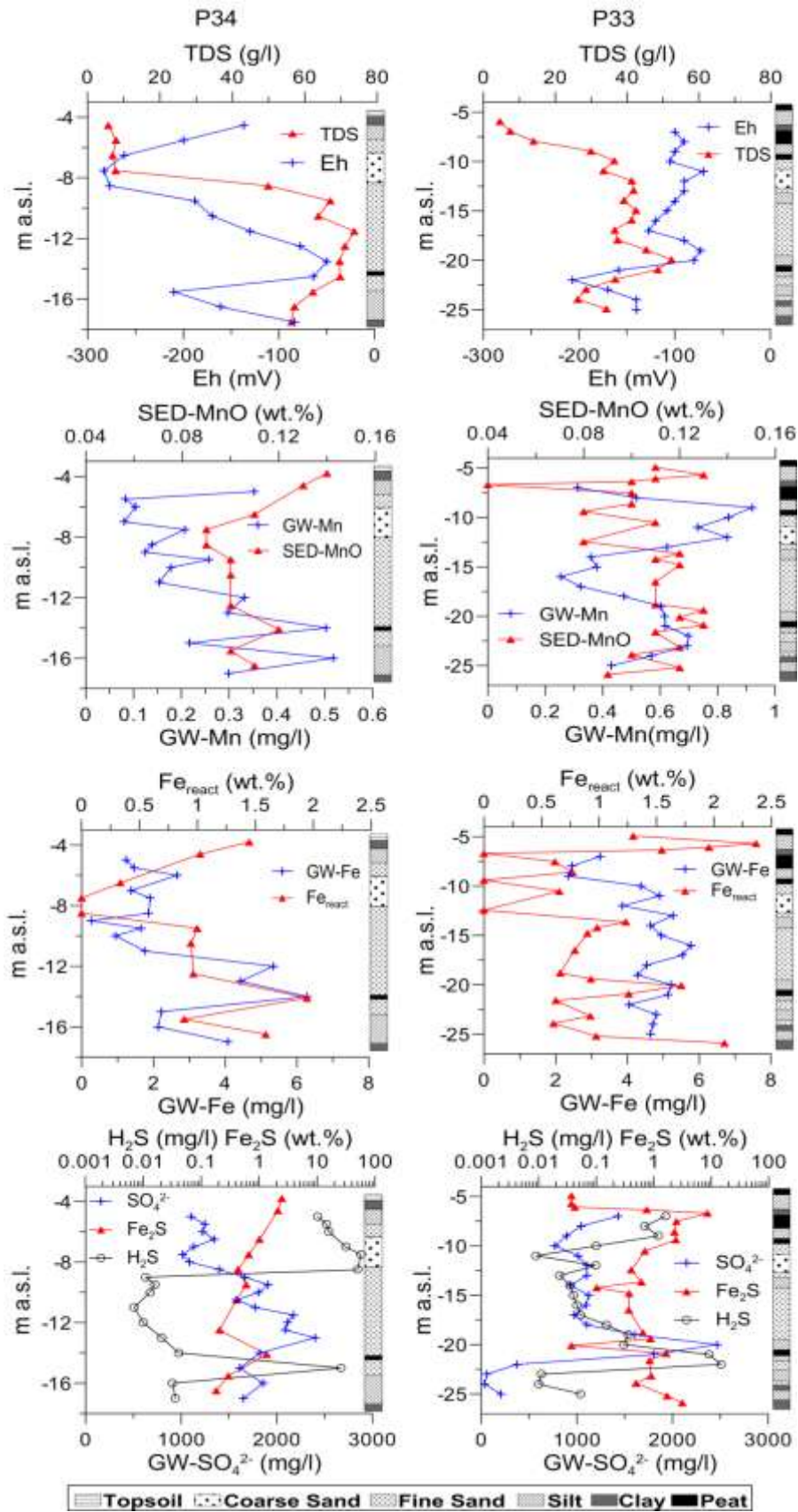


Figure 4.35 - Depth profiles of TDS, Eh and selected redox species in groundwater and sediments; stratigraphy (core logs data) is reported on each plot to facilitate the interpretation.

RESULTS AND DISCUSSION

Table 4.11 - TE concentrations in groundwater samples from P33 and P34. Depth is expressed as relative to mean sea level.

Sample i.d.	Depth (m)	B (mg/l)	Al	P	Fe	Sr	Sc (µg/l)	Ti	Mn	V	Cr	Co	Ni	Cu	Zn	Ga	As	Rb	Ba	Hg	Pb	U
P33-01	-7	3.5	0.8	3.9	3.2	14.1	7.5	182	314	112	11	2.9	35	24	219	5	24	75	214	<0.1	11	0.4
P33-02	-8	3.5	0.9	3.4	2.5	11.5	9.7	148	518	96	24	3.4	36	28	246	1.2	30	57	213	0.6	17	0.1
P33-03	-9	4.2	0.8	3.9	2.4	13.4	5.3	222	920	95	14	3.4	42	35	254	0.8	37	59	172	0.8	13	0.1
P33-04	-10	4	0.8	3.8	4.4	13.5	8	156	838	106	13	6.2	36	13	172	8	35	67	215	0.7	8	0.2
P33-05	-11	3.9	0.7	2.9	4.9	7	6.9	172	731	128	8	4.1	56	23	265	2.9	24	56	253	1	8	0.1
P33-06	-12	4.2	0.4	3.4	3.9	12.7	6.4	127	834	94	120	4.5	23	18	193	3.6	23	46	273	0.5	19	0.1
P33-07	-13	5.7	0.7	3.4	5.3	13.8	16.2	236	624	105	22	4.5	31	25	230	5.9	47	57	208	0.4	31	0.1
P33-08	-14	5.7	1	3.7	4.6	14.4	7.5	193	358	106	13	4.9	24	30	343	5.7	36	57	239	0.2	15	0.2
P33-09	-15	6.7	0.8	3.5	4.9	13.2	9.7	192	379	106	11	3.3	34	27	333	6.5	22	67	265	0.5	14	0.1
P33-10	-16	6.1	1.1	3.1	5.8	13.2	5.3	215	253	106	22	4	44	23	280	4.6	22	46	244	0.5	14	0.2
P33-11	-17	6	0.8	3.9	5.5	13.3	8	222	324	97	33	6.2	23	29	368	4.7	19	45	227	<0.1	15	0.3
P33-12	-18	6.7	0.9	2.9	4.5	13.4	7.7	225	474	91	23	6.4	31	28	321	6.3	29	62	278	0.6	16	0.2
P33-13	-19	7.1	1.5	2.9	4.3	16.5	7.7	239	603	107	73	6.9	28	35	375	8.3	47	40	189	0.8	21	0.4
P33-14	-20	7.7	1.2	3.2	5.2	16.2	5.6	308	617	117	130	4.5	50	20	272	8.9	39	54	173	0.7	27	0.1
P33-15	-21	6.2	1	3.9	5.1	15.1	14.3	183	618	126	23	3.5	24	34	272	5.1	28	42	281	1	30	0.1
P33-16	-22	6.1	0.8	5.5	40	13.5	7.7	201	699	106	13	5.4	29	24	368	10.4	28	57	231	1.5	22	0.2
P33-17	-23	5.6	0.7	4.2	4.8	11.7	5.7	167	695	81	12	2.6	45	18	458	11.4	34	47	251	0.4	26	0.2
P33-18	-24	5.9	0.8	4.5	4.7	10.3	8.7	205	570	86	15	6.6	55	22	326	5.4	45	61	281	0.7	23	0.2
P33-19	-25	5.1	0.6	2.5	4.6	12.3	4.7	134	430	79	12	2.6	25	28	246	3.5	18	37	181	0.5	13	0.2
P34-1	-5	<0.1	0.6	3	1.2	0.8	>0.1	20	352	112	8	<0.1	25	<1	122	<0.1	34	7	54	<0.1	13	<0.1
P34-2	-5.5	<0.1	0.6	2.1	1.5	1.6	>0.1	8	83	96	8	<0.1	6	<1	146	<0.1	28	6	33	<0.1	3	<0.1
P34-3	-6	<0.1	0.8	2.1	2.7	1.7	>0.1	23	104	95	9	<0.1	12	<1	154	<0.1	32	6	29	<0.1	3	<0.1
P34-4	-7	<0.1	0.5	2.8	1.4	1.6	>0.1	24	80	156	10	<0.1	6	<1	102	<0.1	25	7	69	<0.1	2	<0.1
P34-5	-7.5	4	0.5	2.6	1.9	2.7	>0.1	34	208	28	80	0.8	56	<1	165	0.2	<1	16	71	5.2	8	0.1
P34-6	-8.5	5.2	0.4	4.2	1.9	9.2	3.3	114	139	44	1	1.5	1	4	93	3.6	1	48	234	1.4	13	0.1
P34-7	-9	7.3	0.8	7.3	0.3	14.1	16.2	478	124	54	7	4.8	41	52	220	9	44	70	308	0.4	38	<0.1
P34-8	-9.5	7.3	1.6	5.3	1.6	14.2	7.4	236	258	60	3	3.9	14	30	143	7.3	16	72	279	0.2	25	0.2
P34-9	-10	7.3	0.8	5.5	0.9	13.9	9.6	217	179	62	11	3.3	24	27	133	7.3	12	71	269	0.5	24	0.1
P34-10	-11	7	1.4	4.8	1.8	12.7	5.2	181	153	57	42	4	41	23	180	6.2	12	66	234	<0.1	24	0.2
P34-11	-12	7.4	4.3	4.9	5.3	13.7	8	238	332	65	37	6.6	43	29	668	6.8	19	75	223	<0.1	28	0.3
P34-12	-13	8.1	1.9	5.2	4.4	14.5	7.6	208	297	62	3	4.4	11	28	421	6.3	13	72	178	0.6	26	0.2
P34-13	-14	8.4	5.5	9	6.3	15.3	9.7	291	503	68	77	8.7	83	35	375	9.3	37	70	265	0.8	31	0.4
P34-14	-15	7.7	2.2	6.4	2.2	12.4	6.2	138	217	69	140	5.1	101	16	172	8.6	9	64	273	0.7	27	0.1
P34-15	-16	8.8	1.5	7.4	2.1	14.2	14.3	241	518	61	42	5.1	44	34	272	11.4	8	72	283	1	30	0.1

The reported mean composition of B, Sr and Ba for present ocean seawater is 4.5 mg/l, 8.8 mg/l and 21 µg/l, respectively (Turekian, 1968). The quite high Mn and Fe just reflect the reducing conditions present in the aquifer, as explained in the previous section. Another important redox sensitive TE is As, which is often present at remarkable concentrations, exceeding 20 µg/l in most of the samples. In general, some of the analysed TE (as Al, Ti, Zn and Pb) display high or very high concentrations for groundwater. . Their trends will be analysed more in detail in the next sections.

4.5.4 Trace elements profiles in sediments and groundwater

Fig. 4.36 shows a few selected profiles of TE in both sediment and groundwater..

RESULTS AND DISCUSSION

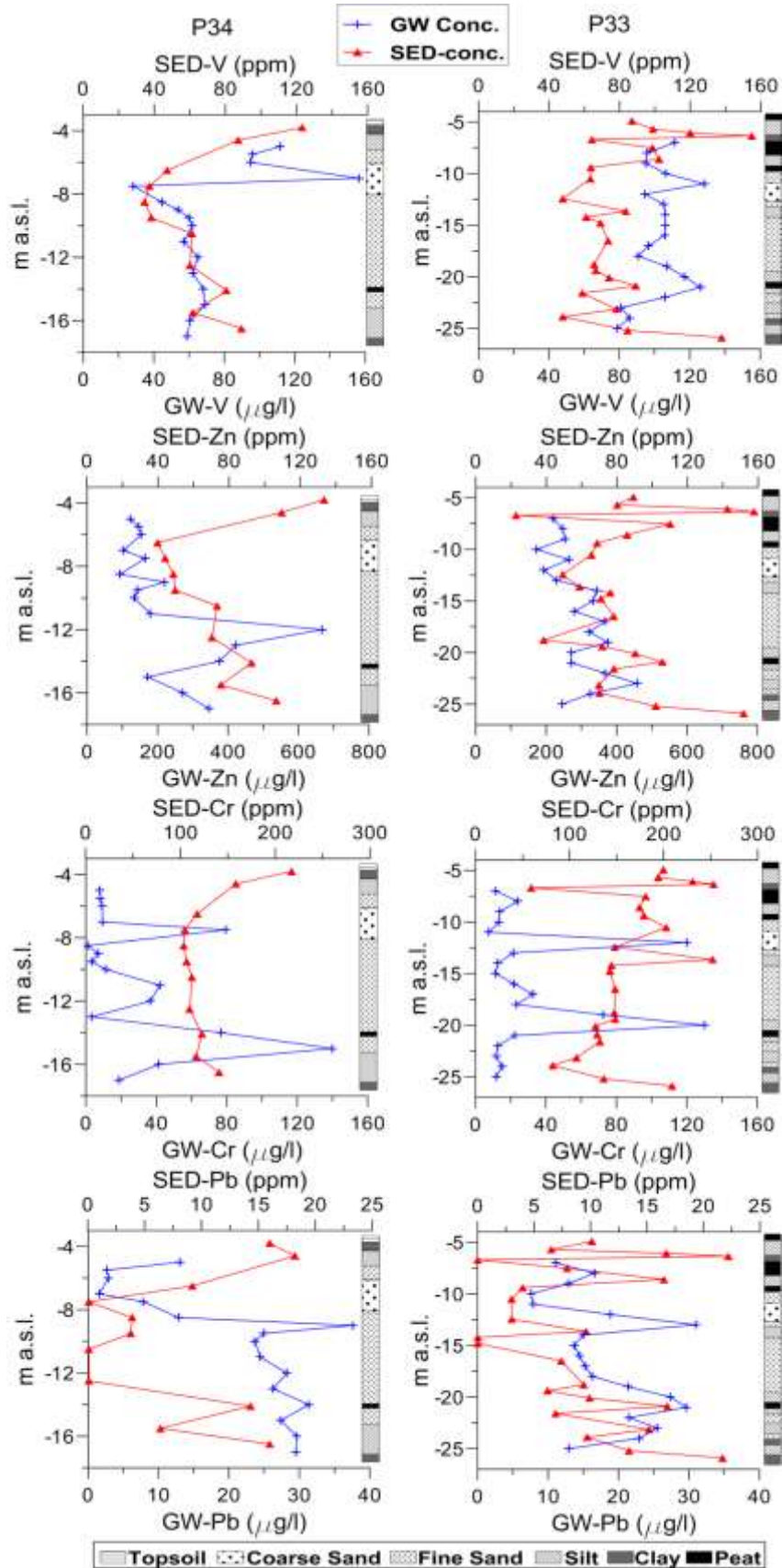


Figure 4.36 - Depth profiles of TE in groundwater and sediments; stratigraphy (core logs data) is reported on each plot to facilitate the interpretation.

The V concentration in sediments follows the grain-size pattern (see Fig. 4.36) with the lowest values in the most permeable layers in both the boreholes P33 and P34. In P34 the V in groundwater (concentrations ranging from 28 to 156 $\mu\text{g/l}$) shows a marked peak, probably due to agrochemical leaching, at the top of the aquifer, and stable concentrations downward despite the elevated salinity. In P33 V shows various peaks not clearly related to salinity or Eh variations, but in general with higher concentrations than in P34.

V could be sensitive to changes in redox conditions. It has two prominent redox species: V(V), which prevails under oxic conditions, and V(IV), which prevails in reduced environments (Breit and Wanty, 1991).

Both species are surface reactive, but V(IV) will be adsorbed far more strongly in natural waters: consequently, V is thought to be removed from solution under reducing conditions (Emerson and Husted, 1991). The elevated salinity and the organic ligands present in this reducing groundwater keep V in solution.

Zn, as already shown, is concentrated in the fine grained sediments; in groundwater (concentrations ranging from 33 to 667 $\mu\text{g/l}$) Zn displays an enrichment in the fine sediments comparable to V enrichment and tends to increase with depth in both P33 and P34, although with a pronounced vertical variability.

Cr displays the same pattern than Zn in the sediments, but in groundwater (concentrations ranging between 1 and 140 $\mu\text{g/l}$) it shows peaks (both in P33 and P34 wells) both in fine graded sediment and coarse sand sediments.

Pb is below detection limits in some sandy sediment; in silt and clay it never exceeds 25 ppm, while in groundwater (concentrations ranging between 1.6 and 37.6 $\mu\text{g/l}$) Pb increases with ionic strength of solution, showing peaks in coincidence with peaty layers. All the selected TE evidence a hundred fold increase in concentration compared to concentrations in mean seawater (Turekian, 1968): this occurrence witnesses the high degree of interaction between liquid and solid phases.

4.5.5 Trace elements partitioning between groundwater and sediments

The direct comparison between sediment and groundwater samples is a quite efficient way to analyse the interaction between liquid and solid phases.

First of all, a correlation matrix can be constructed to evaluate which element or sediment property best matches with other variables. To be concise, only the high correlation degrees will be reported and only Pearson coefficients above 0.6 or below -0.6 will be discussed.

The analysis gives some insights into the interaction between dissolved TE, major ions in groundwater and the aquifer matrix: for example, B present in groundwater is positively correlated to the dissolved Na (0.84) and salinity (0.79), as usually found in saline aquifers (Mondal et al., 2011; Giménez Forcada and Morell Evangelista, 2008); in addition, B displays the highest affinity for dissolved Mg (0.87), however witnessing the role of dolomite dissolution in TE abundance in groundwater. B also correlates quite well with dissolved Ti (0.80), Ga (0.78), Sr (0.78), Ba (0.72) and Pb (0.75).

As mentioned in the previous section, B concentrations in groundwater largely exceed average B seawater concentration (Turekian, 1968): this is consistent with the very high TDS displayed by depth profiles of both the monitoring wells P33 and P43 (Fig. 4.35). Al in groundwater shows a weak positive correlation with salinity (0.62) and with dissolved P (0.68), suggesting that its mobility and the elevated concentrations found in groundwater (Table 4.11) are strongly linked with aqueous complexes and formation of ultrafine colloids.

To prove this hypothesis, Al was analysed in a few selected duplicates of groundwater samples filtered through 0.22 μm polypropylene cartridges: the Al concentration dropped below 0.1 mg/l. The same behaviour was observed for V, Cr, Co, Ni, Cu and U with concentration decreases of more than 80%; all the other TE groundwater concentrations were unaffected by filtration. These findings point to an important control of colloids in the occurrence of TE in groundwater.

P concentration in groundwater is correlated with dissolved K (0.77) and Na (0.73): the most probable source of this nutrient, like for the ammonium, is the decomposition of deep buried SOM (Mastrocicco et al., 2013b). The dissolved Sc has positive correlations with dissolved Mo (0.82) and Cu (0.72), suggesting a common origin of these TE in this saline aquifer. Ti in groundwater is well correlated with dissolved Sr (0.86) and dissolved Co (0.75): Ti concentrations in groundwater are quite elevated and, as mentioned for B, well above the seawater concentration, suggesting dissolution from sediment in reducing alkaline-saline conditions. The filtering through 0.22 μm polypropylene cartridges did not produce appreciable decrease in Ti concentrations. The dissolved Cu is positively correlated with Sr (0.81) and Mo (0.82): in general dissolved Cu concentrations are not elevated even at high salinities (Table 4.11).

On the contrary, Zn groundwater concentrations are much higher, with concentration peaks of more than 400 $\mu\text{g/l}$ (Fig. 4.36 and Table 4.11). Dissolved Zn is weakly correlated with dissolved Fe (0.65), suggesting a release of this metal in iron reducing conditions. The dissolved As is weakly correlated with most of the TE, except dissolved V (0.66), suggesting a possible agricultural origin of Zn from fertilizers (Otero et al., 2005) beside the sedimentary origin. Surprisingly, As is not correlated with pyrite or SOM as it is usually found (Wang et al., 2012), although the As groundwater concentrations are generally high throughout both profiles (Table 4.11). The quite elevated (up to 38 $\mu\text{g/l}$) dissolved Pb concentrations in groundwater are positively the Fereact (0.72) meaning that Pb in groundwater is possibly sourced by iron hydroxides in saline conditions; in addition, Pb correlates with dissolved Mg (0.72), indicating that dolomite is a possible source for the elevated Pb observed groundwater concentrations as well (Table 4.11).

5. SUMMARY AND CONCLUSIONS

5.1 Synthesis

The primary objective of this thesis was to gain a quantitative understanding of the processes that caused groundwater salinization in the Ferrara coastal aquifer. In this final chapter, the main outcomes of the applied multi-disciplinary approach will be evaluated to determine to what extent they contribute to improve current knowledge. Some implications for practical hydrogeological studies will be discussed and research topics needing further understanding will be outlined.

Finally, a list of the related publication is supplied at the end of this chapter (paragraph 5.4) to provide the reader with more detailed information concerning the different aspects on which this thesis has focused over the last three years.

5.2 Conclusions

A detailed hydrodynamic and hydrogeochemical characterization of the Ferrara coastal aquifer, subject to profound natural and anthropogenic changes since the last glaciation to nowadays, demonstrated that groundwater salinization is a factual issue for current and future management of water resources (see chapter 4.1).

Saline and hypersaline water are associated with fine sediments of back barrier and lagoonal environments, relic of Flandrian transgression, while brackish and fresh waters are related to relict dune-beach systems. Hypersaline groundwater found in the deepest portion of the aquifer cannot be associated with lateral seawater intrusion or upconing of present seawater: its features suggest the presence of relict seawater and salts trapped in the back-barrier dunes and lagoonal environments during the Holocene interglacial phases. Relic seawater and salt deposits in fine grained sediments could have been preserved from rapid flushing and gradually released, leading to the formation of hypersaline groundwater.

Field data show that the development of anomalously-high salt contents (i.e., greater than in seawater) may be attributed to direct evaporation of seawater prior to infiltration. Even the high Cl^- concentrations in groundwater from the coastal area can be attributed to this process. Depth-dependent physical aquifer parameterization highlights the presence of an upward vertical gradient due to the dense drainage system that controls the hydrodynamics of the coastal area. As a consequence, saline groundwater previously preserved in the deepest portion of the aquifer, and often confined by low-permeability lenses, has been mobilized and transported via seepage to the shallow part of the aquifer and even discharged in the superficial network of irrigation canals.

The hydrogeological and hydro-geochemical investigations suggest that aquifer salinization does not result in a linear process. In fact, mixing between freshwater end-members and relict

seawater causes the onset of several concurring and competing water-sediment interactions as cation exchange, calcite and dolomite dissolution, oxidation of organic matter, and SO_4^{2-} bacterial reduction, which overlap to salinization. Deviations from the non-reactive mixing line are observed, indeed, for the main ions (Br^- , Na^+ , SO_4^{2-} , Ca^{2+} , and Mg^{2+}) especially in the most saline samples. The more saline groundwater is characterized by the effects of cation exchange and SO_4^{2-} reduction where fossil organic matter is present (paleo-marsh deposits, peat layers). The whole of the processes results in the increase of Ca^{2+} and HCO_3^- contents in the ground waters. The increase in Ca^{2+} , Mg^{2+} , and HCO_3^- shifts the carbonate equilibrium and leads to dolomite/calcite precipitation.

Experience in the field revealed that a detailed vertical characterization is the sole approach that can return a reliable distribution of dissolved species and geochemical patterns within the unconfined aquifer. For this reason different monitoring techniques were applied to acquire depth-dependent profiles of the physical-chemical parameters: they were compared in order to find the most reliable and effective one (see chapter 4.2).

The comparison between the Open-Borehole Logging (OBL) technique and the more robust (but more expensive and time consuming) Multi-Level Sampling (MLS) technique shows that, excluding the distribution of saline to hypersaline water types at the bottom of the aquifer, no significant differences are observed between salinity data recorded by means of the two techniques. It follows that, when the density stratification is from denser groundwater at the bottom to less dense groundwater towards the water table, the OBL method can be successfully used for a preliminary determination of the position of the saltwater wedge and for a general classification of the water types present in the aquifer. However, hydrochemical data (pH, Eh and O_2) collected with the OBL technique do not agree with data acquired by the MLS technique. As matter of fact, more detailed studies on the reactive geochemical processes involving micro and meso-scale structures, like peat layers, can be undertaken only through MLS technique and, this technique is also preferable to OBL when a high level of accuracy in depicting salinity distribution is required to infer recharge from surface water bodies.

A direct comparison between Integrated-Depth Sampling (IDS) and MLS performance was also performed. The conceptual models based respectively on the IDS and the MLS monitoring techniques return different representations of groundwater salinization and therefore of the causes that led to it. The disagreement in the results gained by the two sampling techniques is particularly evident when analysing the TDS versus depth plot, the Cl^-/Br^- molar ratios and the Eh versus pH diagram. Discrepancies between MLS and IDS values concerning major ions concentrations and physical-chemical parameters give a quantitative insight on this disagreement, especially in the case of the redox-dependent dissolved species, testifying that in the IDS technique the artificial mixing within the long well screens masks the actual vertical stratification along the aquifer thickness. The results demonstrate that the IDS technique is not only inaccurate if compared with the MLS technique, but it might also give misleading representations of reality.

Therefore, conceptual models gained via IDS technique cannot be considered in a preliminary study for a coastal aquifer affected by salinization, but they should be decisively avoided, especially when the density contrast between fresh and saline groundwater is large.

The current situation of the Ferrara coastal aquifer was reconstructed through the use of numerical modelling, to confirm the initial hypothesis on the origin of salinization as well (see chapter 4.3). The effects of aquifer autonomous salinization via upward flux and those of the consequent salt loads to surface waters were calculated with a three-dimensional variable-density numerical flow model coupled with a non-reactive solute transport model.

Results show that since seepage water is brackish to saline, salinization of shallow groundwater and surface waters is by now considerable and discharge of salt loads in the superficial network of irrigation canals would intensify in the near future. This process, that is the result of the drainage of lands over the past years, will affect surface water quality and reduce shallow fresh groundwater volumes. Thus, in the future, fresh water resources for agricultural purposes and ecosystems will come under increasing pressure.

A two-dimensional numerical model was implemented along the selected transect A-A' to help deepening the understanding of the key factors that control the hydrodynamic behaviour and the salinity in the local aquifer with respect to a nearby drainage canal.

Results show that the current irrigation scheme governs the groundwater fluxes. In spring and summer the canal used for agricultural irrigation recharges the aquifer, thus diminishing the shallow groundwater salinity also in case of temperature increase (and associated evapotranspiration), as forecasted by future regional climate change. On the contrary, during the cold season the canal is no longer used for irrigation and consequently the freshwater recharge stops, leading to a flow reversal that provokes an increase in shallow groundwater salinity connected to the upward flux of hyper-saline groundwater contained in the fine prodelta sediments. This upward flux slowly salinizes the surface waters bodies connected with the aquifer. Simulations indicate that an increase in temperature or an increase in the severe high rainfall events have only minor influence on the aquifer salinization rate, while an interruption of canal usage could create serious upward movement of the high salinity groundwater currently residing in the aquifer bottom. Besides, the impact of the projected sea level rise seems much more important than temperature and rainfall increase, thus new studies will need to better delineate the forthcoming sea level rise at local scale.

Since climatic changes may enhance the rate of autonomous salinization in the unconfined aquifer of Ferrara, the contribution of water-sediment interaction and the anthropogenic influence on groundwater quality were studied in order to assess whether the change in the present chemical-physical and hydrogeological conditions may also induce the remobilization of geogenic elements. The study focused the attention on nitrogen species (see chapter 4.4) and trace elements (see chapter 4.5).

The prevalent dissolved inorganic N species was NH_4^+ , especially where reducing condition dominates, while NO_3^- prevails where oxidizing condition prevails. Very high NH_4^+ concentrations were found in the salinized anoxic aquifer in coincidence with peaty sediments, and even higher concentrations were in the low-lying aquitard. NH_4^+ extracted from core samples and SED-TOC determinations suggested that NH_4^+ is of natural origin and is likely due to mineralization of organic rich fine sediments, originated in paleo-marsh environments.

Plots of NH_4^+ versus salinity and Sr^{2+} confirm the hypothesis of sediment being the source of NH_4^+ , with the deepest and most mineralized samples displaying the highest NH_4^+ concentrations.

Accordingly, the total trace elements (TE) concentration within the aquifer matrix was higher in the fine sediments, since usually these elements concentrate in the clay fraction, while groundwater concentrations generally increased with the ionic strength of the solution. The only exceptions were V and As that did not follow this trend, being most probably released by fertilizers leaching in the top part of the aquifer and by buried peaty layers in the lower part of the aquifer. In addition, the elevated SOM induced reducing conditions throughout the aquifer profile, which further promoted TE dissolution. The presence of carbonates in the aquifer matrix probably stimulated a high release of Pb and Zn in reducing alkaline-saline conditions, suggesting Pb and Zn surface complexation on carbonate and dolomite minerals. Some TE, like aluminium, were found to be affected by filtration, suggesting the presence of aqueous complexes and formation of ultrafine colloids in coincidence with fine lenses. This latter aspect could be relevant for TE transport and should be accurately studied in future researches.

5.3 Recommendations

5.3.1 Practical implications

Discriminating between past and actual salinization is often difficult or even impossible, especially when only salinity data are collected. It is evident that the current hydrogeological environment and its present border conditions (natural and human) are completely different from those, which allowed originating relic seawater and successively preserving it. The interpretation of present-day observations must take into account that water quality patterns continue evolving starting from the past, by adapting to contemporary boundary conditions. The knowledge of the geological history of the area under investigation is then essential to recognize the potential contribution of past hydrological processes to the present situation.

Moreover, collection of reliable samples resulted of vital importance for the correct identification of aquifer physical properties and groundwater quality distribution. The selection of appropriate monitoring techniques, such as depth-dependent sampling, are therefore as important as that of right analytical and modelling techniques. MSL technique does not require highly-specialized skills or expensive equipment, but still today studies on aquifer salinization are rarely taking advantage of this approach that is conversely common in contaminant fate and transport assessment. The implications of what said so far are not limited to the local situation, but have a wider impact.

In fact, the rational demonstration, for a real site, of how severe can be the misleading in using ease but incorrect conceptual models based on unreliable monitoring techniques, can

represent a warning to water resources managers who have to make difficult choices for planning future groundwater protection and exploitation.

Finally, even if field data are indispensable to understand the hydrogeological system under investigation, numerical models provide a means to test hypothesis based on physical and chemical theory. With the right approach, the conjunctive use of both measurements and simulation leads to better understanding and new insights. In this study numerical scenarios quantified the possible climate change impacts on groundwater salinization and its consequences on water resources quality: moreover, they could be helpful in outlining mitigation strategies to decrease future salt load to groundwater and surface water systems.

As matter of fact, successful choice and implementation of mitigative countermeasures requires a solid knowledge base, through which the relevant conditions and processes are well characterized: however, planning also needs to take into account the economic aspects that were not considered in this study. Nevertheless, the characterization protocol described and applied to this study could be successfully applied in many other similar coastal low lying areas worldwide, suffering from the same issues that are stressing the Ferrara coastal aquifer.

5.3.2 Remaining challenges

The present study used knowledge and methodologies from different earth-scientific disciplines to investigate the salinization of the Ferrara coastal aquifers. None of the methodologies provided complete understanding of the hydrogeological system under consideration when applied separately. The strength of the adopted multi-methodological approach provides an important progress of previous studies that mainly addressed the subject from a single view in this area. Notwithstanding the profuse efforts, some of the topics that were discussed in this thesis are still not fully understood.

For instance, the understanding of the hydrogeological behaviour of low-permeability Holocene strata is inadequate. The observed spatial salinity variations in the pore-water of these layers imply complex flow patterns, which contrast with the often-made assumption of a uniform vertical flow field. This scale issue is relevant on ecological and pollution-oriented applications that require detailed knowledge of the small-scale flow field, such as the quantification of high nutrient loads to surface waters in groundwater discharge areas. It requires the development of methods to characterize groundwater flow in greater detail than those provided by sparse observation wells.

5.4 Related publications

Contributions concerning the characterization of the lowland coastal aquifer of Ferrara and its salinization:

- Colombani N.*, Bonzi L., Calabrese L., Ferrari V., Giambastiani B.M.S., Mastrocicco M., Severi P. (2012). Correlation between hydrochemical facies and depositional environments in a salinized lowland coastal aquifer (Ferrara, IT). Proceedings of 7th EUREGEO, 12-15 giugno 2012, Bologna (IT). Eds. Scappini S., Zapparoli S. Centro Stampa Regione Emilia-Romagna, pp. 363-364.
- Giambastiani B.M.S.*, Colombani N., Fidelibus M.D., Severi P., Mastrocicco M. (2012). Groundwater hypersalinization in a lowland coastal aquifer (Po River Plain, Italy). Proceedings of 22nd Salt Water Intrusion Meeting. 17-22 June 2012, Búzios (BRA). Eds. Cardoso da Silva G.Jr., Gico de Lima Montenegro S.M. - Meta marketing e eventos Publisher; ISBN: 978-85-63243-03-4, pp. 82-85.
- Giambastiani B.M.S., Colombani N., Mastrocicco M.* (2012). Artificial recharge assessment in salinized coastal aquifers: Comacchio case study (IT). Proceedings of the 39th IAH Congress. 16-21 September 2012, Niagara Falls (CAN).
- Giambastiani B.M.S., Colombani N., Mastrocicco M.*, Fidelibus M.D. (2013). Characterization of the lowland coastal aquifer of Comacchio (Ferrara, Italy): hydrology, hydrochemistry and evolution of the system. JOURNAL OF HYDROLOGY, 501, pp. 35-44.
- Giambastiani B.M.S., Colombani N., Mastrocicco M.*, Severi P. (2012). Salinization and freshening processes in the coastal aquifer of Ferrara (IT). Proceedings of BALWOIS2012: V International Scientific Conference on Water, Climate and Environment; 28 May - 2 June 2012, Ohrid (FYROM). Eds Morell M., Popovska C., Morell O., ISBN 978-608-4510-10-9.
- Mastrocicco M., Colombani N.*, Antonellini M. (2012). Freshwater-seawater mixing experiments in sand columns. JOURNAL OF HYDROLOGY, 448-449, pp. 112-118.
- Volta G., Colombani N.* (2013). Continuous monitoring of surface-groundwater interactions in a lowland coastal aquifer. REND. ONLINE SOC. GEOL. IT., 25, 137-139.

Contributions concerning the importance of data acquisition techniques in saltwater intrusion monitoring:

- Colombani N., Giambastiani B.M.S.*, Mastrocicco M. (2015). Combined use of electrical conductivity and temperature to estimate aquifer properties in a forced gradient test. Submitted to JOURNAL OF HYDROLOGY, HYDROL18711.

SUMMARY AND CONCLUSIONS

- Giambastiani B.M.S.*, Colombani N., Mastrocicco M. (2012). Multilevel characterization of vertical hydraulic gradients, permeability, temperature and salinity in a shallow coastal aquifer (Ferrara, Italy). Proceedings of 22nd Salt Water Intrusion Meeting. 17-22 June 2012, Búzios (BRA). Eds. Cardoso da Silva G.Jr., Gico de Lima Montenegro S.M. - Meta marketing e eventos Publisher; ISBN: 978-85-63243-03-4, pp. 140-143.
- Giambastiani B.M.S., Colombani N., Mastrocicco M.*, Severi P. (2012). Cost and time-effective methodology to evaluate aquifer parameters in coastal aquifers. Proceeding of FLOWPATH 2012, 20-22 giugno 2012 Bologna (IT). Percorsi di Idrogeologia.
- Giambastiani B.M.S., Colombani N.*, Salemi E., Mastrocicco M. (2012). Metodica di caratterizzazione multilivello di gradienti idraulici, permeabilità e conducibilità elettrica in acquiferi costieri salinizzati. IV Congresso Nazionale AIGA - Perugia, 6-7 febbraio 2012. ENGINEERING, HYDRO, ENVIRONMENTAL GEOLOGY, 14 (B), pp. 132-133.
- Mastrocicco M., Colombani N.*, Volta G. (2014). Misleading reconstruction of seawater intrusion via integral depth sampling. Submitted to JOURNAL OF HYDROLOGY, HYDROL 18381.
- Mastrocicco M., Giambastiani B.M.S., Severi P., Colombani N.* (2012). The importance of data acquisition techniques in saltwater intrusion monitoring. WATER RESOURCES MANAGEMENT, 26 (10), pp. 2851-2866.

Contributions concerning the implementation of numerical modelling to assess climate change impact on the salinization of the Ferrara coastal aquifer:

- Colombani N., Giambastiani B.M.S., Mastrocicco M.* (2014). Predicting salinization trends in a lowland aquifer: Comacchio (Italy). WATER RESOURCES MANAGEMENT, 29(2), 603-618.
- Colombani N., Giambastiani B.M.S., Mastrocicco M.* (2013). Forecasting Salinization Trends In A Lowland Aquifer: Comacchio (Italy). Proceedings of EWRA: 8th International Conference, 26-29 June 2013, Porto (PT). In Water Resources Management In An Interdisciplinary And Changing Context. Eds. Maia R., Guerreiro de Brito A., Seca Teixeira A., Tentúgal Valente J., Pêgo J.P., FEUP Publisher. ISBN: 978-989-95557-8-5
- Colombani N., Osti A., Volta G., Mastrocicco M.* (2015). Impact of climate change on salinization of coastal water resources. Submitted to WATER RESOURCES MANAGEMENT.
- Mastrocicco M., Colombani N.*, Gargini A. (2014). Modelling present and future Po river interactions with the alluvial aquifers (low Po river plain, Italy). JOURNAL OF WATER AND CLIMATE CHANGE, 5(3), 457-471.

Contributions concerning the effect that salinization could have on the mobilization of major and trace elements:

SUMMARY AND CONCLUSIONS

- Castaldelli G., Colombani N.*, Vincenzi F., Mastrocicco M. (2013). Linking dissolved organic carbon, acetate and denitrification in agricultural soils. ENVIRONMENTAL EARTH SCIENCES, 68 (4), pp. 939-945.
- Castaldelli G.*, Pierobon E., Soana E., Salemi E., Aschonitis V., Colombani N., Mastrocicco M., Bartoli M. (2012). Nitrogen mass balance in a coastal lowland declared vulnerable to nitrate (WFD 2000/60/EC): the relevance of secondary canals in excess nitrogen removal. Proceedings of the 17th Nitrogen Workshop, 26-29th June 2012, Wexford (IRE). Innovations for sustainable use of nitrogen resources, Eds. Richards K.G., Fenton O., Watson C.J. ISBN-10: 1-84170-588-8, pp. 172-173.
- Colombani N., Mastrocicco M.*, Dinelli E. (2014). Trace elements mobility in a saline coastal aquifer of the Po river lowland (IT). Submitted to JOURNAL OF GEOCHEMICAL EXPLORATION, GEXPLO3735.
- Colombani N.*, Mastrocicco M., Vincenzi F., Castaldelli G. (2012). Nitrogen speciation and denitrification in a low land territory receiving synthetic fertilizers (Province of Ferrara, Northern Italy). Proceedings of BALWOIS2012: V International Scientific Conference on Water, Climate and Environment; 28 May - 2 June 2012, Ohrid (FYROM). Eds Morell M., Popovska C., Morell O., ISBN 978-608-4510-10-9.
- Giambastiani B.M.S., Colombani N., Mastrocicco M.* (2014). Detecting small scale variability of trace elements in a shallow aquifer. WATER AIR AND SOIL POLLUTION, doi: 10.1007/s11270-014-2283-4
- Giambastiani B.M.S, Colombani N.*, Mastrocicco M. (2013). High phosphate bearing sediments in a salinized coastal aquifer. Proceedings of GQ13: 8th IAHS Groundwater Quality Conference, 21-26 aprile 2013, Gainesville, Florida (USA).
- Mastrocicco M., Colombani N. *, Castaldelli G. (2013). A step-wise approach to assess the fate of nitrogen species in agricultural lowlands. In "Wastewater reuse and management". Edito da Sharma S.K. and Sanghi R. (Eds.) Springer-Verlag New York, LLC; ISBN 978-94-007-4941-2, 474 p.
- Mastrocicco M., Giambastiani B.M.S., Colombani N.* (2013). Ammonium occurrence in a salinized lowland coastal aquifer. HYDROLOGICAL PROCESSES, 27 (24), pp. 3495-3501.

REFERENCES

- Acosta J.A., Jansen B., Kalbitz K., Faz A., Martínez-Martínez S., 2011. Salinity increases mobility of heavy metals in soils. *Chemosphere* 85(8), 1318-1324.
- Alcalà F.J. and Custodio E., 2008. Using the Cl/Br ratio as a tracer to identify the origin of salinity in aquifers in Spain and Portugal. *Journal of Hydrology* 359, 189-207.
- Allen R.G., Pereira L.S., Raes D., Smith M., 1998. Crop evapotranspiration. Guidelines for computing crop water requirements. Irrigation and Drainage Paper No. 56. FAO, Rome.
- Amorosi A., Centineo M.C., Colalongo M.L., Pasini G., Sarti G., Vaiani S.C., 2003. Facies Architecture and Latest Pleistocene–Holocene Depositional History of the Po Delta (Comacchio Area), Italy. *The Journal of Geology* 111, 39-56.
- Amorosi A., Centineo M.C., Dinelli E., Lucchini F., Tateo F., 2002. Geochemical and mineralogical variations as indicators of provenance changes in Late Quaternary deposits of SE Po Plain. *Sedimentary Geology* 151, 273-292.
- Amorosi A., Colalongo M. L., Fiorini F., Fusco F., Pasini G., Vaiani S.C., Sarti G., 2004. Palaeogeographic and palaeoclimatic evolution of the Po Plain from 150-ky core records. *Global and Planetary Change* 40(1-2), 55-78.
- Amorosi A. and Sammartino I., 2006. Influence of sediment provenance on background values of potentially toxic metals from near-surface sediments of Po coastal plain (Italy). *International Journal of Earth Sciences* 96(2), 389-396.
- Andersen M.S., Nyvang V., Jakobsen R., Postma D., 2005. Geochemical processes and solute transport at the seawater/freshwater interface of a sandy aquifer. *Geochimica and Cosmochimica Acta* 69, 3979-3994.
- Antonellini M. and Mollema P.N., 2010. Impact of groundwater salinity on vegetation species richness in the coastal pine forests and wetlands of Ravenna, Italy. *Ecological Engineering* 36(9), 1201-1211.
- Antonellini M., Mollema P.N., Giambastiani B.M.S., Bishop K., Caruso L., Minchio A., Pellegrini L., Sabia M., Ulazzi E., Gabbianelli G., 2008. Salt water intrusion in the coastal aquifer of the southern Po Plain, Italy. *Hydrogeology Journal* 16(8), 1541-1556.
- Appelo C.A.J. and Postma D., 2005. *Geochemistry, groundwater and pollution*, 2nd Edition, Balkema, Rotterdam, The Netherlands.

REFERENCES

- Aravena R. and Robertson W.D., 1998. Use of multiple isotope tracers to evaluate denitrification in ground water: Study of nitrate from a large-flux septic system plume. *Ground Water* 36(6), 975-982.
- Artegiani A., Paschini E., Russo A., Bregant D., Raicich F., Pinardi N., 1997. The Adriatic Sea general circulation. Part I: Air-sea interactions and water mass structure. *Journal of Physical Oceanography* 27, 1492-1514.
- Balugani E. and Antonellini M., 2011. Barometric pressure influence on water table fluctuations in coastal aquifers of partially enclosed seas: An example from the Adriatic coast, Italy. *Journal of Hydrology* 400, 176-186.
- Balugani E. and Antonellini M., 2010. Measuring Salinity within Shallow Piezometers: Comparison of Two Field Methods. *Journal Water Resource and Protection* 2, 251-258.
- Barlow P.M. and Reichard E.G., 2010. Saltwater intrusion in coastal regions of North America. *Hydrogeology Journal* 18, 247-260.
- Bear J., 1972. *Dinamics of fluids in porous media*. Elsevier, Amsterdam.
- Bear J., Cheng A.H.-D., Sorek S., Quazar D., Herrea I., 1999. *Seawater intrusion in coastal aquifers -concepts, methods and practices*. Kluwer Academic Publishers.
- Böhlke J.K., Wanty R., Tuttle M., Delin G., Landon M., 2002. Denitrification in the recharge area and discharge area of a transient agricultural nitrate plume in a glacial outwash sand aquifer, Minnesota. *Water Resources Research* 38(7), 101-1026.
- Bower C.F. and Holm-Hansen T., 1980. A salicylate-hypoclorite method for determining ammonia in seawater. *Canadian Journal of Aquatic Sciences* 37, 794-798.
- Brambati A., Candian C., Bisiacchi G., 1973. Fortran IV program for settling tube size analysis using CDC 6200 computer. *Istituto di Geologia e Paleontologia, Università di Trieste*.
- Bratton J.F., Bohlke J.K., Krantz D.E., Tobias C.R., 2009. Flow and geochemistry of groundwater beneath a back-barrier lagoon: The subterranean estuary at Chincoteague Bay, Maryland, USA. *Marine Chemistry* 113(1-2), 78-92.
- Breit G.N. and Wanty R.B., 1991. Vanadium accumulation in carbonaceous rocks: a review of geochemical controls during deposition and diagenesis. *Chemical Geology* 91, 83-97.
- Britt S.L., 2005. Testing the in-well horizontal laminar flow assumption with a sand-tank well model. *Groundwater Monitoring and Remediation* 25(3), 73-81.

REFERENCES

- Brun A., Engesgaard P., Christensen T.H., Rosbjerg D., 2002. Modelling of transport and biogeochemical processes in pollution plumes: Vejen landfill, Denmark. *Journal of Hydrology* 256(3-4), 228-247.
- Buggy C.J. and Tobin J.M., 2008. Seasonal and spatial distribution of metals in surface sediment of an urban estuary. *Environmental Pollution* 155(2), 308-319.
- Bureau of Reclamation, 2001. Water testing for permeability. In: *Engineering Geology Field Manual*, US Dept of the Interior, Washington. Vol. 2, Chap. 17.
- Candela L., von Igel W., Elorza F.J., Aronica G., 2009. Impact assessment of combined climate and management scenarios on groundwater resources and associated wetland (Majorca, Spain). *Journal of Hydrology* 376(3-4), 510-527.
- Capaccioni B., Didero M., Paletta C., Didero L., 2005. Saline intrusion and refreshing in a multilayer coastal aquifer in the Catania Plain (Sicily, Southern Italy): dynamics of degradation processes according to the hydrochemical characteristics of groundwater. *Journal of Hydrology* 307, 1-16.
- Carminati E., Dogliosi C., Scrocca D., 2005. Magnitude and causes of natural subsidence of Venice. In: Fletcher C, Spencer T (Eds.) *Flooding and environmental challenges for Venice and its lagoon*. Cambridge University Press, Cambridge, pp. 21-28.
- Cartwright I., Weaver T.R., Fulton S., Nichol C., Reid M., Cheng X., 2004. Hydrogeochemical and isotopic constrains on the origins of dryland salinity, Murray basin, Victoria, Australia. *Applied Geochemistry* 19, 1233-1254.
- Chang S.W., Clement T.P., Simpson M.J., Lee K.K., 2011. Does sea-level rise have an impact on saltwater intrusion? *Advances in Water Resources* 34(10), 1283-1291.
- Christensen T.H., Kjeldsen P., Bjerg P.L., Jensen D.L., Christensen J.B., Baun A., Albrechtsen H.J., Heron G., 2001. Biogeochemistry of landfill leachate plumes. *Applied Geochemistry* 16(7-8), 659-718.
- Cidu S., Vittori Antisari L., Biddau R., Buscaroli A., Carbone S., Carbone S., Da Pelo S., Dinelli E., Vianello G., Zannoni D., 2013. Dynamics of rare earth elements in water–soil systems: The case study of the Pineta San Vitale (Ravenna, Italy). *Geoderma* 193-194, 52-67.
- Colombani N., Mastrocicco M., Dinelli E., 2014. Trace elements mobility in a saline coastal aquifer of the Po river lowland (IT). Submitted to *Journal of Geochemical Exploration*, GEXPL03735.

REFERENCES

- Colombani N., Mastrocicco M., Gargini A., Davis G.B., Prommer H., 2009. Modelling the fate of styrene in a mixed petroleum hydrocarbon plume. *Journal of Contaminant Hydrology* 105(1-2), 38-55.
- Colombani N., Mastrocicco M., Giambastiani B.M.S., 2015a. Predicting salinization trends in a lowland coastal aquifer: Comacchio (Italy). *Water Resources Management* doi: 10.1007/s11269-014-0795-8.
- Colombani N., Osti A., Volta G., Mastrocicco M., 2015b. Impact of climate change on salinization of coastal water resources. Submitted to *Water Resources Management*.
- Colombani N., Volta G., Osti A., Mastrocicco M., 2015c. Misleading reconstruction of seawater intrusion via integral depth sampling. Submitted to *Journal of Hydrology*, HYDROL18381.
- Curzi P.V., Dinelli E., Ricci Lucchi M., Vaiani S.C., 2006. Palaeoenvironmental control on sediment composition and provenance in the late Quaternary deltaic successions: a case study from the Po delta area (Northern Italy). *Geological Journal* 41, 591-612.
- Custodio E., 2010. Coastal aquifers in Europe: an overview. *Hydrogeology Journal* 18, 269-280.
- Danielson R.E. and Sutherland P.L., 1986. In: Klute A. (ed.) *Methods of Soil Analysis, Part I. Physical and Mineralogical Methods*, 2nd Edition. *Agronomy Monograph* 9, 443-461.
- Davis S.N., Whittemone D.O., Fabryka-Martin J., 1998. Uses of chloride/bromide ratios in studies of potable water. *Ground Water* 36(2), 338-350.
- Davis S.N. and De Wiest R.J.M., 1996. *Hydrogeology*. John Wiley & Sons, New York, pp. 463.
- Delaune R.D., Gambrell R.P., Jugsujinda A., Devai I., Hou A., 2008. Total Hg, methyl Hg and other toxic heavy metals in a northern Gulf of Mexico estuary: Louisiana Pontchartrain basin. *Journal of Environmental Science and Health - Part A Toxic/Hazardous Substances and Environmental Engineering* 43(9), 1006-1015.
- Dellwig O., Böttcher M.E., Lipinski M., Brumsack H.-J., 2002. Trace metals in Holocene coastal peats and their relation to pyrite formation (NW Germany). *Chemical Geology* 182(2-4), 423-442.
- Dellwig O., Watermann F., Brumsack H.-J., Gerdes G., Krumbein W.E., 2001. Sulphur and iron geochemistry of Holocene coastal peats (NW Germany): A tool for palaeoenvironmental reconstruction. *Palaeogeography, Palaeoclimatology, Palaeoecology* 167 (3-4), 359-379.

REFERENCES

- de Louw P.G.B., Eeman S., Oude Essink G.H.P., Vermue E., Post V.E.A., 2013a. Rainwater lens dynamics and mixing between infiltrating rainwater and upward saline groundwater seepage beneath a tile-drained agricultural field. *Journal of Hydrology* 501, 133-145.
- de Louw P.G.B., Eeman S., Siemon B., Voortman B.R., Gunnink J., Van Baaren S.E., Oude Essink G.H.P., 2011. Shallow rainwater lenses in deltaic areas with saline seepage. *Hydrology and Earth System Sciences* 15, 3659-3678.
- de Louw P.G.B., Oude Essink G.H.P., Stuyfzand P.J., van der Zee S.E.A.T.M., 2010. Upward groundwater flow in boils as the dominant mechanism of salinization in deep polders. *Journal of Hydrology* 394 (3-4), 494-506.
- de Louw P.G.B., Vandenbohede A., Werner A.D., Oude Essink G.H.P., 2013b. Natural saltwater upconing by preferential groundwater discharge through boils. *Journal of Hydrology* 490, 74-87.
- de Montety V., Radakovitch O., Vallet-Coulomb C., Blavoux B., Hermitte D., Valles V., 2008. Origin of groundwater salinity and hydrogeochemical processes in a confined coastal aquifer: case of the Rhône delta (Southern France). *Applied Geochemistry* 23 (8), 2337-2349.
- Devai I., Patrick Jr. W.H., Neue H.-U., DeLaune R.D., Kongchum M., Rinklebe J., 2005. Methyl mercury and heavy metal content in soils of rivers Saale and Elbe (Germany). *Analytical Letters* 38(6), 1037-1048.
- Dhar R.K., Zheng Y., Stute M., van Geen A., Cheng Z., Shanewaz M., Shamsudduha M., Hoque M.A., Rahman M.W., Ahmed K.M., 2008. Temporal variability of groundwater chemistry in shallow and deep aquifers of Araihasar, Bangladesh. *Journal of Contaminant Hydrology* 99(1-4), 97-111.
- Dillon P., 2005. Future management of aquifer recharge. *Hydrogeology Journal* 13(1), 313-316.
- Dinelli E., Tateo F., Summa V., 2007. Geochemical and mineralogical proxies for grain size in mudstones and siltstones from the Pleistocene and Holocene of the Po River alluvial plain, Italy. In J. Arribas, S. Critelli, and M.J. Johnsson (Eds) *Sedimentary Provenance and Petrogenesis: Perspectives from Petrography and Geochemistry*. Geological Society of America Special Paper, 420, 25-36.
- Directive 2000/60/EC of the European Parliament and of the Council of 23 October 2000. Establishing a framework for Community action in the field of water policy. *Official Journal of the European Communities* L327/1.

REFERENCES

- Doherty J., 2002. PEST: Model-Independent Parameter Estimation: User's Manual, 5th ed., Watermark Numer. Comput., Brisbane, Australia.
- Dou Y., Li J., Zhao J., Hu B., Yang S., 2013. Distribution, enrichment and source of heavy metals in surface sediments of the eastern Beibu Bay, South China Sea. *Marine Pollution Bulletin* 67(1-2), 137-45.
- Du Laing G., De Vos R., Vandecasteele B., Lesage E., Tack F.M.G., Verloo M.G., 2008. Effect of salinity on heavy metal mobility and availability in intertidal sediments of the Scheldt estuary. *Estuarine, Coastal and Shelf Science* 77(4), 589-602.
- Du Laing G., Rinklebe J., Vandecasteele B., Meers E., Tack F.M.G., 2009. Trace metal behaviour in estuarine and riverine floodplain soils and sediments: A review. *Science of the Total Environment* 407(13), 3972-3985.
- Edmunds W.M., 2001. Palaeowaters in European coastal aquifers – the goals and main conclusions of the PALAEWAUX project. In: Edmunds, W.M., Milne, C. (Eds.), *Paleowaters in Coastal Europe: Evolution of Groundwater since the Late Pleistocene*. Special Publications 189. Geological Society, London, pp. 1-16.
- Einarson M.D. and Cherry J.A., 2002. A new multilevel ground water monitoring system using multichannel tubing. *Ground Water Monitoring and Remediation* 22 (4), 52-65.
- Elci A., Gregory P.F., Molz F.J., 2003. Detrimental effects of natural head gradients on chemical and water level measurements in observation wells: Identification and control. *Journal of Hydrology* 281, 70-81.
- Emerson S.R. and Huested S.S., 1991. Ocean anoxia and the concentrations of molybdenum and vanadium in seawater. *Marine Chemistry* 34, 177-196.
- Fakir Y., Mernissi M.E., Kreuser T., Berjami B., 2002. Natural tracer approach to characterize groundwater in the coastal Sahel of Oualidia (Morocco). *Environmental Geology* 43, 197-202.
- Fass T., Cook P.G., Stieglitz T., Herczeg A.L., 2007. Development of saline groundwater through transpiration of seawater. *Ground Water* 45 (6), 703-710.
- Feddes R.A., Kowalik P.J., Zaradny H., 1978. *Simulation of field water use and crop yield*. Pudoc, Wageningen, the Netherlands.
- Feseker T., 2007. Numerical studies on saltwater intrusion in a coastal aquifer in northwestern Germany. *Hydrogeology Journal* 15(2), 267-279.

REFERENCES

- Fetter C.W., 2001. Applied hydrogeology, 4th ed. Prentice Hall, Englewood Cliffs, USA, pp. 598.
- Fidelibus M.D., Calò G., Tinelli R., Tulipano L., 2011. Salt ground waters in the Salento karstic coastal aquifer (Apulia, Southern Italy). In Lambrakis N., Stournaras G & Katsanou K. (Eds.), *Advances in the Research of Aquatic Environment, Environmental Earth Sciences Series*, Springer-Verlag, Berlin. 1, 407-415.
- Fujinawa K., Iba T., Fujihara Y., Watanabe T., 2009. Modeling Interaction of Fluid and Salt in an Aquifer/Lagoon System. *Ground Water* 47(1), 35-48.
- García-Ruiz J.M., López-Moreno J.I., Vicente-Serrano S.M., Lasanta T., Beguería S., 2011. Mediterranean water resources in a global change scenario. *Earth Science Reviews* 105, 121-139.
- Gattacceca J.C., Vallet-Coulomb C., Mayer A., Claude C., Radakovitch O., Conchetto E., Hamelin B., 2009. Isotopic and geochemical characterization of salinization in the shallow aquifers of a reclaimed subsiding zone: the southern Venice Lagoon coastland. *Journal of Hydrology* 378, 46-61.
- Gelberg K.H., Church L., Casey G., London M., Roerig D.S., Boyd J., Hill M., 1999. Nitrate levels in drinking water in rural New York State. *Environmental Research* 80(1), 34-40.
- Ghiglieri G., Oggiano G., Fidelibus M.D., Alemayehu T., Barbieri G., Vernier A., 2009. Hydrogeology of the Nurra Region, Sardinia (Italy): basement-cover influences on groundwater occurrence and hydro-geochemistry. *Hydrogeology Journal* 17(2), 447-466.
- Giambastiani B.M.S., Antonellini M., Oude Essink G.H.P., Stuurman R.J., 2007. Saltwater intrusion in the unconfined coastal aquifer of Ravenna (Italy): a numerical model. *Journal of Hydrology* 340, 91-104.
- Giambastiani B.M.S., Colombani N., Mastrocicco M., Fidelibus M.D., 2013. Characterization of the lowland coastal aquifer of Comacchio (Ferrara, Italy): hydrology, hydrochemistry and evolution of the system. *Journal of Hydrology* 501, 35-44.
- Giménez Forcada E. and Morell Evangelista I., 2008. Contributions of boron isotopes to understanding the hydrogeochemistry of the coastal detritic aquifer of Castellon Plain, Spain. *Hydrogeology Journal* 16, 547-557.
- Giorgi F. and Lionello P., 2008. Climate change projections for the Mediterranean region. *Global Planetary Change* 63, 90-104.

REFERENCES

- Glessner J.J.G. and Roy W.R., 2009. Paleosols in central Illinois as potential sources of ammonium in groundwater. *Ground Water Monitoring and Remediation* 29(4), 56-64.
- Grassi S., Cortecchi G., Squarci P., 2007. Groundwater resource degradation in coastal plains: the example of the Cecina area (Tuscany – Central Italy). *Applied Geochemistry* 22, 2273-2289.
- Gualdi S., Somot S., Li L., Artale V., Adani M., Bellucci A., Braun A., Calmanti S., Carillo A. et al., 2013. The CIRCE simulations – Regional climate change projections with realistic representation of the Mediterranean Sea. *Bulletin of the American Meteorological Society* 94, 65-81.
- Gulis G., Czompolyova M., Cerhan J.R., 2002. An ecologic study of nitrate in municipal drinking water and cancer incidence in Trnava District, Slovakia. *Environmental Research* 88(3), 182-187.
- Guo W. and Langevin C.D., 2002. User's guide to SEAWAT: A computer program for simulation of three-dimensional variable-density ground-water flow. *Techniques of Water-Resources Investigations* 6-A7, pp. 77.
- Hanson R.T., Flint L.E., Flint A.L., Dettinger D.M., Faunt C.C., Cayan D., Schmid W., 2012. A method for physically based model analysis of conjunctive use in response to potential climate changes. *Water Resources Research* 48(2), W00L08.
- Harbaugh A.W., 2005. MODFLOW-2005, the U.S. Geological Survey Modular Ground-water Model - The Ground-water Flow Process: U.S. Geological Survey Techniques and Methods 6, A16.
- Hartog N., Griffioen J., Van der Weijden C.H., 2002. Distribution and reactivity of O₂-reducing components in sediments from a layered aquifer. *Environmental Science and Technology* 36(11), 2338-2344.
- Henderson T.H., Mayer K.U., Parker B.L., Al T.A., 2009. Three-dimensional density-dependent flow and multicomponent reactive transport modeling of chlorinated solvent oxidation by potassium permanganate. *Journal of Contaminant Hydrology* 106, 195-211.
- Hill M.C., Banta E.R., Harbaugh A.W., Anderman E.R., 2000. MODFLOW-2000, the U.S. Geological Survey Modular Ground-Water Model - User guide to the observation, sensitivity, and parameter-estimation processes and three post-processing programs. U.S. Geological Survey Open-File Report 00-184, pp. 210.

REFERENCES

- Hill H.J., Shirley O.J., Klein G.E., 1979. Bound water in shaly sands—its relation to Q_v and other formation properties. *The Log Analyst*, Society of Professional Well Log Analysts XX(3), 3-19.
- Hinkle S.R., Böhlke J.K., Duff J.H., Morgan D.S., Weick R.J., 2007. Aquifer-scale controls on the distribution of nitrate and ammonium in ground water near La Pine, Oregon, USA. *Journal of Hydrology* 333(2-4), 486-503.
- Hinsby K., Condesso de Melo M.T., Dahl M., 2008. European case studies supporting the derivation of natural background levels and groundwater threshold values for the protection of dependent ecosystems and human health. *The Science of the Total Environment* 401(1-3), 1-20.
- Hoque M.A., McArthur J.M., Sikdar P.K., Ball J.D., Molla T.N., 2014. Tracing recharge to aquifers beneath an Asian megacity with Cl/Br and stable isotopes: the example of Dhaka, Bangladesh. *Hydrogeology Journal* 22(7), 1549-1560.
- IPCC, 2014a. *Climate Change 2014: Impacts, Adaptation, and Vulnerability. Part A: Global and Sectoral Aspects. Contribution of Working Group II to the Fifth Assessment Report of the Intergovernmental Panel on Climate Change* [Field CB, VR Barros, DJ Dokken, KJ Mach, MD Mastrandrea, TE Bilir, M Chatterjee, KL Ebi, YO Estrada, RC Genova, B Girma, ES Kissel, AN Levy, S MacCracken, PR Mastrandrea, LL White (eds.)]. Cambridge University Press, Cambridge, United Kingdom and New York, NY, USA.
- IPCC, 2014b. *Climate Change 2014: Impacts, Adaptation, and Vulnerability. Part B: Regional Aspects. Contribution of Working Group II to the Fifth Assessment Report of the Intergovernmental Panel on Climate Change* [Barros, VR, CB Field, DJ Dokken, MD Mastrandrea, KJ Mach, TE Bilir, M Chatterjee, KL Ebi, YO Estrada, RC Genova, B Girma, ES. Kissel, AN Levy, S MacCracken, PR Mastrandrea, LL White (eds.)]. Cambridge University Press, Cambridge, United Kingdom and New York, NY, USA.
- Jang C.S. and Liu C.W., 2005. Contamination potential of nitrogen compounds in the heterogeneous aquifers of the Choushui River alluvial fan, Taiwan. *Journal of Contaminant Hydrology* 79(3-4), 135-155.
- Jayasingha P., Pitawala A., Dharmagunawardhane H.A., 2011. Vulnerability of coastal aquifers due to nutrient pollution from agriculture: Kalpitiya, Sri Lanka. *Water Air and Soil Pollution* 219, 563-577.
- Jiao J.J., Wang Y., Cherry J.A., Wang X., Zhi B., Du H., Wen D., 2010. Abnormally high ammonium of natural origin in a coastal aquifer-aquitard system in the Pearl River Delta, China. *Environmental Science and Technology* 44, 7470-7475.

REFERENCES

- Jorstad L.B., Jankowski J., Acworth R.I., 2004. Analysis of the distribution of inorganic constituents in a landfill leachate-contaminated aquifer: Astrolabe Park, Sydney, Australia. *Environmental Geology* 46(2), 263-272.
- Kass A., Gavrieli I., Yechieli Y., Vangosh A., Starinsky A., 2005. The impact of freshwater and wastewater irrigation on the chemistry of shallow groundwater: a case study from the Israeli Coastal Aquifer. *Journal of Hydrology* 300, 314-331.
- Kim K.-Y., Chon C.-M., Park K.-H., Park Y.-S., Woo N.C., 2008. Multi-depth monitoring of electrical conductivity and temperature of groundwater at a multilayered coastal aquifer: Jeju Island, Korea. *Hydrological Processes* 22(18), 3724-3733.
- Konikow L.F. and Hornberger G.Z., 2006. Modeling effects of multimode wells on solute transport. *Ground Water* 44 (5), 648-660.
- Kurtzman D., Netzer L., Weisbrod N., Graber E., Ronen D., 2011. Steady-state homogeneous approximations of vertical velocity from EC profiles. *Ground Water* 49(2), 275-279.
- Lambeck K., Antonioli F., Anzidei M., Ferranti L., Leoni G., Scicchitano G., Silenzi S., 2011. Sea level change along the Italian coast during the Holocene and projections for the future. *Quaternary International* 232, 250-257.
- Landon M.K., Green C.T., Belitz K., Singleton M.J., Esser B.K., 2011. Relations of hydrogeologic factors, groundwater reduction-oxidation conditions, and temporal and spatial distributions of nitrate, Central-Eastside San Joaquin Valley, California, USA. *Hydrogeology Journal* 19, 1203-1224.
- Langevin C.D., Thorne D.T.Jr., Dausman A.M., Sukop M.C., Guo W., 2007. SEAWAT Version 4: A Computer Program for Simulation of Multi-Species Solute and Heat Transport: U.S. Geological Survey Techniques and Methods, 6-A22, pp 1-39.
- Langevin C.D. and Zygnerski M., 2013. Effect of Sea-Level Rise on Salt Water Intrusion near a Coastal Well Field in Southeastern Florida. *Ground Water* 51(5), 781-803.
- Lebbe L., Van Meir N., Viaene P., 2008. Potential Implications of Sea-Level Rise for Belgium. *Journal of Coastal Research* 24(2), 358-366.
- Lenahan M.J. and Bristow K., 2010. Understanding sub-surface solute distributions and salinization mechanisms in a tropical coastal floodplain groundwater system. *Journal of Hydrology* 390, 131-142.

REFERENCES

- Leven C. and Dietrich P., 2006. What information can we get from pumping tests?-comparing pumping test configurations using sensitivity coefficients. *Journal of Hydrology* 319, 199-215.
- Lewandowski J. and Nützmann G., 2010. Nutrient retention and release in a floodplain's aquifer and in the hyporheic zone of a lowland river. *Ecological Engineering* 36(9), 1156-1166.
- Li Q., Cai S., Mo C., Chu B., Peng L., Yang F., 2010. Toxic effects of heavy metals and their accumulation in vegetables grown in a saline soil. *Ecotoxicology and Environmental Safety* 73(1), 84-88.
- Li J., Li F., Liu Q., Zhang Y., 2014. Trace metal in surface water and groundwater and its transfer in a Yellow River alluvial fan: evidence from isotopes and hydrochemistry. *The Science of the Total Environment* 472, 979-988.
- Linderfelt W.R. and Turner J.V., 2001. Interaction between shallow groundwater, saline surface water and nutrient discharge in a seasonal estuary: The Swan - Canning system. *Hydrological Processes* 15(13), 2631-2653.
- Lorenzen G., Sprenger C., Baudron P., Gupta D., Pekdeger A., 2012. Origin and dynamics of groundwater salinity in the alluvial plains of western Delhi and adjacent territories of Haryana State, India. *Hydrological Processes* 26, 2333-2345.
- Loring D.H., 1991. Normalization of heavy-metal data from estuarine and coastal sediments. *ICES Journal of Marine Science* 48(1), 101-115.
- Lorite-Herrera M., Hiscock K., Jiménez-Espinosa R., 2009. Distribution of dissolved inorganic and organic nitrogen in river water and groundwater in an agriculturally-dominated catchment, South-East Spain. *Water Air and Soil Pollution* 198, 335-346.
- Martinelli L., Zanuttigh B., Corbau C., 2010. Assessment of coastal flooding hazard along the Emilia Romagna littoral, IT. *Coastal Engineering* 57, 1042-1058.
- Mastrocicco M., Colombani N., Castaldelli G., Jovanovic N., 2011a. Monitoring and modelling nitrate persistence in a shallow aquifer. *Water Air and Soil Pollution* 217(1-4), 83-93.
- Mastrocicco M., Colombani N., Di Giuseppe D., Faccini B., Coltorti M., 2013a. Contribution of the subsurface drainage system in changing the nitrogen speciation of an agricultural soil located in a complex marsh environment (Ferrara, Italy). *Agricultural Water Management* 119, 144-153.

REFERENCES

- Mastrocicco M., Colombani N., Petitta M., 2011b. Modelling the density contrast effect on a chlorinated hydrocarbon plume reaching the shore line. *Water Air and Soil Pollution* 220(1-4), 387-398.
- Mastrocicco M., Colombani N., Salemi E., Castaldelli G., 2011c. Groundwater nitrogen speciation in intensively cultivated lowland areas. In *Advances in the Research of Aquatic Environment*, Springer, XXVIII, pp. 512, ISBN 978-3-642-24075-1. Eds. Lambrakis N., Stournaras G., Katsanou K. 2, 291-298.
- Mastrocicco M., Colombani N., Salemi E., Castaldelli G., 2010. Numerical assessment of effective evapotranspiration from maize plots to estimate groundwater recharge in lowlands. *Agricultural Water Management* 97(9), 1389-1398.
- Mastrocicco M., Colombani N., Salemi E., Vincenzi F., Castaldelli G., 2012a. The role of the unsaturated zone in determining nitrate leaching to groundwater. In "Groundwater Quality Sustainability", IAH Book Series (IAH Selected Papers), Eds. Zuber A., Maloszewski P., Witczak S., Malina G. - Taylor & Francis Books (UK) ISBN-13:9780415698412.
- Mastrocicco M., Colombani N., Sbarbati C., Petitta M., 2012b. Assessing the effect of saltwater intrusion on petroleum hydrocarbons plumes via numerical modelling. *Water Air and Soil Pollution* 223(7), 4417-4427.
- Mastrocicco M., Giambastiani B.M.S., Colombani N., 2013b. Ammonium occurrence in a salinized lowland coastal aquifer. *Hydrological Processes* 27(24), 3495-3501.
- Mastrocicco M., Giambastiani B.M.S., Severi P., Colombani N., 2012c. The importance of data acquisition techniques in saltwater intrusion monitoring. *Water Resources Management* 26, 2851-2866.
- Mc Donald J.M. and Harbaugh A.W., 1988. MODFLOW, a modular 3D finite difference groundwater flow model. U.S. Geological Survey Open File Report 83-875, pp. 586.
- McMahon P.B. and Chapelle F.H., 2008. Redox processes and water quality of selected principal aquifer systems. *Ground Water* 46(2), 259-71.
- Mollema P.N., Antonellini M., Dinelli E., Gabbianelli G., Greggio N., Stuyfzand P.J., 2013. Hydrochemical and physical processes influencing salinization and freshening in Mediterranean low-lying coastal environments. *Applied Geochemistry* 34, 207-221.
- Mollema P.N., Antonellini M., Gabbianelli G., Laghi M., Marconi V., Minchio A., 2012. Climate and water budget change of a Mediterranean coastal watershed, Ravenna, Italy. *Environmental Earth Sciences* 65, 257-276.

REFERENCES

- Mondal N.C., Singh V.P., Singh S., Singh V.S., 2011. Hydrochemical characteristic of coastal aquifer from Tuticorin, Tamil Nadu, India. *Environmental Monitoring and Assessment* 175, 531-550.
- Nash J.E. and Sutcliffe J.V., 1970. River flow forecasting through conceptual models. Part I: A discussion of principles. *Journal of Hydrology*, 10(3), 282-290.
- Nativ R. and Weisbrod N., 1994. Management of a multilayered coastal aquifer – an Israeli case study. *Water Resources Management* 8, 297-311.
- Netzer L., Weisbrod N., Kurtzman D., Nasser A., Graber E.R., Ronen D., 2011. Observations on Vertical Variability in Groundwater Quality: Implications for Aquifer Management. *Water Resources Management* 25, 1315-1324.
- Ortega-Guerrero A., 2003. A. Origin and geochemical evolution of groundwater in a closed-basin clayey aquitard, Northern Mexico. *Journal of Hydrology* 284(1-4), 26-44.
- Otero N., Vitòria L., Soler A., Canals A., 2005. Fertilizer characterisation: Major, trace and rare earth elements. *Applied Geochemistry* 20, 1473-1488.
- Oude Essink G.H.P., van Baaren E.S., de Louw P.G.B., 2010. Effects of climate change on coastal groundwater systems: A modeling study in the Netherlands. *Water Resources Research* 46(10), W00F04.
- Park S.C., Yun S.T., Chae G.T., Yoo I.S., Shin K.S., Heo C.H., Lee S.K., 2005. Regional hydrochemical study on salinization of coastal aquifers, western coastal area of South Korea. *Journal of Hydrology* 313(3-4), 182-194.
- Parkhurst D.L., 1995. User's guide to PHREEQC – A computer program for speciation, reaction-path, advective-transport, and inverse geochemical calculations: U.S. Geological Survey Water - Resources Investigations Report 95-4227, pp. 143.
- Post V. and Abarca E., 2010. Preface: saltwater and freshwater interactions in coastal aquifers. *Hydrogeology Journal* 18, 1-4.
- Post V., Kooi H., Simmons C., 2007. Using hydraulic head measurements in variable-density ground water flow analyses. *Ground Water* 45(6), 664-671.
- Prommer H., Tuxen N., Bjerg P.L., 2006. Fringe-controlled natural attenuation of phenoxy acids in a landfill plume: Integration of field-scale processes by reactive transport modelling. *Environ Science Technology* 40(15), 4732-4738.

REFERENCES

- Puckett L.J., Cowdery T.K., McMahon P.B., Tornes L.H., Stoner J.D., 2002. Using chemical, hydrologic, and age dating analysis to delineate redox processes and flow paths in the riparian zone of a glacial outwash aquifer-stream system. *Water Resources Research* 38(8), 91-920.
- Ranjana P., Kazama S., Sawamoto M., 2006. Effects of climate change on coastal fresh groundwater resources. *Global Environmental Change* 16(4), 388-399.
- Ridd P.V. and Stieglitz T., 2002. Dry season salinity changes in arid estuaries fringed by mangroves and saltflats. *Estuarine Coastal and Shelf Science* 54(6), 1039-1049.
- Ritchie J.T., 1972. Model for predicting evaporation from a row crop with incomplete cover. *Water Resources Research* 8(5), 1204-1213.
- Robbins G.A. and Martin-Hayden J.M., 1991. Mass balance evaluation of monitoring well purging: Part I. Theoretical models and implications for representative sampling. *Journal of Contaminant Hydrology* 8(3-4), 203-224.
- Rodvang S.J. and Simpkins W.W., 2001. Agricultural contaminants in Quaternary aquitards: A review of occurrence and fate in North America. *Hydrogeology Journal* 9(1), 44-59.
- Sanchez-Martos F., Pulido-Bosch A., Molina-Sanchez L., Vallejos-Izquierdo A., 2002. Identification of the origin of salinization in groundwater using minor ions (Lower Andarax, Southeast Spain). *Science of the Total Environment* 297, 43-58.
- Seitzinger S.P., Gardner W.S., Spratt A.K., 1991. The effect of salinity on ammonium sorption in aquatic sediments. Implications for benthic nutrient recycling. *Estuaries* 14(2), 167-174.
- Shalev E., Lazar A., Wollman S., Kington S., Yechieli Y., Gvirtzman H., 2009. Biased monitoring of fresh water-salt water mixing zone in coastal aquifers. *Ground Water* 47(1), 49-56.
- Simeoni U. and Corbau C., 2009. A review of the Delta Po evolution (Italy) related to climatic changes and human impacts. *Geomorphology* 107, 64-71.
- Šimunek J., Šejna M., Saito H., Sakai M., van Genuchten M.Th., 2008. The HYDRUS-1D Software Package for Simulating the Movement of Water, Heat, and Multiple Solutes in Variably Saturated Media, Version 4.0, HYDRUS Software Series 3, Department of Environmental Sciences, University of California Riverside, Riverside, California, USA, pp. 315.
- Stefani M. and Vincenzi S., 2005. The interplay of eustasy, climate and human activity in the late Quaternary depositional evolution and sedimentary architecture of the Po Delta system. *Marine Geology* 222-223, 19-48.

REFERENCES

- Stueber A.M. and Walter L.M., 1991. Origin and chemical evolution of formation waters from Silurian-Devonian strata in the Illinois basin, USA. *Geochimica and Cosmochimica Acta* 55, 309-325.
- Stuyfzand P.J., 2008. Base exchange indices as indicators of salinization or freshening of (coastal) aquifers. In: Proc. 20th SWIM, Naples (FI), USA, 2008, pp. 262-265.
- Stuyfzand P.J., 1989. A new hydrochemical classification of watertypes. IAHS Publication 182, 89-98.
- Stuyfzand P.J. and Stuurman, R.J., 2008. Origin, distribution and chemical mass balances of non-anthropogenic, brackish and (hyper)saline groundwaters in the Netherlands. In: Proc. 1st SWIM-SWICA Joint Saltwater Intrusion Conference, Cagliari (Italy), 151-164.
- Teatini P., Ferronato M., Gambolati G., Bertoni W., Gonella M., 2005. A century of land subsidence in Ravenna, Italy. *Environmental Geology* 47(6), 831-846.
- Teatini P., Ferronato M., Gambolati G., Gonella M., 2006. Groundwater pumping and land subsidence in the Emilia-Romagna coastland, Italy: modeling the past occurrence and the future trend. *Water Resources Research* 42, 1-19.
- Teuchies J., Vandenbruwaene W., Carpentier R., Bervoets L., Temmerman S., Wang C., Maris T., Cox T.J.S., Van Braeckel A., Meire P., 2013. Estuaries as Filters : The Role of Tidal Marshes in Trace Metal Removal. *PLoS ONE* 8(8), e70381.
- Thornthwaite C.W., 1948. An approach toward a rational classification of climate. *Geographical Review* 38, 55-94.
- Tiessen H. and Moir J.O., 1993. Total and organic carbon. In: Carte M.E. (Eds.) *Soil Sampling and Methods of Analysis*, Lewis Publishers, MI (USA), pp. 187-211.
- Turekian K.K., 1968. *Oceans*. Prentice-Hall.
- Vandecasteele B., Buysse C.A., Tack F.M.G., 2008. Metal uptake in maize, willows and poplars on impoldered and freshwater tidal marshes in the Scheldt estuary. *Soil Use and Management* 22(1), 52-61.
- Vandenbohede A. and Lebbe L., 2012. Groundwater chemistry patterns in the phreatic aquifer of the central Belgian coastal plain. *Applied Geochemistry* 27, 22-36.
- Vandenbohede A., Luyten K., Lebbe L., 2008. Effects of global change on heterogeneous coastal aquifers: a case study in Belgium. *Journal of Coastal Research* 24(2B), 160-170.

REFERENCES

- Vienken T., Dietrich P., 2011. Field evaluation of method for determining hydraulic conductivity from grain size data. *Journal of Hydrology* 400, 58-71.
- Vukovic M. and Soro A., 1992. Determination of Hydraulic Conductivity of Porous Media From Grain-Size Composition, Water Resources Publication, Highlands Ranch, Colorado, pp. 83.
- Wang Y., Jiao J.J., Cherry J.A., 2012. Occurrence and geochemical behaviour of arsenic in a coastal aquifer-aquitard system of the Pearl River Delta, China. *Science of the Total Environment* 427-428, 286-297.
- Watson T.A., Werner A.D., Simmons C.T., 2010. Transience of seawater intrusion in response to sea level rise. *Water Resources Reserch* 46(12), W12533.
- Werner A.D., Bakker M., Post V.E.A., Vandenbohede A., Lu C., Ataie-Ashtiani B., Simmons C.T., Barry D.A., 2013. Seawater intrusion processes, investigation and management: Recent avances and future challenges. *Advances in Water Resources* 51, 3-26.
- Werner A.D. and Gallagher M.R., 2006. Characterisation of sea-water intrusion in the Pioneer Valley, Australia using hydrochemistry and three-dimensional numerical modelling. *Hydrogeology Journal* 14, 1452-1469.
- Werner A.D. and Simmons C.T., 2009. Impact of sea-level rise on sea water intrusion in coastal aquifers. *Ground Water* 47(2), 197-204.
- Wood W.W., Rizk Z.S., Alsharhan A.S., 2003. Timing of recharge and the origin, evolution and distribution of solutes in a hyperarid aquifer system, in Alsharhan, A.S., Wood, W.W., (Eds.), *Water Resources Perspectives: Evaluation, Management and Policy*. Elsevier, Amsterdam, The Netherlands, pp. 295-312.
- Worthington P.F., 1998. Conjunctive interpretation of core and log data through association of effective and total porosity models. In: Harvey, P.K. & Lovell, M.A. (Eds), *Core-Log Integration*, Geological Society, London, Special Publications 136, pp. 213-223.
- Yamanaka M. and Kumagai Y., 2006. Sulfur isotope constraint on the provenance of salinity in a confined aquifer system of the southwestern Nobi Plain, central Japan. *Journal of Hydrology* 325, 35-55.
- Zalidis G., Stamatiadis S., Takavakoglou V., Eskridge K., Misopolinos N., 2002. Impacts of agricultural practices on soil and water quality in the Mediterranean region and proposed assessment methodology. *Agriculture Ecosystems and Environment* 88, 137-146.